SRP-22 ALAR FOX

Fall DSE 2022: Regional Passenger Transport

Report Version No. 3.0

Tuesday 31st January, 2023 | Delft (Netherlands)

AE3200 Design Synthesis

Group 1:

Marcos Cabanas	4782151
Albert Chou	5010292
Megha Dinesh	4995686
Berend Domhof	4659724
Doroteya Doneva	4664892
Tim Hokke	5072395
Alvaro Lanza Rausell	5067251
Adrian Masle	5032148
Gabriel Sa	4662733
Inès van Teeffelen	5001145

TUDelft

This page is intentionally left blank

SRP-22 ALAR FOX

Fall DSE 2022: Regional Passenger Transport

Report Version No. 3.0

Tuesday 31st January, 2023 | Delft (Netherlands)

by

Group 1:

Marcos Cabanas	4782151
Albert Chou	5010292
Megha Dinesh	4995686
Berend Domhof	4659724
Doroteya Doneva	4664892
Tim Hokke	5072395
Alvaro Lanza Rausell	5067251
Adrian Masle	5032148
Gabriel Sa	4662733
Inès van Teeffelen	5001145

Instructor:	Dr.ir. Roelof Vos
Coaches:	Nathan Eskue, M.Sc.
	Dr.ir. Rudolf Saathof
Institution:	Delft University of Technology
Place:	Faculty of Aerospace Engineering, Delft
Project Duration:	November 2022 - February 2023

Cover Image: Rendering of the SRP-22 Alar Fox flying over winter fields [own work]

TU Delft

Preface

This technical report is the result of ten weeks of work for ten Bachelor of Science students of the Faculty of Aerospace Engineering at the Delft University of Technology. Over 4000 man hours, countless investigations of research papers, a considerable number of Python scripts, and pushing the limits of our engineering capabilities have been summarized in over six deliverables, this one being the most extensive, intensive, and complete of them. With this report, we conclude the Design Synthesis Exercise and our Bachelor studies.

During the DSE, we had the privilege to incorporate all the knowledge learned during the Aerospace Engineering bachelor into practice. The design process was challenging, yet exciting and very rewarding. We are proud to present the SRP-22, a regional passenger aircraft using a fuel cell powertrain, into which we poured our heart, soul, and efforts into. The aviation industry is ready and prepared for an innovative breakthrough, and we hope that, with our findings, we are able to add our grain of salt to this breakthrough impact.

We would like to extend our most sincere gratitude to our principal tutor - Dr.ir. R. Vos - and to our coaches - N. Eskue M.Sc, and Dr.ir. R. Saathof - for all their guidance and time spent with us to make this idea a reality. Furthermore, we would like to thank S. Link M.Sc for her expertise on hydrogen combustion engines, P. Proesmans M.Sc for his knowledge on average temperature response, and M. van Dongeren from *AeroDelft* for the fuel cell design and hydrogen transfer. Finally, we would like to thank our respective friends and family members, for their supportive efforts all throughout the four years of our university studies, and especially throughout these past ten weeks.

DSE Group 1, SRP-22 ALAR FOX
Delft, January 2023

Summary

This report entails the design of a regional passenger aircraft, serving 48 passengers and entering the market by 2035. It is known as the SRP-22 ALAR FOX, however, in general, SRP-22 is used. The propulsion system is designed with hydrogen as its fuel. The hydrogen is converted to electricity with a low-temperature proton-exchange membrane fuel cell, which in turn is used by the electric motors, to power the propellers. There are four electric motors with one six-bladed propeller each. Two propellers are located under the wing near the fuselage and deliver 80% of the total power. The remaining two propellers are positioned on the wing tips, delivering the remaining 20%. The benefit of these wingtip propellers is an expected drag reduction of around 10%, due to the attenuation of wingtip vortices.

The hydrogen is stored in a composite tank, located behind the aft pressure bulkhead. The fuel cell is placed under the cabin floor, just in front of the pressure bulkhead, such that less tubing is required to transport the hydrogen. The boil-off of the hydrogen is used to transform the hydrogen from its liquid state to its gaseous state, through the usage of glass rods. After that, the hydrogen is heated up until about 80°C, which is the operating temperature of the fuel cell. The control system is controlled through a mechanical-powered hydraulic system. The elevator design includes horns to relieve the hinge moment.

One of the main goals was to reduce the environmental impact of the aircraft. The average temperature response of the SRP-22 is almost 83 times lower than that of the ATR 42 by 2064, which supports this goal. Noise has also been taken into account, which mainly stems from the propellers and airframe. It is found that the noise levels are well below the limits set by ICAO.

The unit list price of the SRP-22 will be $19 million when using more optimistic fuel cell prices, while a least optimistic estimate results in a unit list price of $37 million. Moreover, the direct operational cost is around 10% lower than those of the ATR 72. Because of the usage of electric motors, the maintenance cost is expected to be lower than for a turboprop aircraft.

Executive Overview

The Design Synthesis Exercise (DSE) is the final project of the Aerospace Engineering Bachelor program at Delft University of Technology. In the DSE, ten students are given ten weeks to design a regional passenger aircraft with the goal of minimizing the global warming impact of aircraft operation while still providing market-competitive performance, price, and operational costs.

This final report concludes the design of the SRP-22 ALAR FOX regional passenger aircraft. The Executive Overview is used to show all design specifications in a comprehensive manner.

Project Objective

As the demand grows for short-haul flights together with an outdated fleet of regional aircraft, a new market is emerging for more efficient and sustainable alternative aircraft. Over the next 20 years, current market predictions forecast a $\approx$ 2000 unit demand, as airlines seek new alternatives that will lower maintenance and operational costs. The aim of the entire project is to present a design proposal for a regional passenger aircraft with at least a 20% reduction of block fuel per seat over 500 nautical miles compared to market competitors while providing market-competitive performance, price, and operational costs. As a result, the Mission Need Statement (MNS) and the Project Objective Statement (POS) are defined as follows:

Mission Need Statement (MNS)

To minimize the environmental impact of regional passenger aircraft, while providing market-competitive performance, price and operational costs.

Project Objective Statement (POS)

Design a regional passenger aircraft with at least a 20% reduction of block fuel per seat over 500 nmi compared to market competitors, in ten weeks by ten students, entering service by 2035.

Client Requirements

The client requirements for the design of the aircraft are listed. These requirements summarize the stakeholder view and give a general overview of the design frame. All client requirements are listed in Table 1.

Table 1: Client Requirements

Client Req.	
RA-CLI-1	The aircraft shall be able to carry a number of passengers in the range of 46-50.
RA-CLI-2	The aircraft shall have a minimum design range of 1000 nmi, at full passenger capacity.
RA-CLI-3	The aircraft shall be compliant with CS/FAR 25 regulations.
RA-CLI-4	The aircraft shall have a reduction in block fuel of at least 20% on a 500 nmi mission compared to reference aircraft.
RA-CLI-5	The aircraft shall have a maximum wingspan ICAO Code C (<36 m).
RA-CLI-6	The aircraft shall have an asking unit price of 36 million USD or lower.
RA-CLI-7	The aircraft shall have a cash operating cost per seat mile on a 500 nmi mission of 0.16 USD or lower.
RA-CLI-8	The aircraft shall enter service in 2035.

Aside from the mentioned client requirements, there are many more detailed requirements that showcase technical specifications. In addition to all requirements, there are mission objectives. These must always be kept in mind during the design process and describe additional goals considering the design.

Weight Estimations

The Class I weight estimation uses the OEM/MTOM ratio following from the build-up method in the Class II weight estimation. Together with the power- and wing loading, this is used to design the subsystems (Table 2). Most of all, the MTOM and W/P ratio are used to both size the power train and determine flight performance.

Table 2: Weight Estimations Outputs

Outputs	Value	Unit
MTOM	18650	[kg]
OEM	12770	[kg]
m_{F}	683	[kg]
W/P	0.077	[N/W]
W/S	3270	[N/m^2]

Aircraft Geometries

The main aircraft geometries are those of the fuselage and the wing (Table 3). The S_{h}/S ratio is equal to 0.17 (resulting in a horizontal tail area of 10.3 m^2) and the vertical tail area is about 14 m^2.

Table 3: Main Aircraft Geometries

Parameter	Value	Unit
Fuselage Length	23.9	[m]
Fuselage Diameter	3.0	[m]
Wing Span	26.8	[m]
Wing Surface Area	59.9	[m^2]

Aerodynamics

As the aircraft contains wing-tip propellers, a **drag reduction of approximately 10%** to the conventional case is expected. The chosen airfoil is the **NACA 63(4)421**, for its overall good aerodynamic performance, along with a high t/c ratio. The maximum flap deflection is 40°. The aerodynamic performance is assessed for cruise, takeoff, and landing configuration (Table 4).

Table 4: Aerodynamic Overview

Cruise	
C_{L}	0.63
$C_{\mathrm{L}}/C_{\mathrm{D}}$	20
α	4°
Takeoff/Landing	
$(C_{\mathrm{L}}/C_{\mathrm{D}})_{\mathrm{flaps},40^\circ}$	11.6
$(C_{\mathrm{L}}/C_{\mathrm{D}})_{\mathrm{flaps},15^\circ}$	15.2
Airfoil	
t/c	0.21
Stall behaviour	gradual

Propulsion

The propulsion system consists of 10 fuel cells stacked together, from which the generated electricity is used by the electric motors, which in turn power the propellers (Figure 1). The always-present boil-off is used as an advantage, as it is actually stimulated in order to create the gaseous hydrogen required to run the fuel cell. In total, there are four motors and propellers present, with six-bladed propellers.

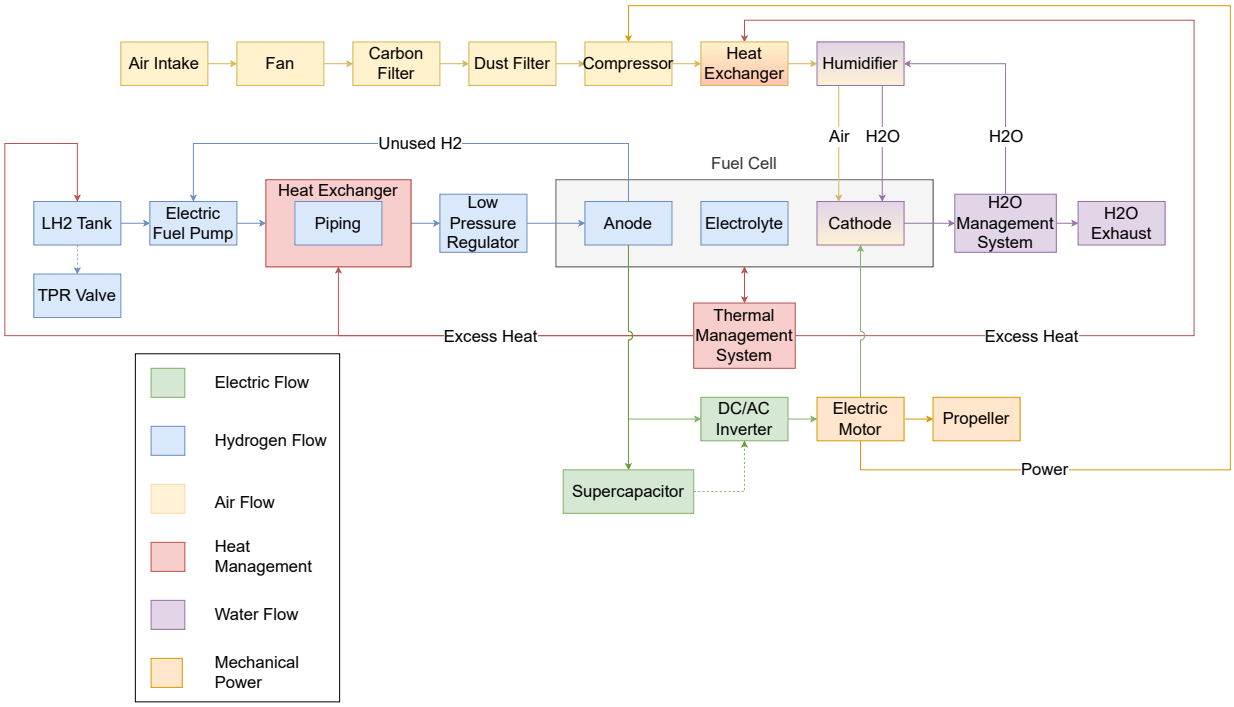

Figure 1: Propulsion System Architecture Block Diagram

Flight Performance

The most interesting aircraft ranges are the range at design payload, the range including divergence, and the ferry range (Figure 2). The takeoff length is equal to **1160 m**, being the summation of the runway length (855 m) and the distance traveling over an object of 50 ft (305 m), while the landing field length is 1125 m. The aircraft is able to climb up to cruise altitude (FL280) within 74.5 nmi with a climb time of approximately 20.3 minutes. Furthermore, a bank angle of 40° can be achieved.

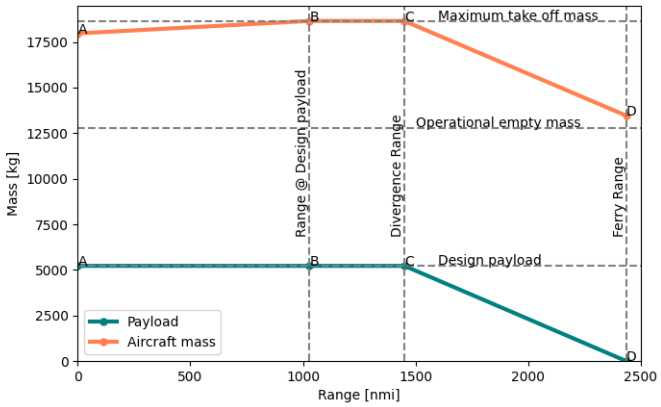

Figure 2: Payload Range Diagram

Finance

Manufacturing accounts for the biggest part of the cost influencing the unit list price of the SRP-22. The SRP-22 will be sold for **$19 million** for the most optimistic fuel cell price prediction. The least optimistic estimate results in a unit list price of **$37 million**. Finally, when comparing to the ATR 72, the direct operational cost of the SRP-22 are **10% lower** for optimistic fuel cell price. In the least optimistic estimate, the SRP-22's direct operational cost is comparable with the ATR-42.

Table 5: Financial Overview

Definition	Value [USD$]	Notes
R&D Cost	1,470 million	FY2035
Manufacturing Cost	14,600 million	FY2035 (1000 aircraft)
Unit List Price	19 million	FY2035 most optimistic case
Unit List Price	37 million	FY2035 least optimistic case
Direct Operational Cost	0.19	per seat nmi FY2035 most optimistic case
Direct Operational Cost	0.26	per seat nmi FY2035 least optimistic case
Total Operational Cost	0.39	per seat nmi FY2035 most optimistic case
Total Operational Cost	0.55	per seat nmi FY2035 least optimistic case
Total Program Operational Cost	3,290 million	FY2035 most optimistic case
Total Program Operational Cost	4,600 million	FY2035 least optimistic case

Sustainability

To compare the environmental impact of the aircraft, the average temperature response is used. This calculates the radiative forcing and its respective temperature response stemming from the operations of the aircraft and its influence for up to 30 years. The average temperature response of the SRP-22 is significantly lower than that of its counterparts that use kerosene. In 2064, the SRP-22 is expected to have an average temperature response of 0.00035, whereas the ATR 42 is expected to have an average temperature response of 0.029. This means that the average temperature response of the SRP-22 is expected to be almost **83 times lower than that of the ATR 42** by 2064. The average temperature response of the SRP-22 is shown in Figure 3. The noise levels at lateral, flyover and approach points are estimated and shown in Table 6. It is concluded that the noise does not exceed the set limits.

Table 6: Noise Levels

Certification Point	Total Noise [EPNdB]	Noise Limit [EPNdB]
Lateral	88.5	94
Flyover	85.3	89
Approach	87.6	98

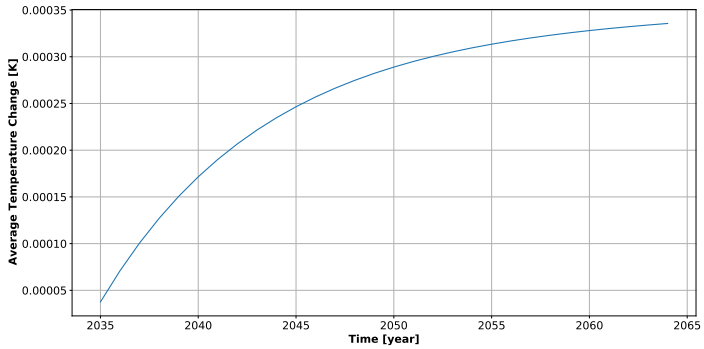

Figure 3: Average Temperature Response of the SRP-22

Aircraft Overview

The 3D layout of the aircraft can be found in Figure 4

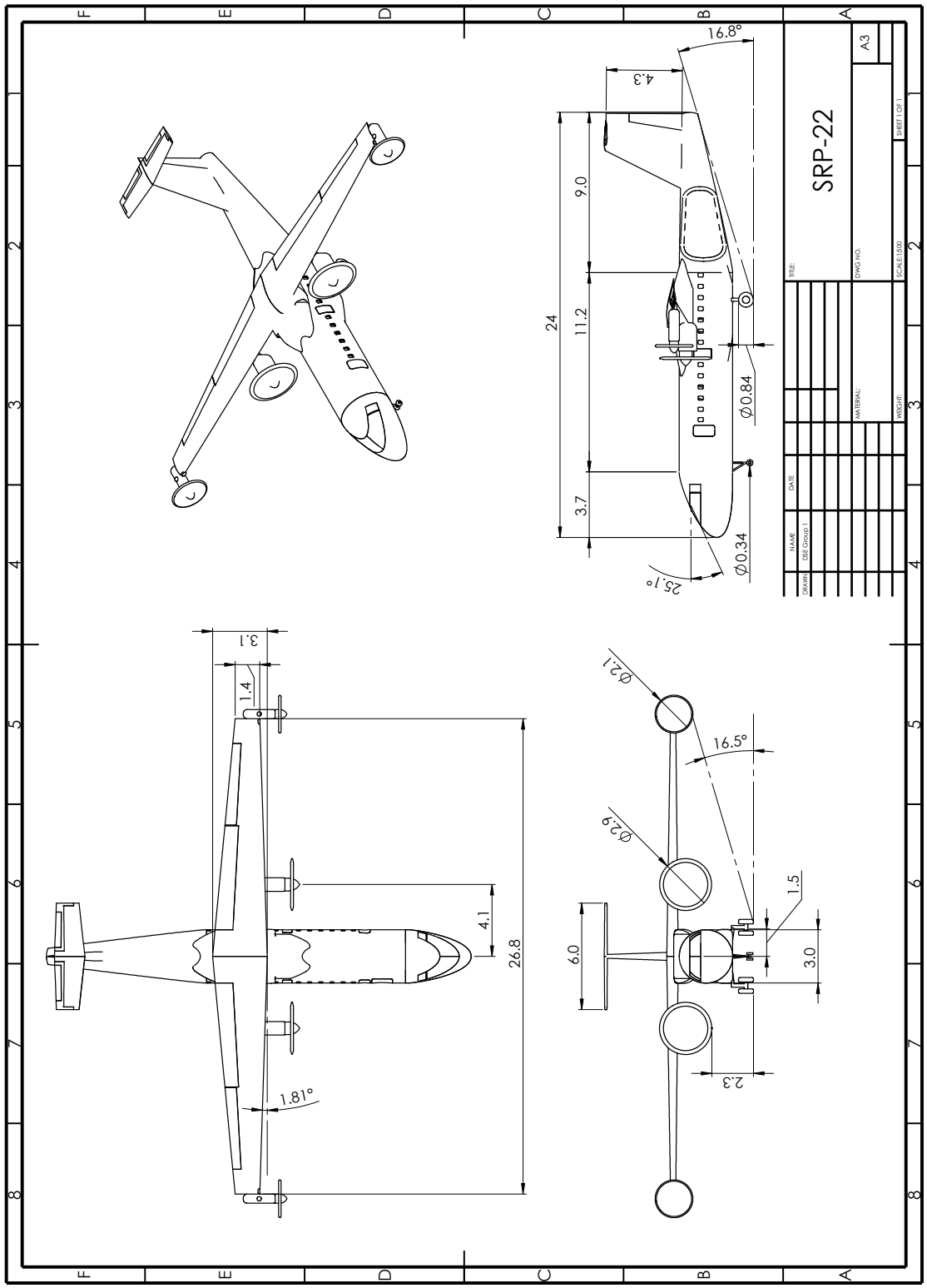

Figure 4: Four view drawing of SRP-22

Contents

Nomenclature

Abbreviations

Abbr.	Definition
AC	Alternating Current
AEP	Aircraft Estimated Price
APU	Auxiliary Power Unit
ATR	Average Temperature Response
CAD	Computer-Aided Design
CD	Conceptual Design
CF	Carbon Fiber
CFD	Computational Fluid Dynamics
CFRP	Carbon Fibre Reinforced Polymer
c.g.	Center of Gravity
CO2	Carbon Dioxide
CP	Certification Program
CS	Certification Specification
DC	Direct Current
DD	Detailed Design
DOC	Direct Operating Cost
DOT	Design Option Tree
DSE	Design Synthesis Exercise
EASA	European Aviation Safety Agency
EPN	Effective Perceived Noise
EPS	Expanded Polystyrene Insulation
FAA	Federal Aviation Administration
FAR	Federal Aviation Regulations
FL	Flight Level
FC	Fuel Cell
FY	Fiscal Year
G.I.	Gravimetric Index
GPS	Global Positioning System
HLD	High-Lift Device
HEPA	High Efficiency Particulate Air
HEPS	Hybrid-Electric Parallel/Series
HES	Hybrid-Electric Series
ICAO	International Civil Aviation Organization
IFR	Instrument Flight Rules
ISA	International Standard Atmosphere
KIAS	Knots Indicated Airspeed
KTAS	Knots True Airspeed
LE	Leading Edge
LEMAC	Leading Edge of the Mean Aerodynamic Chord
LH2	Liquid Hydrogen

Abbr.	Definition
LTPEM	Low Temperature Proton Exchange Membrane
LNC	Load Classficiation Number
MAC	Mean Aerodynamic Chord
MLI	Multi Layer Insulation
MOI	Moment of Inertia
MTOW	Maximum Takeoff Weight
MTOM	Maximum Takeoff Mass
MNS	Mission Need Statement
MZFM	Maximum Zero Fuel Mass
NACA	National Advisory Committee for Aeronautics
OEI	One Engine Inoperative
OME	Operating Empty Mass
pax	Passengers
PEMFC	Proton-Exchange Membrane Fuel Cell
PMAD	Power Management and Distribution
PoO	Probability of Occurrence
POS	Project Objective Statement
RAMS	Reliability, Availability, Maintainability and Sustainability
R&D	Research and Development
Re	Reynolds Number
RF	Radiative Forcing
ROC	Rate of Climb
ROI	Return On Investment
RPM	Revolutions Per Minute
SAF	Sustainable Aviation Fuel
SERA	Standardised European Rules of the Air
SoC	Severity of Consequences
SMR	Steam Methane Reforming
SRP	Sustainable Regional Propeller
SWOT	Strengths-Weaknesses-Opportunities-Threats
TAS	True Airspeed
TBD	To Be Decided
TPR	Temperature-Pressure Relief
TRL	Technology Readiness Level
VHF	Very High Frequency
VFR	Visual Flight Rules

Symbols

Latin	Definition	Unit
A	Area	[m^2]
A	Aspect ratio	[$-$]
b	Wing span	[m]
b	Rib spacing	[m]
c	Chord	[m]
$\bar{c}$	Mean Aerodynamic Chord	[m]
c_d	Airfoil Drag coefficient	[-]
c_l	Airfoil Lift coefficient	[-]
c_r	Root chord length	[m]
c_t	Tip chord length	[m]
C_D	Drag coefficient	[-]
C_{D_o}	Zero-lift drag coefficient	[-]
C_L	Lift coefficient	[$-$]
ch_l	Chord length at certain wingspan	[m]
D	Drag	[N]
d	Diameter	[m]
E	Endurance	[s]
E	Young's modulus	[N/m]
e	Oswald efficiency	[-]
e	Specific Energy Density	[MJ/kg]
F	Force	[N]
g	Gravitational constant	[N/kg]
h	Height	[m]
I	Area Moment of Inertia	[kg m^2]
K_c	Buckling Coefficient	[-]
K_p	Propeller constant	[-]
L	Lift	[N]
l	Length	[m]
M	Mach number	[-]
M	Moment	[Nm]
$\dot{m}$	Mass flow	[kg/s]
n	Load factor	[-]
n	Number	[-]
P	Power	[kW]
P	Pressure	[Bar]
q	Pitch rate	[rad/s]
R	Radius	[m]
r	Radius	[m]
R	Range	[m]
Re	Reynolds number	[-]
S	Surface area	[m^2]
sp_h	Spar height at certain wingspan	[m]
T	Thrust	[N]
t	Time	[s]
t	Thickness	[m]
V	Velocity	[kts]
V	Volume	[m^3]
V	Voltage	[V]
w	Width	[m]
x	Position	[m]
x_{cg}	Center of gravity location	[m]
y_{MAC}	Mean aerodynamic chord location	[m]

Subscript	Definition
a	Aileron
a	Available
ac	Aerodynamic center
air	Air
aft	Aft position
Al	Aluminium
avg	Average
backup	Backup
BL	Boundary layer
c	Cabin
cg	Centre of gravity
clean	Clean configuration
con	Contingency
cr	Cruise
cell	Cell level
div	Divergence
Des	Design point
e	Elevator
fuel	Fuel
f	flaps
f	Fuselage
FC	Fuel cell
h	Horizontal tail
i	Inner
l	Rolling moment
LE	Leading Edge
LFL	Landing Field Length
lg	Landing Gear
L2	Lift at Takeoff Safety Speed
m	Moment
main	Main engine
max	Maximum
MAC	Mean Aerodynamic Center
min	Minimum
mlg	Main Landing Gear
MTO	Maximum Take-off
n	Yawing moment
n_d	Undamped natural
nlg	Nose Landing Gear
nc	Nose cone
o	Outer
O2	Oxygen
OE	Operational Empty
PL	Payload
p	Roll rate
p	Propeller
pax	Passengers
pres	Pressure
q	Pitch rate
r	Required
r	Yaw rate
root	Root position

Greek	Definition	Unit
α	Angle of Attack	[°]
β	Sideslip Angle	[°]
Δ	Change	[-]
δ	Change	[-]
δ_{f}	Flap deflection	[°]
δ_{r}	Rudder deflection	[°]
δ_{a}	Aileron deflection	[°]
δ_{e}	Elevator deflection	[°]
ζ	Damping ratio	[-]
η	Efficiency	[$-$]
θ	Angle	[°]
λ	Taper ratio	[-]
Λ	Sweep angle	[°]
λ	Eigenvalues	[-]
ν	Poisson ratio	[-]
ρ	Density	[kg/m^3]
σ	Stress	[MPa]
τ	Shear stress	[N/m^2]
ω	Angular Frequency	[1/rad]

Subscript	Definition
S	Stall
shell	Tank Shell
skin	Skin
strut	Landing gear strut
SR0	Stall
t	Tail
tip	Tip position
tank	Liquid Hydrogen Tank
TAS	True Airspeed Speed
tc	Tail cone
TO	Take-off
tot	Total
ult	Ultimate
v	Vertical tail
w	Wing
w	Weight
wet	Wetted wing
X	X-direction
Y	Sideforce
y	Y-direction
Z	Z-direction
ZF	Zero Fuel

1 Introduction

As the aviation industry progresses to become increasingly more sustainable on all fronts, the regional aircraft market will likely see a surge in demand for new aircraft with inferior environmental impact. In a growing economy, more and more people will need to travel longer distances in shorter times, often invoking air travel. Conventionally however, more air travel results in greater climate impact. As of 2022, the aviation industry is responsible for 2.1% of all human-induced carbon emissions, and a whopping 12% of all transport-source emissions. With no immediate action, these figures are expected to increase, even with the totality of emissions increasing. As a result, the Air Transport Action Group together with the International Civil Aviation Organization has set a decarbonization plan to stabilize and cap aviation emissions, with civil aviation operations culminating in net-zero emissions by 2050. To achieve this, revolutionary means of propulsion must be integrated into the market.

Over the last decade, great leaps forward have been undertaken with the release of the A320 neo family, the A350, the B737 max family and the B787, aircraft efficiencies have drastically improved to maintain increased demand while consuming less fuel and emitting less carbon dioxide. Nevertheless, these designs are primarily economically motivated, with less emphasis on their overall climate impact. Other more radical alternatives, such as the TU Delft - KLM Flying V or the ZeroAvia retrofitted Dornier 228, have already theoretically and experimentally proven that total decarbonization is truly achievable. What is predominant in the aforementioned examples is that most of these aircraft target a mid-range to long-haul market, with little oversight of the regional market. Furthermore, airlines and operators welcome this change as long as its economic performance remains unaffected or with little change.

The aim of this report is to present the conceptual design of a regional passenger transport aircraft that integrates a novel propulsion system to reduce greenhouse emissions while remaining market-competitive in terms of both unit cost and cash operating cost. The aircraft is expected to comply with CS/FAR-25 regulations, with an entry-into-service date by 2035. This report is the culmination of ten weeks and over 4000 man-hours in an attempt to prove that the future of regional air travel lies within new green technologies, and can remain economically feasible for the manufacturer, operator, and customer.

The report is divided into twenty two parts. In Chapter 2 the requirement compliance matrix and design objectives are presented. Following this, in Chapter 3 the functional flow and functional breakdown structure of the aircraft is depicted. To choose the best configuration a trade-off was performed in Chapter 4. Next, in Chapter 5, a market analysis provides a general overview of potential markets. Chapter 6 shows the design N2 chart, providing an overview of inputs and outputs from different subsystems. Chapter 7 and Chapter 8 provide the class I, class II and aircraft sizing respectively. To generate sufficient lift, Chapter 9 looks into airfoil selection and sizing of high lift devices. Chapter 10 sizes the airframe, integration of the hydrogen storage tank and material selection. Following this, in Chapter 11, an overview of all electrical systems are depicted. In Chapter 12 and Chapter 13 the propulsion system is thoroughly designed and integrated, together with other systems such as hydraulics. To be able to manufacture the aircraft, a general plan was set up in Chapter 14. To make sure the SRP-22 is both statically and dynamically stable, Chapter 15 performs this analysis. In Chapter 16 shows the flight performance, such as payload range, gust maneuver and flight profile diagrams. The technical budget breakdown is presented in Chapter 17. In Chapter 18 the analysis on financial feasibility is performed, both an cost and return on investment. Following this, in Chapter 19, the climate impact and noise levels are considered, showing the sustainability of the aircraft. The operations and logistics of flight operations and hydrogen infrastructure are considered in Chapter 20. Chapter 21 looks at reliability, availability, maintainability and safety. Next, in Chapter 22 the project risks is analysed. Chapter 23 provides an overview of the future planning of the project, such that the SRP-22 can enter service in 2035. Finally, in Chapter 24 the verification and validation together with the requirement comliance form the basis for the recommendations and conclusion in Chapter 25 and Chapter 26.

2
Requirements and Objectives

To define the design space of the project, an extensive list of requirements is constructed. These include user requirements, system requirements, and mission requirements. Moreover, design objectives are set which would drive the design process. Finally, requirement compliance must be checked and if design objectives are met, showing the feasibility of the initial aircraft design.

2.1. Design Requirement Compliance

All design requirements and their compliance are presented in Table 2.1. A division is made from leading requirements, subrequirements and sub-subrequirements. Furthermore, the categories to divide all requirements are bold along with their abbreviation. A distinction between top (TOP) and system (SYS) requirements was made. Top requirements include all user requirements, while system requirements entail all additional requirements defined to ensure the design will fulfill its purpose.

The requirement compliance matrix shows if the SRP-22 complies with all set requirements. If the design complies it receives a check mark (✓). If the requirement is conditionally met or indecisive it receives a tilde (∼). This means the requirement needs more research before it can be determined if it complies or not. Finally, if a requirement is not yet met it will be set as TBD. This will require a meeting with the customer, during which acceptance of failing to meet the requirement or changing the design will be the outcome. In the last column of Table 2.1 the sections that show compliance are presented.

A main focus while designing the aircraft is to ultimately comply with all CS/FAR 25 regulations. As this is not possible during the conceptual design phase, the most important regulations are presented in the requirement matrix and complied with. Any additional requirements from CS/FAR 25 shall be considered during later design phases and testing.

Table 2.1: Requirement Compliance Matrix

Requirement ID	Requirement	✓/∼/TBD	Sections
Performance (PER)			
RA-TOP-PER-1	The aircraft shall be able to carry a number of passengers in the range of 46-50.	✓	Figure 8.1, Section 16.1 and Appendix A
RA-TOP-PER-2	The aircraft shall have a minimum design range of 1,000 nmi, at full passenger capacity.	✓	Section 16.1
RA-TOP-PER-3.1	The aircraft shall have a minimum cruise speed of 275 KTAS.	✓	Section 16.4 and Section 16.5
RA-TOP-PER-3.2	The aircraft shall comply with approach speed category C (<141 knots).	✓	Section 16.5
RA-TOP-PER-4.1.1	The aircraft shall have a maximum take-off field length of 1.37 km over a 15 m obstacle on a runway with dry pavement (sea level ISA + 10 °C day).	✓	Section 16.5
RA-TOP-PER-4.1.2	The aircraft shall have a maximum take-off field length of 1.37 km over a 15 m obstacle on a runway with dry pavement at 1.5 km above mean sea level (ISA + 10 °C day).	✓	Section 16.5

Continued on next page

Table 2.1 – *Continued from previous page*

RA-TOP-PER-4.2.1	The aircraft shall have a maximum landing field length of 1.37 km over a 15 m obstacle on a runway with dry pavement at maximum landing weight (sea level ISA + 10 °C day).	✓	Section 16.5
RA-TOP-PER-4.2.2	The aircraft shall have a maximum landing field length of 1.37 km over a 15 m obstacle on a runway with dry pavement at maximum landing weight at 1.5 km above mean sea level (ISA + 10 °C day).	✓	Section 16.5
RA-TOP-PER-5.1	The aircraft shall have a minimum initial cruising altitude of FL280.	✓	Section 16.5
RA-TOP-PER-5.2	The aircraft shall have a horizontal distance to climb up to a cruising altitude of less than 200 nmi.	✓	Section 16.5
Safety and Reliability (SRE)			
RA-TOP-SRE-2.1	The aircraft shall comply with VFR.	TBD	
RA-TOP-SRE-2.2	The aircraft shall comply with IFR.	TBD	
RA-TOP-SRE-3	The aircraft shall be capable of flight in known icing conditions.	✓	Section 11.2
RA-SYS-SRE-1	The aircraft shall have the following lights: icing, anti-collision, and landing.	✓	Section 11.1
RA-SYS-SRE-2.1	The aircraft shall contain an approved-type emergency exit within 9.1 m of the furthest seat on one side of the fuselage cross-section and 13.7 m on the other side of the fuselage cross-section.	✓	Figure 8.1
RA-SYS-SRE-2.2	The aircraft shall have at least one Type I and one Type III emergency exit on each side of the fuselage cross-section [1] (CS 25.807).	✓	Appendix A and Section 8.1
RA-SYS-SRE-3	The aircraft shall be protected against catastrophic effects from lightning.	✓	Figure 10.3
RA-SYS-SRE-4	The aircraft shall be able to withstand the calculated ultimate load factors (maneuver or gust).	✓	Chapter 10
RA-SYS-SRE-5	The aircraft shall carry contingency fuel (five minutes of holding flight), airport divergence fuel (to get to an alternate airport[2] within 100 nmi) and final reserve fuel (30 additional minutes) [2].	✓	Section 16.1 and Section 7.2
RA-SYS-SRE-6	The aircraft propeller clearance shall be a minimum of 18 cm from the ground.	✓	Section 8.5 and Appendix A
Sustainability (SUS)			
RA-TOP-SUS-1	The aircraft shall have a reduction in block fuel of at least 20% per passenger on a 500 nmi mission compared to reference aircraft.	✓	Section 7.2
RA-TOP-SUS-2.1	At the lateral noise measurement point, the maximum noise level shall not exceed 94 EPNdB [3].	✓	Section 19.3
RA-TOP-SUS-2.2	At the flyover noise measurement point, the maximum noise level shall not exceed 89 EPNdB [3].	✓	Section 19.3

Continued on next page

Table 2.1 – *Continued from previous page*

RA-TOP-SUS-2.3	At the approach noise measurement point, the maximum noise level shall not exceed 98 EPNdB [3].	✓	Section 19.3
Dimensions (DIM)			
RA-TOP-DIM-1.1.1	The aircraft shall have a minimum seat width of 44 cm.	✓	Appendix A and Figure A.1
RA-TOP-DIM-1.1.2	The aircraft shall have a minimum arm rest width of 5 cm.	✓	Appendix A and Figure A.1
RA-TOP-DIM-1.1.3	The aircraft shall have a minimum seat pitch of 76 cm.	✓	Appendix A and Figure A.2
RA-TOP-DIM-1.2.1	The aircraft shall have a minimum stand-up height in the aisle of 1.9 m.	✓	Appendix A and Figure A.1
RA-TOP-DIM-1.2.2	The aircraft shall have a minimum aisle width of 46 cm.	✓	Appendix A and Figure A.1
RA-TOP-DIM-2	The aircraft shall have a maximum wingspan compliant with ICAO Code C (<36 m).	✓	Section 8.2 and Appendix A
RA-SYS-DIM-1.1	The aircraft shall contain a lavatory with minimum dimensions of 91×91 cm [4].	✓	Appendix A and Figure A.3
RA-SYS-DIM-1.2	The aircraft shall contain a galley storage area with minimum dimensions of 76×91 cm [4].	✓	Appendix A and Figure A.3
RA-SYS-DIM-2	The aircraft shall have a minimum overnose angle of 25.1 degrees [5].	✓	Appendix A and Figure A.4
Cost (COS)			
RA-TOP-COS-1	The aircraft shall have a maximum asking unit price of 31 million USD in FY2022.	✓	Section 18.2
RA-TOP-COS-2	The aircraft shall have a maximum cash operating cost per seat mile on a 500 nmi mission of 0.16 USD in FY2022.	$\sim$	Section 18.3
Timing (TIM)			
RA-TOP-TIM-1	The aircraft shall enter service by 2035.	TBD	Section 23.3
Crew (CRE)			
RA-TOP-CRE-1.1	The aircraft shall carry a minimum of two pilots, and one cabin crew member to serve up to 50 passengers.	✓	Section 7.2
RA-TOP-CRE-1.2.1	The aircraft shall have a minimum crew baggage mass of 14 kg per crew member.	✓	Section 7.2
RA-TOP-CRE-1.2.2	The aircraft shall have a minimum crew baggage volume of 0.1 m^3 per crew member.	✓	Table 8.1
Passengers (PAS)			
RA-TOP-PAS-1.1.1	The aircraft shall have a minimum passenger baggage mass of 40 lbs per passenger.	✓	Section 7.2 and Section 16.5
RA-TOP-PAS-1.1.2	The aircraft shall have a minimum passenger baggage volume of 0.14 m^3 per passenger.	✓	Section 8.1
Undercarriage (UCG)			
RA-SYS-UCG-1	The aircraft shall contain an anti-skid brake system.	✓	Section 8.5
RA-SYS-UCG-2.1	The aircraft shall have a maximum lateral tip-over angle of 55° at the most forward c.g. position[1].	✓	Section 8.5 and Appendix A
RA-SYS-UCG-2.2	The aircraft shall prevent tip-back at the most aft c.g. position.	✓	Section 15.1 and Appendix A

Continued on next page

Table 2.1 – *Continued from previous page*

RA-SYS-UCG-3	The load on the nose wheel shall be between 8% and 15% of the total aircraft weight [4].	✓	Section 8.5
Maneuverability, Stability, Controllability (MSC)			
RA-SYS-MSC-1	The aircraft shall be able to perform a 40° bank angle turn.	✓	Section 16.4
RA-SYS-MSC-2	The aircraft shall be able to perform a steep approach landing with a glide angle greater than 4.5°.	✓	Section 16.5
RA-SYS-MSC-3	The scrape angle of the aircraft shall be such that it prevents tail strikes.	✓	Figure 8.1
RA-SYS-MSC-4	The aircraft shall be able to perform a 45° change in bank angle in 1.4s.	✓	Section 15.4
RA-SYS-MSC-5	The x-location of the neutral point shall be larger than the x-location of the center of gravity.	✓	Section 15.2
RA-SYS-MSC-6	The non-dimensional roll rate shall be larger than 0.07.	✓	Section 15.3
RA-SYS-MSC-7	The vertical tail shall be able to counteract a yawing moment generated by a one, inner engine inoperative mission.	✓	Figure 15.4
RA-SYS-MSC-8.1	The slope of the elevator control force over velocity shall be larger than 0.	✓	Section 15.4
RA-SYS-MSC-8.2	The hinge moment derivative due to deflection shall be less than 0.	✓	Section 15.4
RA-SYS-MSC-8.3	The elevator efficiency shall be less than 0.	✓	Section 15.4
RA-SYS-MSC-9	The pitching-moment-due-to-angle-of-attack derivative shall be less than 0.	✓	Section 15.3
RA-SYS-MSC-10.1	The sideforce-due-to-sideslip derivative shall be less than 0.	✓	Section 15.3
RA-SYS-MSC-10.2	The rolling-moment-due-to-sideslip derivative shall be less than 0.	✓	Section 15.3
RA-SYS-MSC-10.3	The yawing-moment-due-to-sideslip derivative shall be larger than 0.	✓	Section 15.3
RA-SYS-MSC-11.1	The side-force-due-to-roll-rate derivative shall be less than 0.	✓	Section 15.3
RA-SYS-MSC-11.2	The roll damping derivative shall be less than 0.	✓	Section 15.3
RA-SYS-MSC-11.3	The yawing-moment-due-to-roll-rate derivative shall be less than 0.	✓	Section 15.3
RA-SYS-MSC-12.1	The side-force-due-to-yaw-rate derivative shall be larger than 0.	✓	Section 15.3
RA-SYS-MSC-12.2	The rolling-moment-due-to-yaw-rate derivative shall be larger than 0.	✓	Section 15.3
RA-SYS-MSC-12.3	The yawing-moment-due-to-yaw-rate derivative shall be less than 0.	✓	Section 15.3
RA-SYS-MSC-13.1	The damping ratio of the short period motion shall be larger than 0.30 and less than 2.00.	✓	Section 15.5
RA-SYS-MSC-13.2	The damping ratio of the phugoid motion shall be larger than 0.04.	✓	Section 15.5

Continued on next page

Table 2.1 – *Continued from previous page*

RA-SYS-MSC-14.1	The roll mode time constant shall be less than 1.4 s.	✓	Section 15.5
RA-SYS-MSC-14.2	The damping ratio of the Dutch roll shall be larger than 0.08.	✓	Section 15.5
RA-SYS-MSC-14.3	The product of undamped natural frequency and damping ratio of the Dutch roll shall be larger than 0.15 rad/s.	✓	Section 15.5
RA-SYS-MSC-14.4	The undamped natural frequency of the Dutch roll shall be larger than 0.4 rad/s.	✓	Section 15.5
RA-SYS-MSC-14.5	The minimum time to double the amplitude in the spiral motion shall be larger than 20 s.	✓	Section 15.5
RA-SYS-MSC-15	The Lateral Departure Control Parameter shall be larger than 0	✓	Section 15.5
Operations and Maintenance (OPM)			
RA-SYS-OPM-1	The luggage compartment shall be easily accessible and ergonomically serviceable.	TBD	
RA-SYS-OPM-2	The aircraft shall have the required systems to be able to communicate with the ground and other aircraft.	✓	Section 20.3
RA-SYS-OPM-3	The aircraft shall allow for easy access for catering.	TBD	
RA-SYS-OPM-4	The aircraft shall allow for energy source replenishment within 40 minutes.	✓	Section 20.2

2.2. Design Objectives compliance

Even though the design space is defined by its requirements, design objectives shall be used to achieve goals and constantly be kept in mind during the design process. Table 2.2 shows all identified objectives. Subsequently, the extent of compliance with the design objectives is discussed.

Table 2.2: Design Objectives

#	Identifier	Objective
1	RA-OBJ-1	Minimize the environmental impact of the entire aircraft life-cycle.
2	RA-OBJ-2	Minimize the usage of hazardous materials.
3	RA-OBJ-3	The aircraft can be converted to a cargo configuration, such that standard sized cargo pallets are able to fit in the fuselage.
4	RA-OBJ-4	The aircraft is visually appealing and has a modern aesthetic in order to be marketable and reflect its advanced design.
5	RA-OBJ-5	The preliminary design of the aircraft shall be finished by 2029.[3]
6	RA-OBJ-6	The aircraft has a target cruise speed of 350 KTAS.
7	RA-OBJ-7	The aircraft shall have similar takeoff performance to the DHC Dash 8 Q300 in hot climates.
8	RA-OBJ-8	The aircraft has built-in stairs to reduce change-over time and lower operational airport cost.
9	RA-OBJ-9	The aircraft design can be used to design aircraft family members with different seating capacities.
10	RA-OBJ-10	The target seat width is 46 cm.
11	RA-OBJ-11	The aircraft has a wingspan compliant with ICAO Code B (<24 m).

RA-OBJ-1: The environmental impact of the entire aircraft life-cycle of the SRP-22 is 87 times lower than the most modern version its direct competitor, the ATR 42-600. This is based on the Average Temperature Response metric, which can be found in Chapter 19.

RA-OBJ-2: Due to the principal use of recyclable non-hazardous materials, at least 91% of the SRP-22 can be recycled. This can be found in Chapter 10.

RA-OBJ-3: SRP-22 can be converted to a freighter aircraft by stripping the cabin of its furnishing and reinforcing the floor, resulting in a cargo capacity of 6000 kg. This can be found in Section 8.6.

RA-OBJ-4: The electric motor configuration with its wingtip mounted propellers reflect the novel propulsion system and thereby the innovative design of the aircraft. This will aid in marketing of the aircraft. The full aircraft configuration can be found in Appendix A.

RA-OBJ-5: The preliminary design will be finished before 2027 according to project development Gantt chart which can be found in Chapter 23

RA-OBJ-6: The SRP-22 is designed for a cruise speed of 275 knots. Since the average route length of the SRP-22 will be around 300 nautical miles, it was decided that achievement of this objective was not pursued because the 350 knots cruise speed would only decrease the average route flight time by a maximum of 15 minutes which can be found in Chapter 5.

RA-OBJ-7: The SRP-22 is capable of takeoff in hot and high conditions, similar to the DHC Dash 8. The takeoff performance compliance at an airport altitude of 2,300 m and 40° Celsius ambient temperature is shown in Chapter 16.

RA-OBJ-8: SRP-22 is equipped with an internal extendable stairway to allow for quick passenger turnaround, lower remote airport dependency with regards to mobile stairways and avoid mobile stairway use airport fees. This is shown in Chapter 20.

RA-OBJ-9: Due to the limited scope of this design phase, this objective is not investigated and therefore not met at this stage.

RA-OBJ-10: The seat width of the SRP-22 cabin is 0.5m, which can be found in Chapter 8.

RA-OBJ-11: The wingspan of SRP-22 is 26.8m, therefore this objective is not met.

2.3. Requirement Importance

To develop the proper end-product, it is of utmost use that all requirements are ranked in order of importance. This is not done on an individual basis, but rather on a category basis. Do note that the weights during later trade-offs may differ, as the importance is variable through different design phases. This list represents the importance of all categories when evaluating the end-product. The order from the most important to the least important categories is given below, together with a short explanation for each category's position.

1. Sustainability
As the main design objective is to minimize the global warming impact of aircraft operation and manufacturing, sustainability has been ranked as the most important. Sustainability greatly affects multiple subsystems, such as the propulsion system and materials used for the structure. As such, sustainability shall have the highest weight in the trade-off for all design options and hence shall be given priority.

2. Safety and Reliability
Safety and Reliability has high priority, as an aircraft is often rated on its safety. Customers will not want to fly in an aircraft they do not believe to be safe. Furthermore, if the aircraft of an airline regularly crash, it damages the name of the company. Hence this has been designated as a top priority. Moreover, this category is highly regulated through CS-25 rules and therefore drives a large part of the design.

3. Cost
For an aircraft to be profitable during its lifetime, manufacturing and operational cost shall be limited. Cost has been given a high priority to make the aircraft attractive to the client.

4. Performance
The aircraft needs to perform according to customer's expectations. It should fly at a minimum speed, be able to take off and land on specified runways, and carry a certain amount of passengers or load. Therefore, performance is ranked as relatively important.

5. Maneuverability, Stability, Controllability
In addition to aircraft performance, the pilot must be able to fly the aircraft properly. Therefore, maneuverability, stability and controllability is next. The overall goal regarding this category is that the aircraft is pleasurable to fly.

6. Operations and Maintenance
Operations and Maintenance include both operations on the ground (such as refueling) and during flight (such as GPS determination). An easy and fast operable aircraft is preferred, as it reduces the ground time and hence greater flight time can be made. The same holds for maintenance.

7. Timing
The client requires that the aircraft enter service by 2035. The reason this requirement is a down the line is that it may be possible to extend this deadline in agreement with the client if the proper reasoning is given.

8. Dimensions
The dimensions ensure the passengers can sit comfortably, stand in the aisle, and can use the overhead baggage compartment. This is driving the size and cross-section of the fuselage but is considered less important than all of the above as comfort is not the main priority.

9. Undercarriage
The undercarriage will be designed later and has to serve its purpose. It should ensure takeoff and landing are performed safely and proper steering is possible. This system is supporting the aircraft, and hence not one of the most important categories.

10. Passengers and Crew
The final two categories have to do with the baggage of the passengers and crew. This drives the size of the baggage compartment, which again drives the size of the fuselage. As this is more of an input on the sizing of the aircraft (dimensions), it is given the lowest priority. Passengers are put above the crew as the passengers paid for a ticket whereas the crew is at work.

[1]URL `https://arc.aiaa.org/doi/pdf/10.2514/1.46564` [cited 01 Dec 2022]
[2]URL `https://www.mark-pearson.com/airport-distances/#nationwide_results` [cited 01 Dec 2022]
[3]URL `https://www.faa.gov/aircraft/air_cert/airworthiness_certification` [cited 02 Dec 2022]

3 Functional Flow and Breakdown

In this chapter, the functional analysis of the aircraft operations is presented. Before designing an aircraft, a functional analysis must be performed, which includes a functional breakdown and a functional flow. The functional breakdown of the aircraft operations presents an overview of the aircraft functions, as seen in Figure 3.2. The functional flow represents the relation between these functions, as seen in Figure 3.1. The principle function of the aircraft is ”Transport Payload X over range Y between airports of type Z”. This is broken down into several top level functions, which are further broken into first, second and third level functions.

Functional Flow

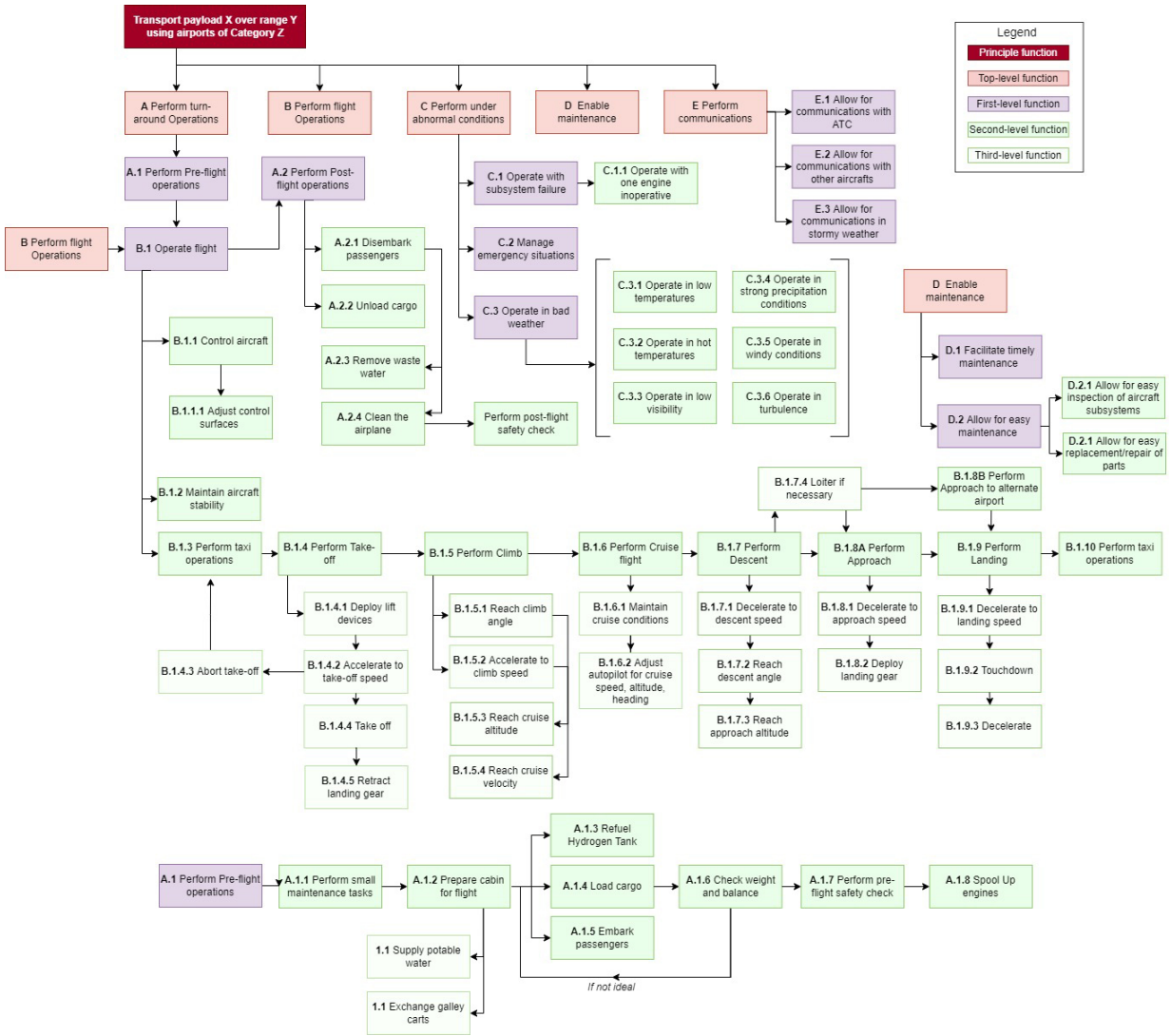

Figure 3.1: Functional Flow Block Diagram of the SRP-22

Functional Breakdown

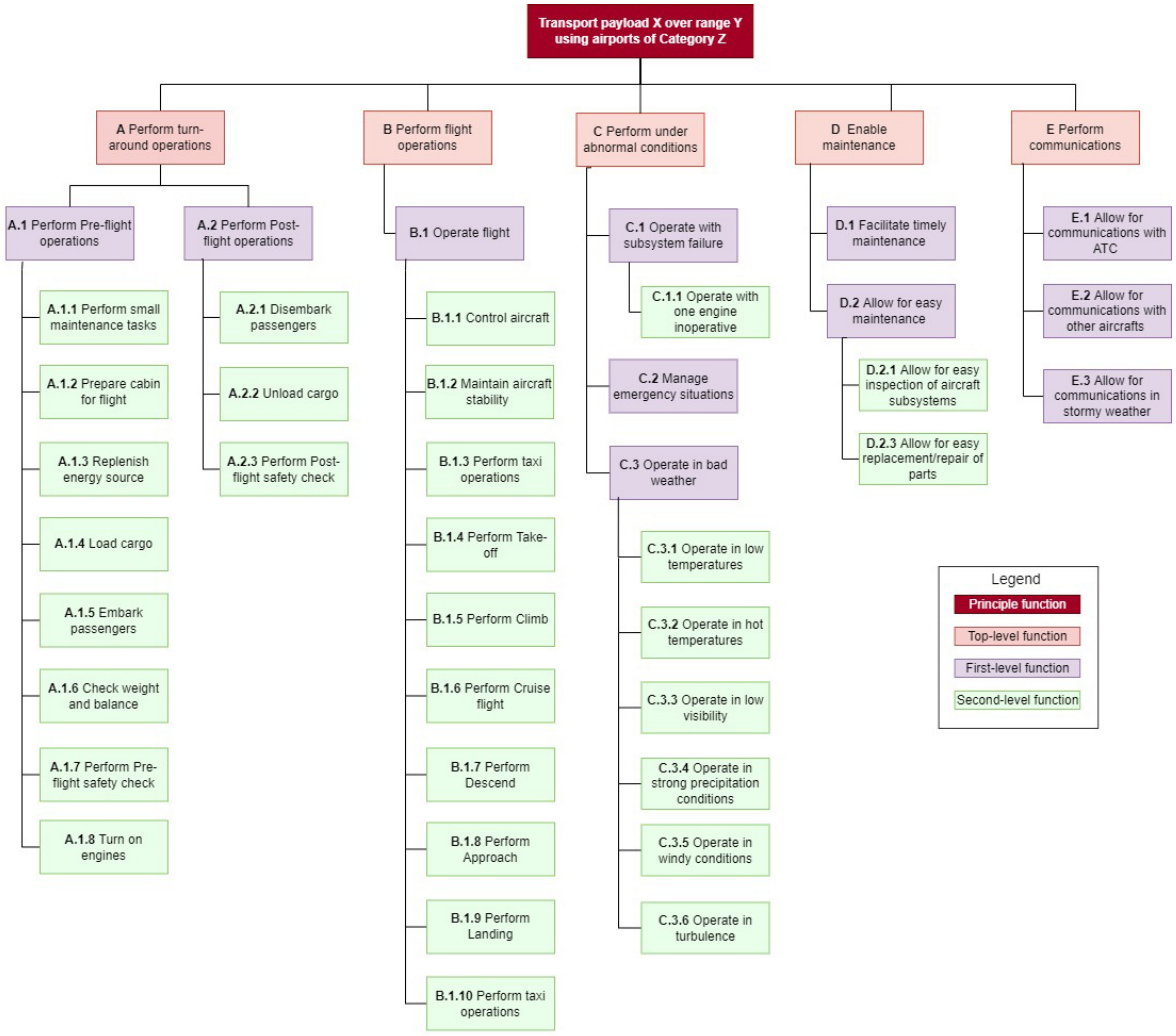

Figure 3.2: Functional Breakdown Diagram

4
Design Trade-Off

Earlier in the design process, four design concepts were explored and a trade-off was performed to choose the best design option for further design. The designs are evaluated based on cost, aerodynamics, climate impact, and the risk of the design. This chapter includes an overview of the propulsion system configurations, the trade-off methodlogy and finally, the results of the trade-off.

4.1. Propulsion System Configurations

Hydrogen Combustion - This configuration has the most conventional layout besides hydrogen storage. LH2 combustion works in a very similar manner as jet A1 fuel, needing only minor changes to the turboprops. Therefore, it has a very similar configuration to the ATR 72 with an aft-mounted storage tank.

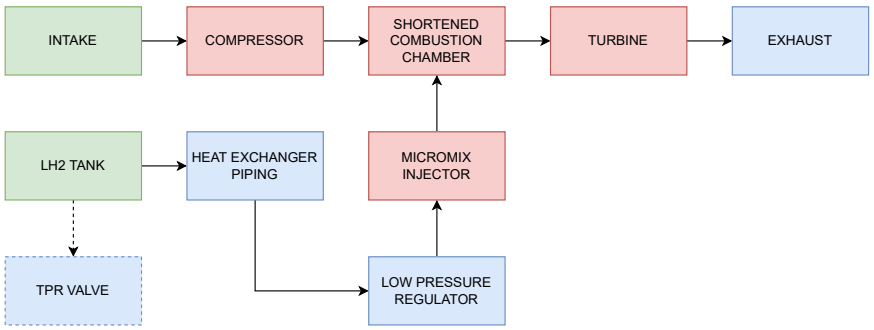

Figure 4.1: Hydrogen Combustion Components

Hydrogen Fuel Cell - The hydrogen fuel cell configuration makes use of electric motors for propulsion. A total of four electric motors, of which two are mounted on the wing tips, are selected. These tip-mounted motors allow for an increased L/D, thus improving efficiency and providing a drag reduction of 10%. Moreover, the storage tank is located behind the rear pressure bulkhead, while the fuel cell is just in front.

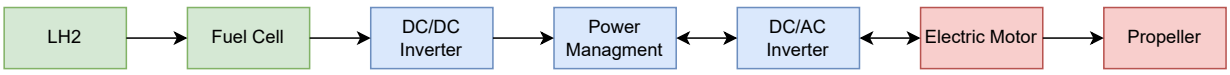

Figure 4.2: Full H2 Fuel Cell Configuration

Hybrid-Electric Series - The HES configuration makes use of a turbo generator running on SAF placed in the tailcone. In addition, it has a large battery pack to store electric energy for peak performance. The battery pack is generally very heavy and increases the OEM significantly. Due to this configuration also having a fully electric propulsion system, it will use the same motor layout as the fuel cell configuration.

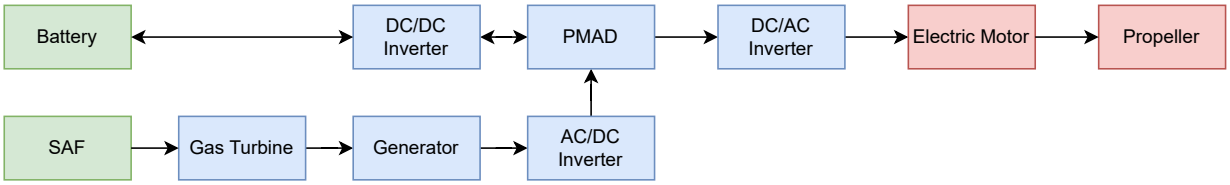

Figure 4.3: Series architecture

Hybrid-Electric Parallel/Series - The HEPS configuration makes use of conventional turboprop engines running on SAF together with a battery pack powering two electric motors mounted at the wingtips. This configuration also has a similar increase in OEM due to the battery pack as the HES configuration.

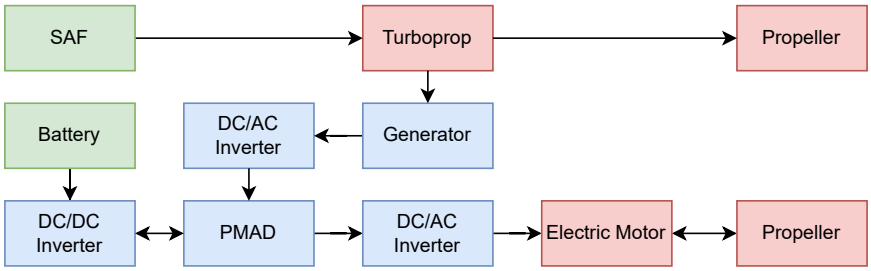

Figure 4.4: Parallel/Series architecture

4.2. Trade-off Methodology

The considered criteria were Cost, Aerodynamics/Planform, Climate Impact, and Risk. These criteria use a scale that runs from 1 (hardly important) to 5 (extremely important). Below the reasoning behind each criterion for the different design options can be found.

Risk

With regard to safety, the main distinction shall be made between hydrogen and electricity. For hydrogen, the risk would lie in a pressure build-up within the tank, whereas for electricity the main risk would be a fire breaking out. Furthermore, the turboprops are certified and hence can be considered to be fairly safe with respect to the electric propellers. Because of the above, hydrogen combustion is considered the best option having the least safety risks.

Technological maturity is quantified in TRLs. Multiple current projects are researching hydrogen usage in combustion and fuel cell systems, with an entry of service in 2035 as well. Being optimistic both combustion and LT-PEM fuel cells will have TRL9 by 2035 [6] [1] [2]. For hybrid electric design, the batteries are the critical factor as the SAF already exists and is produced[3]. Li-ion batteries already exist, however, compared to Li-air or Zinc-air, Li-ion has significantly lower specific energy than Li-air. Moreover, lithium is a scarce resource, making Zinc-air a good contender. However, Li-air and Zinc-air, need further technical development and won't be TRL9 by 2035.

Lastly, operations readiness by 2035 focusing on the fueling infrastructure for the hybrid electric configurations is not as optimistic as the ones with hydrogen as fuel. Hydrogen supply is a very likely option before 2035[4],[5]. When it comes to the electrical supply for batteries, very few studies or projects exist and the existing ones are either very preliminary[7] or don't provide enough charging capabilities[6].

Cost

The cost analysis considered all costs related to fuel, propulsion systems, and operations. For fuel, cost is analyzed over a 500 nmi per seat mile and also over the aircraft's lifetime of 25 years, considering four flights per day, 300 days a year. This adds up to about 60,000 flight hours throughout its lifetime. The propulsion system cost considers all components that differ per configuration, such as batteries, turboprop, electric motors, and fuel cells. For the cost of the rest of the aircraft, it is assumed that the cost is equal and thus is not considering the difference in size per aircraft. For the operational cost, maintenance and component replacement are considered over the lifetime of parts in the propulsion system. Therefore the total cost compromises of mainly the propulsion system cost and operations cost explained above over the entire life span of the aircraft of 25 years. The cost per seat mile, flight, and total cost can be found in Section 4.3, Table 4.1.

Climate Impact

The Life-Cycle CO_2 Emissions per aircraft per year per seat, with relevant values are presented in Table 4.1. Material supply, energy supply, production, downstream, use, and end-of-life phases of each fuel were taken into account during calculations.[8]

The values of CO_2 intensity were provided by J. Mukhopadhaya and D. Rutherford [9]. These represent the amount of CO_2 emitted in the entire life cycle such that the fuel provides 1 MJ of energy. Then, using the power required for a 500nmi flight, the CO_2 emissions for that mission are obtained. This is then multiplied by 4 flights a day and then 300 days per year, to finally obtain the yearly CO_2 Emissions per aircraft. Additionally, all values are normalized by dividing the emission by seat number, finally presenting the Life-Cycle CO_2 Emissions per aircraft per year per seat. All relevant values are presented in Table 4.1.

4.3. Results

All data in Table 4.1 is compared to a baseline value, which is taken from the reference aircraft (ATR-72).

Table 4.1: Values used for Trade-off

		H2 Combustion		H2 FC		HEPS		HES	
	Baseline	**Value**	**Delta%**	**Value**	**Delta%**	**Value**	**Delta%**	**Value**	**Delta%**
Fuel cost	0.053	0.036	-32.1	0.019	-64.2	0.054	1.9	0.048	-9.4
Total cost	43.95	31.30	-28.8	20.19	-54.1	51.75	17.7	45.51	3.5
L/D	16.90	19.80	17.2	22.00	30.2	22.00	30.2	22.00	30.2
Span	27.00	26.83	-0.6	25.22	-6.6	33.23	23.1	35.67	32.1
CO_2	80.50	1.74	-97.8	0.92	-98.9	15.4	-80.9	19.1	-76.3
RF	1.03	1.19	15.5	0.61	-41.1	1.16	12.6	1.41	13.0
Safety		8.00		6.00		7.00		6.00	
Technology		8.00		7.00		4.00		4.00	
Operations		8.00		8.00		4.00		4.00	

Table 4.2: Trade-off Results

			H2 Combustion	**H2 FC**	**HEPS**	**HES**
Category	Unit	Weight	Score	Score	Score	Score
Cost						
Fuel cost	[USD $/pax/nmi]	3	8	9	6	6
Total cost	[USD Mil$]	4	7	9	5	6
Aerodynamics/Planform						
L/D	-	3	7	8	8	8
Span	[m]	2	6	6	5	4
Climate Impact						
CO_2 Emissions	[Tonnes]	5	11	11	10	10
Radiative Forcing	[W/m2 (E-07)]	5	5	8	6	6
Risk						
Safety	-	2	8	6	7	6
Technology	[TRL]	5	8	6	5	5
Operations	-	4	8	8	6	6
Sum			253	268	215	215
% of max. attainable score			69.7%	73.8%	59.2%	59.2%

After all data is gathered, a score is given to each category derived from their percentage difference from the baseline value. A six represents a difference in the range of 10% to -10%, a value of seven in the range of -10% to -30%, and so on, where the scores are ranging from 1 to 11. This score is then multiplied by the weight assigned for the category as defined in the second column of Table 4.2. All weighted scores are summed in the second to last row, after which the final row shows the score as a percentage of the total score available. Table 4.2 contains the trade-off results.

4.4. Trade-off Sensitivity Analysis

First, all of the criteria weights were changed one at a time. This did not change the result of the trade-off itself as H2 fuel cell continued to be the best option in every scenario. However, it did narrow the gap between LH2 fuel cell and combustion, bringing the score of combustion to around 1-3% of the fuel cell when Radiative Forcing and Safety were given a weight of 1. Next, a combination of two criteria weights was changed to see what the impact would be on the result. In this analysis, LH2 combustion only outperformed LH2 fuel cell (by 1.4%) in the case that both total cost and the RF weights were reduced to 1. While reducing both CO_2 and Radiative Forcing weights to 1 brings LH2 combustion to within 1% of the fuel cell, reducing technology and operations maturity to 1 increases the difference to more than 10%. Finally, some criteria were removed altogether. This also did not affect the result of the trade-off unless Radiative Forcing was removed. In this case, LH2 combustion and fuel cell were equal in score. In this analysis, the Hybrid Electric configurations did not make any major improvements in their scores or ranking.

The H2 fuel cell outscores the other configurations in most cases, with minute changes to the result occurring only with very extreme (and unlikely) adjustments. This sensitivity analysis, therefore, substantiates the validity of the trade-off method and its results.

4.5. Conclusion

Looking at the results in Table 4.2, it can be seen that the hydrogen fuel cell scores the best, with hydrogen combustion closely behind. While hybrid configurations are almost 15 % behind. The design using liquid hydrogen fuel cells was chosen as the configuration that will be further developed, although hydrogen combustion performed well in some of these criteria as well, it did significantly worse for Radiative Forcing. Even though the technological readiness for hydrogen combustion is higher than for the fuel cell, the fuel cell technology development necessary is still concluded to be realistic. Moreover, the H2 fuel cell configuration allows for more aerodynamic innovation due to the use of electric motors.

[1]URL https://www.airbus.com/en/newsroom/stories/2020-11-hydrogen-combustion-explained [Cited 21 Dec. 2022]

[2]URL https://www.airbus.com/en/newsroom/press-releases/2022-11-airbus-reveals-hydrogen-powered-zero-emission-engine [Cited 21 Dec. 2022]

[3]URL https://skynrg.com/ [Cited 21 Dec. 2022]

[4]URLhttps://www.airbus.com/en/newsroom/press-releases/2022-11-airbus-teams-up-to-advance-green-hydrogen-availability-at-airports [Cited 21 Dec. 2022]

[5]URL https://skynrg.com/producing-saf/saf-production-plant-in-the-port-of-amsterdam/ [Cited 21 Dec. 2022]

[6]URL https://www.pipistrel-aircraft.com/products/other-products/charging-infrastructure/ [Cited 21 Dec. 2022]

[7]URL https://www.transportenvironment.org/discover/airline-contrails-warm-planet-twice-much-co2-eu-study-finds/ [Cited 21 Dec 2022]

5 Market Analysis

The market analysis is used to provide insight to both the status quo and projections of the regional aircraft market and the market feasibility of the SRP-22 program. The market analysis includes the market volume, market share and preliminary cost targets of the aircraft.

5.1. Market Volume

Current market

Although not universally defined, regional air transport consists of flights that transport up to 100 passengers and/or cargo on short-haul routes (i.e. routes shorter than 810nmi [10]). These routes usually connect small cities or remote regions. These flights are performed by two aircraft types with different propulsion systems: regional jets and turboprops.

The total worldwide commercial aircraft fleet was approximately 25,000 aircraft in 2017, of which about 6000 were turboprops and regional jets accounting for 23.8% of the total [11]. This share is visualized relative to other aircraft types in Figure 5.1. Regional aircraft with a 20 to 120 seat capacity are responsible for 24% of the total annual flights worldwide [12].

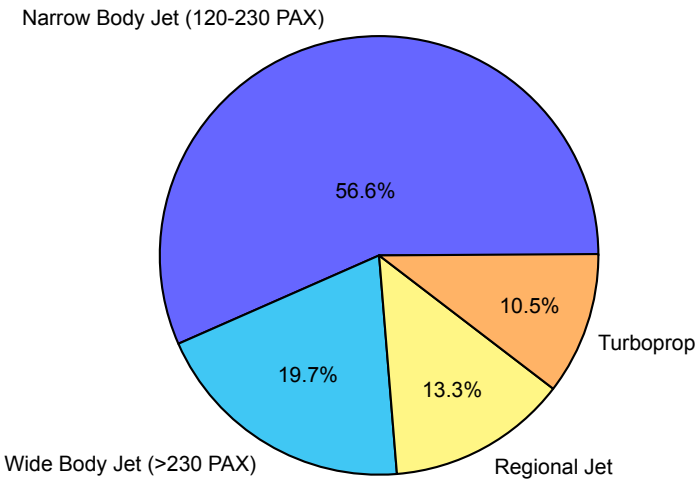

Figure 5.1: 2017 Global Market Segmentation [11]

Both aircraft types have their strengths and weaknesses, making them suitable for different routes. The distribution per region of turboprops and regional jets is presented in Figure 5.2. For example, it can be seen that over half of the regional jets are North America based. The choice for either aircraft can mainly be attributed to the following characteristics:

Turboprop strengths

- Lowest fuel consumption per block hour among <150 seat aircraft on routes below 300 nmi [13];
- Strong performance on challenging routes (short/unpaved runways etc.);
- Long service life.

Regional jet strengths

- Better *perceived* safety and in-flight experience and compared to turboprop aircraft, especially in the U.S. market;
- Significantly faster on routes above 400 nmi [14];
- More innovation within the jet propulsion field [14];
- Higher range, making regional jets more versatile for airlines.

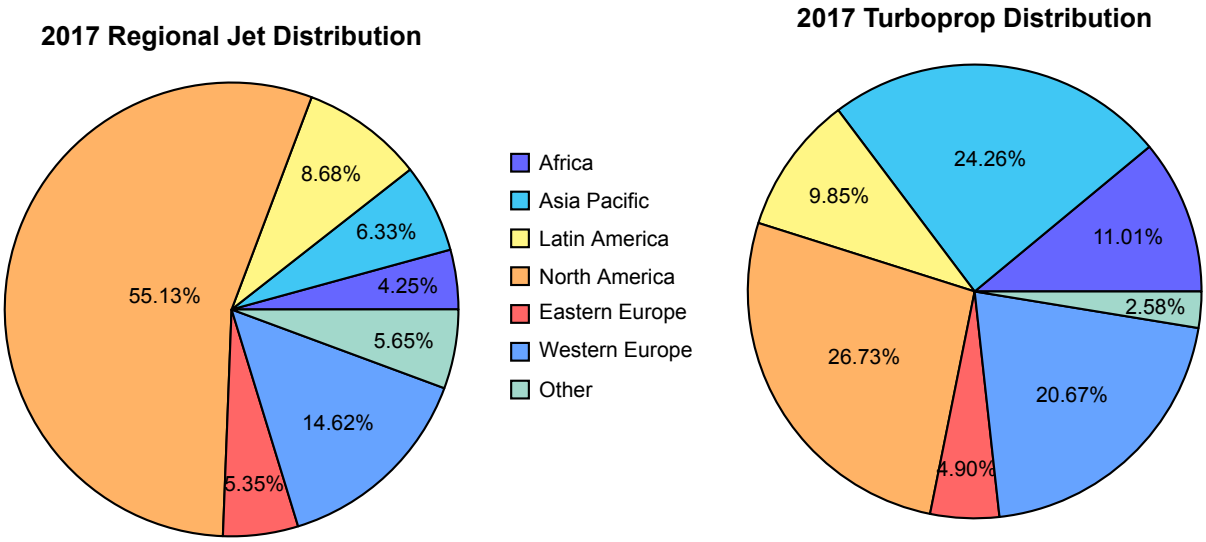

Figure 5.2: 2017 Worldwide regional aircraft distribution [11]

Currently the main players in the turboprop market are the aircraft manufacturer ATR and De Havilland Canada (DHC) which make up about 40% of the market share with the ATR-42/72 and Dash-8 aircraft families respectively. Due to higher operational costs and production complications of the latter, it is forecasted that ATR will prevail within the turboprop market [11]. The regional jet market has two main players: Embraer with their ERJ-series and until 2020 Bombardier with the CRJ-series, which was sold to Mitsubishi in June 2020[1]. These two aircraft families make up a large majority of the active regional jets today[2].

Market Forecast

The total forecast of worldwide regional aircraft deliveries is presented in Table 5.1. The air transport market demand in the upcoming decades depends upon a combination of factors, which differ per region in the world based on their geographical nature and economic and societal development.

Table 5.1: Regional aircraft fleet and delivery forecast (20-120 pax) for 2019-2050 [12]

Fleet forecast	**2019**	**2030**	**2040**	**2050**
Aircraft in service	5,630	6,690	7,040	6,910
Delivery forecast		**2020-2030**	**2030-2040**	**2040-2050**
Aircraft deliveries		3,230	2,250	2,950
		Total 2030-2050:	5200	

The demand for regional air passenger transport in the western world will depend on socio-economic factors and competition with land transport modes such as trains. The European Union's sustainability agreements and "green flying" initiatives will require heavy reduction in CO2 emissions and noise pollution to stay relevant in this market. In regions where alternative transport modes are not feasible, the demand for air transport will be less vulnerable [15].

The regional aircraft market within North America requires special attention, as its landscape is partly dominated by the so-called *Scope Clause*. These clauses are contracts between major airlines and pilot trade unions which limit the number and size of aircraft that can be flown by its regional subsidiaries. Since about 700 out of 1,100 total active regional jets are operated in North America, this is of major importance to manufacturers [2]. This is one of the reasons it is important to design regional aircraft in families, to allow for sales of aircraft on markets with the demand for different aircraft capacities.

5.2. Market Share

To estimate the potential market share, the market volume needs to be determined. In order to do this, the following criteria are considered:

- **Only routes under 500 nautical miles are considered**, since the difference in flight time between SRP-22 and regional jets, is under 45 minutes, as seen in Figure 5.3 is deemed acceptable. Moreover, 95 % of worldwide turboprop routes and 70% of worldwide regional jet routes are below 500 nautical miles [12].
- **Only regional flights in Europe, North America, Australia, China, India, and Japan are considered**, since these regions are the large regional aircraft markets with concrete plans for developing a hydrogen economy in the upcoming decades [3][4][5][6][7] [16];
- **Only flights from or to major hubs that are close to future hydrogen production plants or import location are considered**, since it is unlikely that hydrogen infrastructure will be available on remote 'spoke' airports. **The design range of the SRP-22 is 1000 nautical miles, which allows for round trips from hubs to remote airports without refueling at the remote airport for routes under 500 nautical miles.**

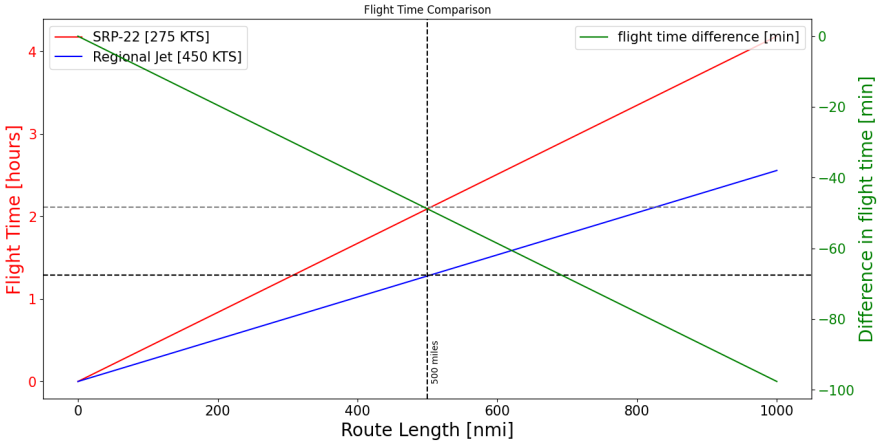

Figure 5.3: Flight time comparison between SRP-22 and a typical regional jet

To get an estimate of the number of aircraft that fly on the routes that are suitable for SRP-22, a dataset containing over 67,000 flights between 3300 airports on 540 airlines[8] is filtered by taking the following steps:

1. A list is made of airports in all considered regions that are above 10 million annual passengers and are close to a potential hydrogen production plant, import location, or other transport infrastructure for the 2045 scenario. Another list is made for the 2035 scenario, by only considering major hubs above 20 million passengers;
2. The total route list is then filtered for routes that have one of the airports as their source airport and that use aircraft with a seating capacity between 20 - 100 seats. One route is considered to be a combination of two airports (so LIS-MAD and MAD-LIS are one route);
3. The routes are filtered for a maximum distance of 500 nautical miles. The resulting routes in Europe are shown Figure 5.4 for both an expected infrastructure scenario in 2035 and 2045 respectively.

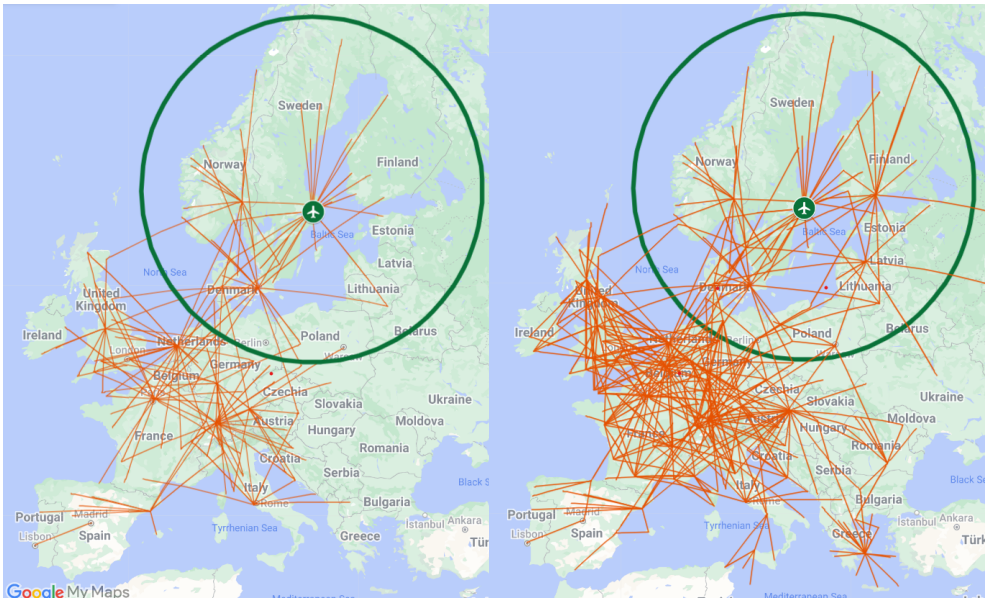

(a) 2035 scenario (13 hubs, ≈200 routes) **(b)** 2045 scenario (60 hubs, ≈600 routes)

Figure 5.4: Regional route maps of the SRP-22 in Europe. Stockholm Arlanda Airport is shown as an example hub, with the green circle being the 500 nautical mile radius

4. To estimate the total number of aircraft that fly on these routes, a rough estimate is made by dividing the total regional aircraft fleet in 2017 by the total number of routes flown with regional aircraft:

$$\frac{\textit{regional aircraft fleet}}{\textit{total regional routes}} = \frac{6000}{7500} = 0.8 \textit{ aircraft per regional route} \tag{5.1}$$

Based on the resulting routes, it can be seen in Figure 5.5 that the average route length is 278 nmi. This means that the lower cruise speed of the SRP-22 compared to regional jets will have a small impact on the flight duration, as seen in Figure 5.3. In Figure 5.6 it can be seen that **with small number of hydrogen airport hubs, already a large number of routes can be covered.** It is assumed that airports are adapted with hydrogen infrastructure from large to small.

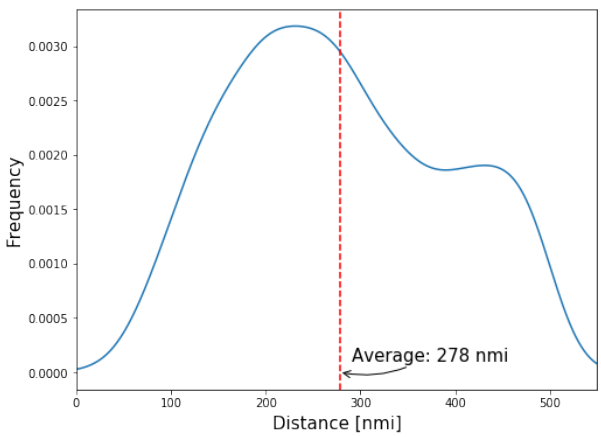

Figure 5.5: Distance distribution of considered routes

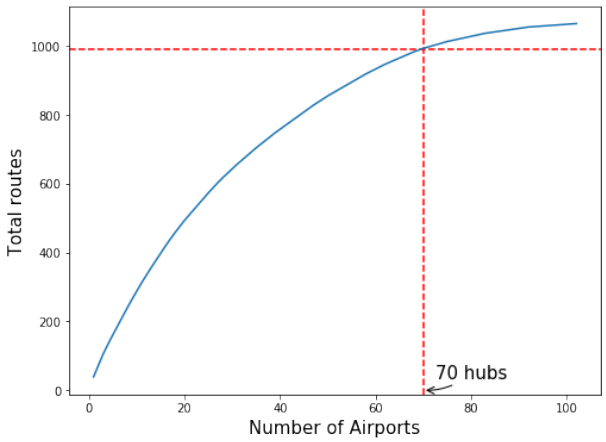

Figure 5.6: Total routes per number of hydrogen airports

The route distribution per region is shown in Figure 5.7. It can be seen that **if only Europe and North America live up to the expected infrastructure scenario, already over 85% of the expected hydrogen aviation market is created.**

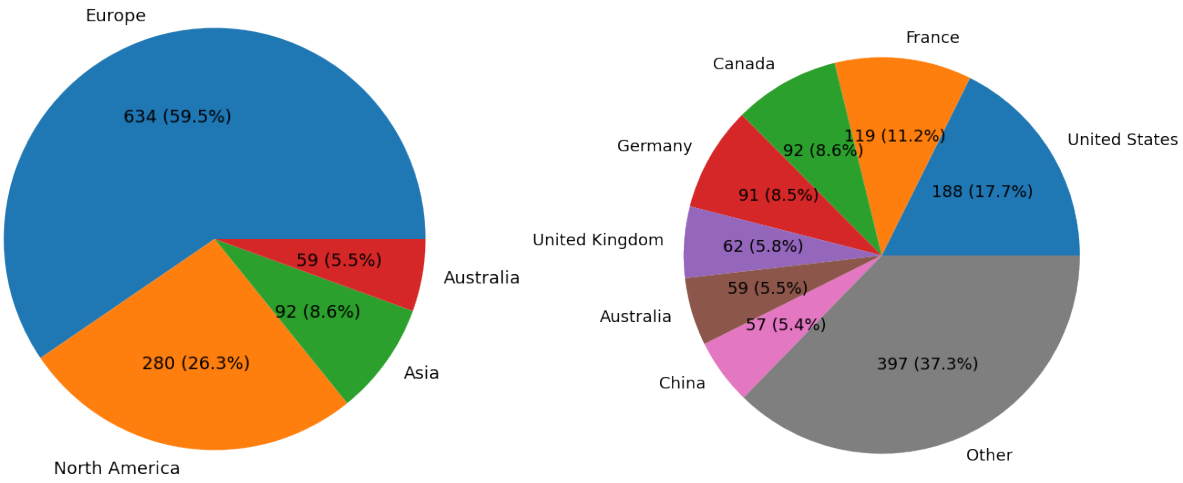

(a) Routes per continent

(b) Routes per country

Figure 5.7: Routes distribution per region. Routes are matched to their departure airport (2045 scenario)

To estimate the number of potential aircraft sales in the upcoming decades, the following assumptions are made:

- The fraction of regional aircraft that need to be replaced are approximated by the data in Table 5.1. For the time frame 2035 - 2045, approximately 3 out of every 8 regional aircraft will be replaced;
- By 2045 about 70 of the largest hubs that are considered are equipped with a hydrogen infrastructure, opening a total of 1000 routes for SRP-22 as can be seen in Figure 5.6;
- In the first decade of the program (2035 - 2045) the market share with respect to competitors on these routes is 50%. This is based on the significant advantage of the SRP-22 program with respect to 'traditional' competitors in the EU, which strives for climate-neutrality by 2050[9]. North America is the other main regional air transport market which is dominated by scope clauses, limiting the number of seats to 76 [10]. This gives SRP-22 the advantage to the main regional hydrogen aircraft competitor: the Airbus ZeroE regional turboprop with 100 seat capacity[11].

So to obtain the total number of aircraft sales in 2035 - 2045, the number of routes, aircraft per route, the aircraft that need to be replaced and the market share are taken into account:

$$Sales_{2035-2045} = 1000 \cdot 0.8 \cdot \frac{3}{8} \cdot 0.5 = 150 \tag{5.2}$$

It is assumed that the number of aircraft sales will double in the two decades that follow, due to the expectation of many new routes opening up worldwide as a result of climate-neutrality targets in combination with an increased production capacity of the SRP-22 program. The total expected sales of the SRP-22 program over 30 years are shown in Table 5.2.

Table 5.2: Expected sales of SRP-22 over 30 years

Decade	**2035-2045**	**2045-2055**	**2055 - 2065**	**2035 - 2065**
Aircraft sales	150	300	600	$\approx$ **1000**

5.3. Competitive Cost

To compete with existing regional aircraft manufacturers, one of the major emphases mentioned in Figure 5.1 is to reduce the cost of the aircraft in both the asking unit price and operational cost. The reduction of the asking unit price of the aircraft is compared to existing regional aircraft. The reference aircraft that are compared are shown in Table 5.3. All prices are listed in USD, since its the most used currency in the aviation industry [12].

Table 5.3: Aircraft asking unit price adjusted to inflation to FY2022 in $USD[13]

Aircraft Model	**Listed unit price** (USD, millions)	**Year**	**Unit price** (Inflation-adjusted to FY2022, USD, millions)
ATR-42-600	19.5	2012	25.3
ATR-72-600	18.6	2007	26.7
DHC-8 Q300	26.0	2017	31.6
DHC-8 Q400	32.2	2022	32.2
Saab 2000	15.0	1999	26.8
An140	9.0	2011	11.9
BAe 146-100	8.0	1984	22.9
ERJ-145	21.0	2022	21.0
CRJ-200	39.0	2019	45.5
ERJ-140	15.2	2000	26.3

All listed unit prices shown in Table 5.3 that are not listed in 2022 have been adjusted with consideration of inflation. The average unit cost of all reference aircraft in 2022 is approximately $27 million USD. Existing regional aircraft remain market value is evaluated to determine potential asking unit price, as within the North American turboprop market as of 2022, the lowest aircraft age is 15 years old [15]. This leads to a high demand in the North American market for replacing aging aircraft with new regional aircraft. The total average remaining market value of registered regional aircraft to the FAA in 2018 is shown in Table 5.4.

Table 5.4: Remaining market value of existing regional aircraft [17] adjusted to inflation to FY2022 in $USD

	Number of Aircraft	**Weighted Average Market Value** (USD, million)	**Standard Deviation** (USD, million)	**Upper Limit** (USD, millions)	**Lower Limit** (USD, millions)
Regional jet w/ more than 60 PAX	1111	15.8	7.0	22.8	8.8
Regional jet w/ less than 60 PAX	706	1.4	0.2	1.6	1.2
Turboprop w/ more than 60 seats PAX	45	11.2	3.1	14.3	8.1
Turboprop w/ 20-60 PAX	96	2.7	2.0	4.7	0.7

As shown in Table 5.4, the weighted average market value of aircraft is averagely depreciated by over 50% compared to the asking unit price shown in Table 5.3, where the weighted average of all remaining market value is ranged between $14.1 to 5.7 million USD per aircraft.

For the SRP-22 to achieve a competitive advantage in terms of aircraft price, both the asking unit price and the remaining market value of regional aircraft are considered. 20% contingency percentage for the asking unit price is considered to be the average asking unit price for the extensive research and development cost on the integration of new technology to reduce environmental impact. Additionally, the 20% contingency percentage also takes into account the market competitor already having mature manufacturing and assembly processes, which allows the manufacturers to reduce the asking unit price. However, considering the market remaining value of aircraft for air carriers, a deduction of 10% of the upper limit average remaining market value is considered. Leading to a design unit asking price of approximately 31 million USD.

The aircraft operational cost is separated into two sectors, direct operational cost, and indirect operational cost. Direct operational costs are the operating costs that are directly related to the aircraft flight operations, whereas indirect operational costs relate to marketing expenses, general administration expenses, passenger services, etc. As reported by the FAA in 2018, 48% of the total operational cost were direct operating costs for passenger air carriers with over $1 billion USD in revenue annually [18].

Direct operational costs consist of two segments, variable cost, and fixed cost. Fuel cost, maintenance cost, and crew cost all contribute towards the variable cost, whereas aircraft depreciation, rental insurance, etc. contribute towards the fixed cost. 72.2% of the direct operating cost is contributed by variable costs, the remaining 27.8% is contributed by fixed costs. The relative percentage contribution of fuel, maintenance, and crew cost is shown in Figure 5.8

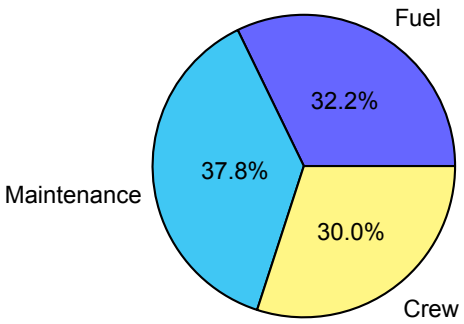

Figure 5.8: Variable Cost Segmentation[18]

As shown in Figure 5.8 fuel and maintenance cost contributes 70% to the total variable cost. Fixed cost and crew cost could not be reduced by design (single pilot operations are not an option, according to CS25 regulations) as it is interrelated towards the logistics and operations of the air carriers, hence the total percentage of contribution that could be designed for within the operational cost is approximately 24%. Compared to reference aircraft that are discussed previously in Table 5.3, operational costs of turboprop and regional jet aircraft are displayed in Table 5.5.

Table 5.5: Fuel cost percentage calculation based on operational cost [4]

Aircraft	**Direct Operational Cost / Block Hour (USD Inflation-adjusted)**	**Fuel Cost Percentage**
ATR-42-600	$2310	24.7%
ATR-72-600	$2950	20.7%
CRJ-200	$2830	53.7%
ERJ-145	$2320	42.8%

As shown in Table 5.5, the average direct operational cost of all 4 aircraft is approximately $2600 USD per block hour, with adjustment to inflation and inflation of Jet-A fuel cost as of December 1st[7], leading to ATR-42-600 having the lowest operational cost of approximately $2310 USD. Averagely, each regional aircraft trip is 1.5 block hours, with an average traveling distance of 356nmi [12], leading to ATR-72-600 having the lowest cost per seat-nmi with approximately $0.17 USD per seat-nmi.

Hence, to meet the user requirements of reducing 10% lower cash operating cost per seat mile on 500 nmi missions, and the design objective for minimizing environmental impact, the SRP-22 aircraft design should have a lower fuel cost percentage than the ATR-72-600 and the operational cost should be designed for lower than $0.16 USD per seat-mile, which is approximately $1,770 USD per block hour.

5.4. SWOT and Stakeholder Analysis

To determine the competitive advantages and disadvantages, the strengths, weaknesses, opportunities, and threat analysis of the novel regional aircraft are shown in Figure 5.9.

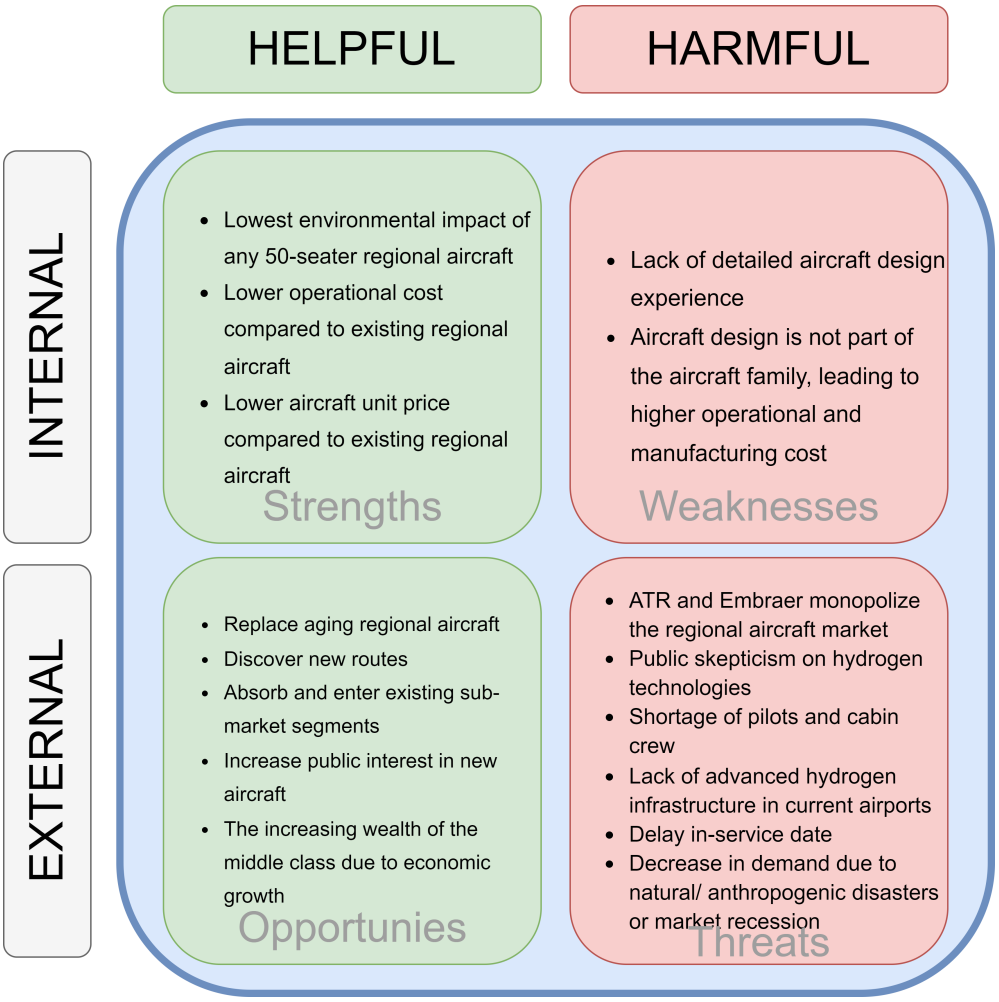

Figure 5.9: SWOT Analysis of the SRP-22 program

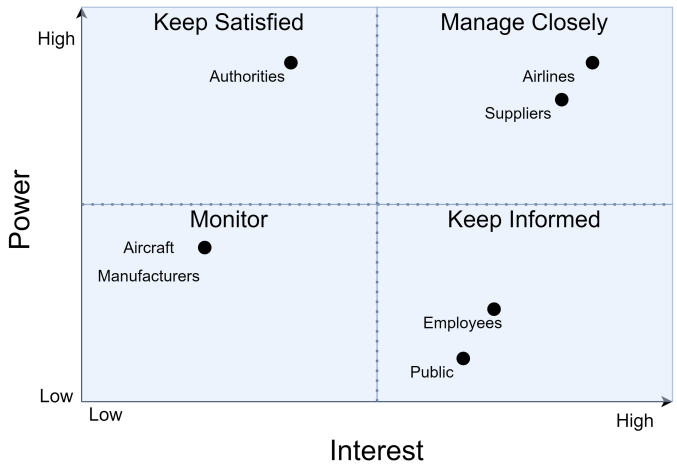

Figure 5.10: Stakeholder Analysis of the SRP-22 program

As shown from Figure 5.9, the competitive advantage of the novel regional aircraft is that the design will be designed to lower both the operational cost and competitive advantage, providing the opportunities of disrupting the current regional aircraft. However, the competitive disadvantage is the lack of detailed design experience and aircraft family consideration, leading to barriers to entering the regional aircraft market. Stakeholders of the SRP-22 project are derived from the SWOT analysis and are mapped in Figure 5.10. The following stakeholders are considered:

- **Airlines**: The end user of SRP-22 aircraft.
- **Aircraft Manufacturers**: Companies such as ATR or Embraer are direct competition and the SRP-22 project will obtain certain market segments that ATR or Embraere currently possess.
- **Authorities**: Regulation authorities such as the EASA or the FAA influence the certification and verification process.
- **Suppliers**: SRP-22 project requires multiple sources of suppliers such as fuel cell and electric motor suppliers.
- **Public**: End user of the service from the airline.
- **Employees**: Involved in the SRP-22 program.

[1]URL https://www.mhi.com/news/190625.html [cited 30 Nov. 2022]
[2]URL https://www.flightglobal.com/airframers/lively-debate-about-potential-for-new-50-seat-jet/134075.article [cited 24 Nov. 2022]
[3]URL https://www.csis.org/analysis/hydrogen-hubs-proposals-guideposts-future-us-hydrogen-economy [cited 15 Jan. 2023]
[4]URL https://www.csiro.au/hydrogen-map [cited 15 Jan. 2023]
[5]URL https://fuelcellsworks.com/news/in-2019-83-new-hydrogen-refuelling-stations-worldwide/ [cited 15 Jan. 2023]
[6]URL https://www.researchgate.net/figure/e-Three-major-clusters-of-Chinas-hydrogen-energy-industry_fig2_347297183 [cited 15 Jan. 2023]
[7]URL https://www.spglobal.com/marketintelligence/en/news-insights/latest-news-headlines/geography-matters-hydrogen-hub-proposals-spring-up-across-north-america-70997688 [cited 15 Jan. 2023]
[8]URL https://openflights.org/data.html [cited 15 Jan. 2023]
[9]URLhttps://commission.europa.eu/strategy-and-policy/priorities-2019-2024/european-green-deal_en [cited 17 Jan. 2023]
[10]URL https://airinsight.com/since-there-is-no-new-regional-jet-that-is-scope-clause-complaint-lets-talk-about-turboprops/ [cited 15 jan. 2022]
[11]URL https://www.engineering.com/story/airbus-unveils-stunning-new-zero-emission-concepts [cited 15 Jan. 2023]
[12]URL https://www.iata.org/en/iata-repository/publications/economic-reports/exchange-rates-and-aviation-examining-the-links/ [cited 30 Nov. 2022]
[13]URL https://aerocorner.com/ [cited 23 Nov. 2022]
[14]URL https://thedocs.worldbank.org/en/doc/777021436899472389-0190022009/render/AirTransportAirCargoAD.pdf [cited 26 Jan. 2023]
[15]URL https://jet-a1-fuel.com/ [cited 1 Dec. 2022]

N2 Chart

Feed Forward		INPUT	
Feed Backward	OUTPUT	ANALYSIS	OUTPUT
		INPUT	DESIGN ACTVIVITY

CLASS I WEIGHT	C_D0, C_D_TO		mtow	mtow, CL/CD			mtow		masses	masses	mass fraction of climb, mtow, C_D0	masses							Mases	
	WING LOADING		W/S, W/P	Sw							Sw		W/S	Sw					W/S	
	ROC, velocities	**FLIGHT PROFILE**	Velocities						velocity	flight altitudes and velocities	rho, Range		flight altitudes and velocities							
n_p	n_p		**PROPULSION SYSTEM**		tank and engine size,location&configuration				efficiencies		P_TO, eta_p	T_TO, type of propulsion, mass of engine	propulsion placement & size						propulsion placement & size	
Swet/s				**WING**	wing size & configuration			wing size & configuration		Sw		Sweep, S, S_fwet	wing size & configuration	wing Sweep, planform	wing planform	wing size & configuration, MAC, LEMAC	wing size & configuration	wing size & configuration, MAC	wing size & configuration	
Swet/S					**FUSELAGE**	fuselage size&configuration		l_f, l_ultimate				l_f, w_f, h_f	fuselage size & configuration			fuselagee size & configuration	fuselagee size & configuration		fuselage size & configuration	
						CG POSITION	cg locations	cg locations								xcg_oew, xcg_fuel, x_cg cargo	xcg_oew, xcg_fuel, x_cg cargo	xcg range		
						empennage size & location	**UNDERCARRIAGE**					undercarriage configuration	undercarriage size & configuration			undercarrige size, location & configuration	undercarrige size, location & configuration		undercarrige size & configuration	
						empennage size & location		**EMPENNAGE**				S, sweep	empennage size & configuration		empennage size & configuration	empennage size & configuration	empennage size & configuration	empennage size & configuration	empennage size & configuration	
									PAYLOAD RANGE											
										V-N DIAGRAM		V_D							n_ult, n	
	ROC, climb gradient	ROC	P								**CLIMB PERFORM**		ROC							
	masses					mass fractions	mtow		masses	masses	mtow	**CLASS II**	mtow				mass fractions		mass fractions	
CL, CD	CL,CD, CD0			HLD size,location & configuration					CL/CD_cruise	CL_max, CL,alpha	cdo, clmax	wing,vertical and horizontal tail size	**AERO CHARACTERISTICS**	airfoil characteristics, CL	lift curve	CL,alpha, x_ac, mc_ac	cm_alpha, CL,alpha, x_ac, mc_ac	x_ac, mc_ac		
	CL,CD new			control surfaces size,location & configuration				control surfaces size location & configuration		CL_max		HLD size	new aero characteristics for landing, TO	**HLD**			HLD size,location & configuration	HLD size,location & configuration		
															CONTROL SURFACES	*Control surfaces size, location & configuration*	*Control surfaces size, location & configuration*	*Control surfaces size, location & configuration*		
						fwd_cg, aft_cg		empennage size & configuration								**GROUND STABILITY**				
								empennage size & configuration						HLD size,location & configuration	*Control surfaces size, location & configuration*		**FLIGHT STABILITY**			
								empennage size & configuration							elevator trim, control force curve			**CONTROL**		
												masses							**STRUCTURES**	Part & subpart design configuration
												masses							Part & subpart design configuration	**MATERIALS**

7 Weight Estimations

First weight estimations shall be performed for the further design of the aircraft. A wing loading diagram is constructed which gives W/P and W/S ratios. Furthermore, the combination of Class I and Class II weight estimations leads to the final combined weight estimation which is used for the design of several subsystems.

7.1. Wing Loading Diagram

The wing loading diagram is used to determine the necessary shaft power of the aircraft. The construction of the wing loading diagram was done by the usage of the method as defined by R. Vos [4]. The design point was chosen from the wing loading diagram with $\frac{W}{P} = 0.077$ N/W and $\frac{W}{S} = 3270$ N/m^2, which is constrained by rate of climb and one engine inoperative takeoff. The design point was mostly chosen for a high $\frac{W}{P}$, as this means less power is required. Fuel cells are quite heavy and placed in the aft. More power required in turn means more fuel cells, causing the center of gravity to be further aft. As can be seen in Figure 7.1, it would have been possible to choose the design point to be intersecting with both the landing constraint and the takeoff (OEI) case, leading to a lower $\frac{W}{S}$.

After the mass of the aircraft is computed, the design point can be revisited. Along with the chosen design points, the design points for three reference aircraft are shown.

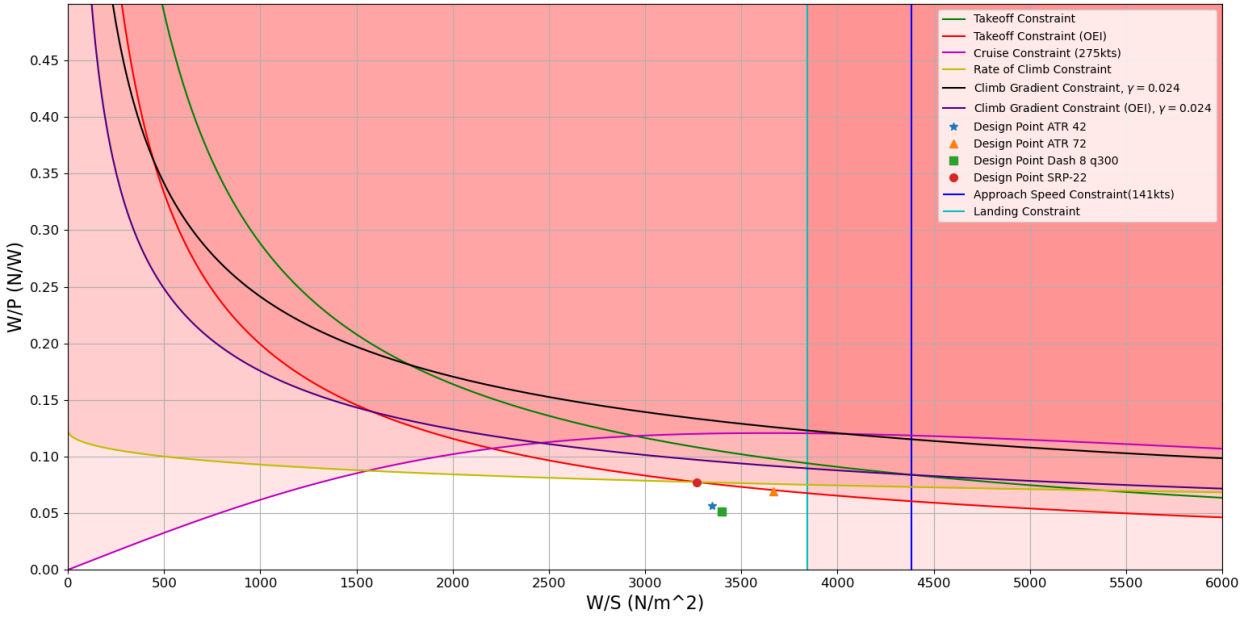

Figure 7.1: Wing Loading Diagram

7.2. Class I Weight Estimation

For the class I weight estimation, the method as described by R. Vos was used [4]. This method uses the Breguet range equation to find the equivalent range, from which the fuel fraction can be calculated. To comply with requirement RA-TOP-PER-2, the equivalent range was found to be equal to about 1440 nmi. The $\frac{m_{OE}}{m_{MTO}}$ ratio is estimated from both statistical data and additional inputs stemming from the expected powertrain mass. The payload mass is constructed for an aircraft carrying 48 passengers. The total efficiency was calculated, taking into account the efficiencies of the fuel cell, the wiring, the inverter, the electric motor and finally the propeller. The L/D ratio during cruise was used from the aerodynamic estimations as will be elaborated upon later in the report. The main inputs and results are shown in Table 7.1.

Table 7.1: Inputs and Outputs of Class I

Inputs	Value	Unit	Inputs	Value	Unit	Outputs	Value	Unit
$\left(\frac{L}{D}\right)_{\text{cr}}$	16.8	-	R	1440	[nmi]	MTOM	18290	[kg]
e_{fuel}	120	[MJ/kg]	f_{con}	0.05	-	OEM	12410	[kg]
$\frac{m_{\text{OE}}}{m_{\text{MTO}}}$	0.679	-	R_{div}	100	[nmi]	m_{fuel}	669	[kg]
$\frac{m_{\text{fuel}}}{m_{\text{MTO}}}$	0.027	-	E	30	[min]			
m_{PL}	5225	[kg]	V_{cr}	275	[KTAS]			
η_{tot}	0.47	-						

The payload mass presented in Table 7.1 consists of passengers and luggage. The passengers were set at a weight of 200 lbs, the calculated mass for the luggage of the passengers would then be 18 kg, thus complying with **RA-TOP-PAS-1.1.1**.

After computing the MTOM, the wing loading diagram was revisited. If the design point was chosen to intersect with the landing constraint, the objective of a wingspan under 24 m would be met as a wingspan of 23.9 m could be reached. However, this would also lead to an increase in the power loading by 13.2%, and hence the choice was made to use the old design point.

Furthermore, the fuel mass for the 500 nmi mission is computed to be equal to 241 kg, which leads to $\approx$ 5 kg of fuel per passenger. According to Von Schoenberg, the ATR 42-600 has a lower block fuel per seat than the Dash-8 q300, hence this aircraft is taken as a comparison [14]. The results are shown in Table 7.2. Note that block fuel is taken per kg. If rather the energy difference would be taken into account, the energy density shall be used. This difference is also shown.

Table 7.2: Comparison of Block Fuel per Passenger on 500 nmi

Aircraft	Block Fuel per Passenger [kg]	Relative Difference to ATR 42-600 [kg]	Relative Difference to ATR 42-600 [MJ]
ATR 42-600	27	0%	0%
SRP-22	5	-81.7%	-48.7%

As the comparison of fuel mass is not relevant to comply with the block fuel reduction requirement, the difference in required energy is determined to be a better metric. This reduction is mainly caused by the wingtip mounted propellers and the high efficiency of the fuel cells compared to conventional combustion. This ultimately results in almost halving the required energy and thus complying with RA-TOP-SUS-1.

7.3. Class II Weight Estimation

The Class II weight estimation was mostly taken from Raymer, with some additions/changes due to the fact a hydrogen aircraft is designed [19]. For example, as there is no fuel in the wing nor the fuel cell, less bending relief is present. To compensate for this, the wing weight was estimated using the Torenbeek method, with the m_{MTO} rather than the m_{ZF} [20]. By using this method in this manner, no bending relief is taken into account, with the m_{MTO} as an input. Furthermore, regular engine weight estimations are not applicable. Both the mass of the fuel cell and the electric motors were estimated using the peak power stemming from the wing loading diagram, taking into account losses due to efficiencies. For every fuel cell delivering 250 kW a mass of 80 kg was assigned, while the electric motors were scaled with a power density of 8 kW/kg. The same was done for the inverter mass. Everything else is the same as for a conventional aircraft and hence the Raymer method was applied. After calculating all component masses, these were added up to obtain a more accurate m_{OE}. The percentages of all component masses relative to the total OEM can be found in Figure 7.2. Adding all components up leads to a **OEM of 12,470 kg**. The sensitivity of the Class II with regard to an increase in MTOM has been evaluated. An increase of the MTOM by 7.2% leads to an increase of the OEM of 2.8%, which is deemed acceptable.

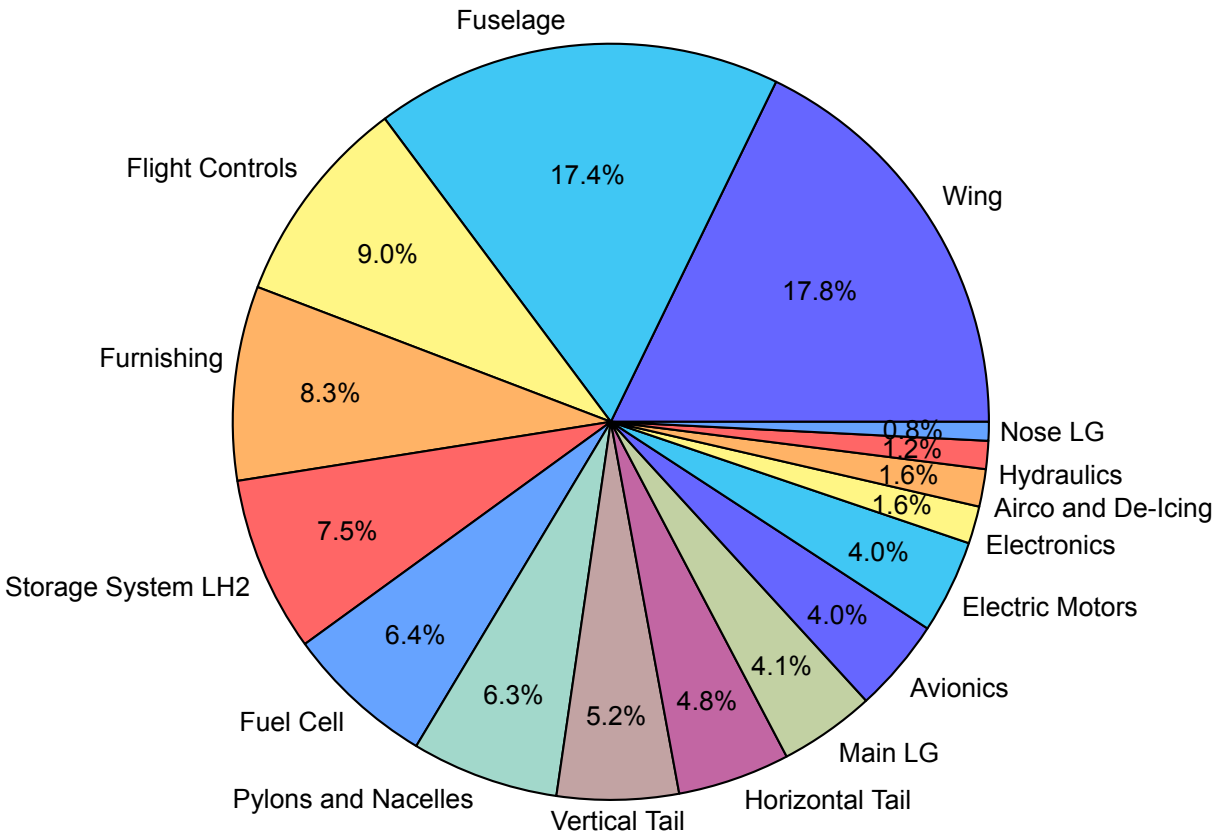

Figure 7.2: OEM Breakdown

7.4. Final Weight Estimation

After both the Class I and Class II have been conducted, the outcomes can be combined. As mentioned, the Class II takes the MTOM of the Class I as an input to determine a more specific OEM. This newly calculated OEM is in turn used to obtain a more accurate OEM/MTOM fraction for the Class I estimation. As can be deduced from Table 7.1 and the value resulting of the Class II weight estimation, the difference between the two weight fractions is 0.8%. This difference is smaller than 1%, hence the newly obtained OEM/MTOM fraction (equal to **0.684**) was used in the Class I. This resulted in the estimated masses as shown in Table 7.3.

Table 7.3: Final Weight Estimations

Outputs	Value	Unit
MTOM	18650	[kg]
OEM	12770	[kg]
m_{fuel}	683	[kg]

The current Class I does not take into account specific flight phases but rather uses an approximation of its fuel burn. As a means of validation, a different code using the chemical reaction within the fuel cell was used [21]. The power during different flight phases was calculated, from which the required mass flow could be obtained through the chemical reaction [22].

The outcome of these calculations was a required fuel mass of 818 kg of hydrogen for the 1000 nmi mission, including all contingencies. This means an increase of 19.8% in the required fuel mass with respect to the value of the Class I. This results from several factors, including the fact that several values used in the method are uncertain, such as the voltage the fuel cell will use. Furthermore, this method is more specific, hence a difference could be expected. As the method is basically combining two methods (power calculations and a chemical reaction), it was used as a validation tool rather than a real estimation.

8
Aircraft Sizing

An initial sizing and design of the geometry of the fuselage, wing, empennage, and undercarriage is undertaken to achieve some basic aircraft geometries. Furthermore, the aircraft center of gravity location is estimated based on Class I and Class II weight estimations. The initial dimensions are presented in this chapter and would be re-iterated in later stages of the design process.

8.1. Fuselage Design

The main purpose of the fuselage is to protect the payload - the passengers, cabin luggage, and larger cargo. In addition, the fuselage provides structural support for the attachment of interfaces (wings, empennage etc.) whilst also housing the cockpit and other key aircraft systems [23]. The summary table with the final values is presented in Table 8.2.

Fuselage Cross Section

In this subsection, the fuselage cross-sectional profile of the SRP-22 will be defined. First, it is decided that a design with a constant cross-section will be adopted instead of a variable cross-sectional shape. This brings benefits in terms of minimizing the complexity of the production of the fuselage, resulting in a reduction of production cost [20]. Another advantage stemming from this design choice is that the future development of lengthened and shortened variants of the base model can be more easily incorporated [24].

The shape of the fuselage cross-section is determined. Common shapes of commercial aircraft's cross-sections include (near) circular, double-bubble and rectangular. The rectangular profile is often adopted by aircraft without a pressurized cabin. However, as the cabin is pressurized during flight, a circular or double bubble design is optimal as the internal pressure is distributed evenly along the cross-section, lowering the skin thickness and thus the fuselage's structural weight [24]. The decision of choosing between a circular shape or a double bubble shape depends on the storage of additional propulsion systems and cargo. The double bubble shape provides additional space to accommodate cargo and fuel storage without compromising on the cabin's floor area and the comfort level of the passengers.

With the cross-sectional shape being decided, the configuration is followed up with determining the arrangement of the cabin. The maximum number of seats abreast is defined by CS-25 regulations, stating that no more than three seats abreast may be placed on each side of the aisle in any row [1]. The three abreast, four abreast, and five abreast configurations are shown in Figure 8.2. Having more seats abreast leads to a shorter cabin length, a wider fuselage diameter, and more underfloor storage space. The inner diameter of the cross-section should be adequately sized such that the seat width, aisle width, aisle height, and passenger headroom (definitions shown in Figure 8.1) meet the user requirements specified in Section 2.1. A CAD software is used to visually determine the minimum inner diameter of the fuselage ($d_{f,i}$). Subsequently, the thickness of the fuselage (Δd) can be approximated by the empirical relation shown in Equation 8.1 [24].

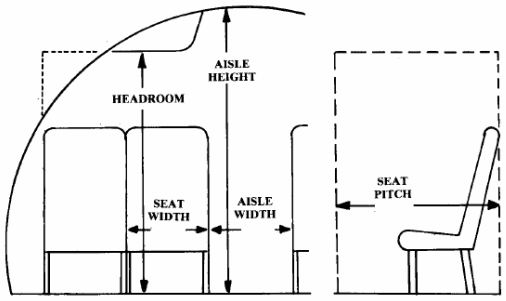

Figure 8.1: Definitions of cabin and seats parameters [19]

$$\Delta d = d_{f,o} - d_{f,i} = 0.084 + 0.045 \cdot d_{f,i} \tag{8.1}$$

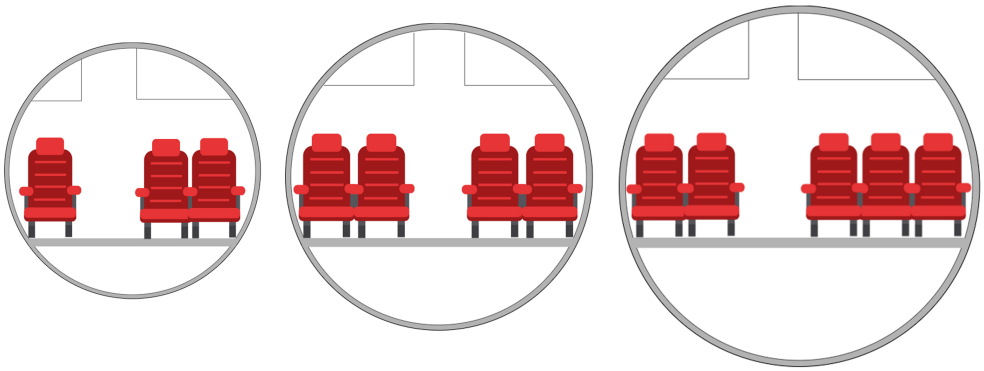

Figure 8.2: Cross-section of the various seating configurations. From left to right: three abreast, four abreast and five abreast

Fuselage Sizing

The fuselage can be divided into three sections: the nose, the cabin, and the tail. During subsonic flight, one of the main forms of drag is skin friction drag [23]. By adhering the design of the fuselage to the optimal fineness ratio the minimization of skin friction drag is ensured. Literature suggests that the ideal fineness ratio for a subsonic aircraft is about 1:8, meaning the ideal fuselage length is eight times as long as the cross-section diameter of the aircraft [25]. In Figure 8.3, some common geometric parameters and their symbols are presented. The results for each seat configuration are presented in Table 8.1. The slenderness ratio has been defined as the ratio between the fuselage length and the fuselage outer diameter. One can find information regarding the way each parameter is computed in the following sections.

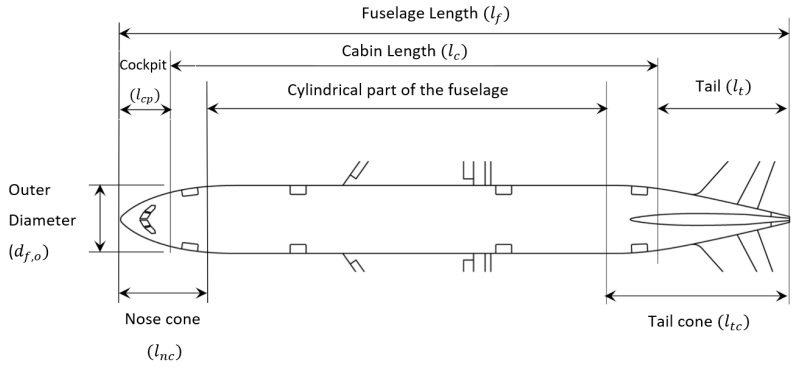

Figure 8.3: Definition of geometric fuselage parameters [23]

Table 8.1: Fuselage sizing and cabin sizing for different seat configurations

Seating configuration	n_{pax}	$d_{f,i}$ **[m]**	$d_{f,o}$ **[m]**	l_f **[m]**	l_c **[m]**	t_f **[m]**	**Slenderness Ratio**
Three abreast	48	2.5	2.7	25.6	17.3	0.20	9.5
Four abreast	48	2.8	3.0	23.9	13.0	0.21	7.9
Five abreast	50	3.5	3.7	20.8	10.8	0.24	5.6

The four abreast setup is selected due to its near-ideal slenderness ratio (close to 8 [25]) thus minimizing skin friction drag compared to the fuselages designed for the other two seat configurations. The setup also provides the option of designing a lengthened or shortened variant of the base aircraft in the future without compromising on the aerodynamic performances.

Nose Cone Sizing

The nose is where the cockpit of the aircraft is situated. It must provide sufficient space for pilots, avionics, and instruments. In commercial aircraft, the design of nose cones is driven by the performance of said aircraft in drag divergence. As the designed cruise speed of the SRP-22 is lower than $M < 0.5$, the effect of drag divergence is negligible, meaning a less slender nose is required [23]. To reflect this, a nose cone fineness ratio of 1.2 is selected for the final design of the aircraft, resulting in an approximated nose cone length of 3.6 m.

Cabin Sizing

In commercial airliners, the cabin is the section where passengers sit. Sizing of the cabin should ensure adequate spacing for the passenger seating, crew seating, cabin provisions (toilets, galleys), large items of luggage, and emergency exits. A full-economy configuration is chosen for the SRP-22 to maximize the number of seats in the cabin without compromising an increasing fuselage length. As seen in Figure 8.3, the cabin length typically extends into both the nose- and tail cone. The required length allocated for the cabin section of the SRP-22 is approximated by the method presented by R. Vos [23]. This resulted in a cabin with 12 rows of seats and a cabin length of 12.3 m. The seating plan of the aircraft is presented in Figure 8.4. Furthermore, to accommodate for the luggage as defined by requirement **RA-TOP-PAS-1.1.2**, along with the overhead luggage compartment (5.7 m^3), some cabin space is used for a front luggage compartment, which has a volume of 3.5 m^3. The crew luggage is placed in a compartment within the cockpit section. The volume of the said crew luggage space is 0.71 m^3 which is compliant with the volume per requirement **RA-TOP-CRE-1.2.2**.

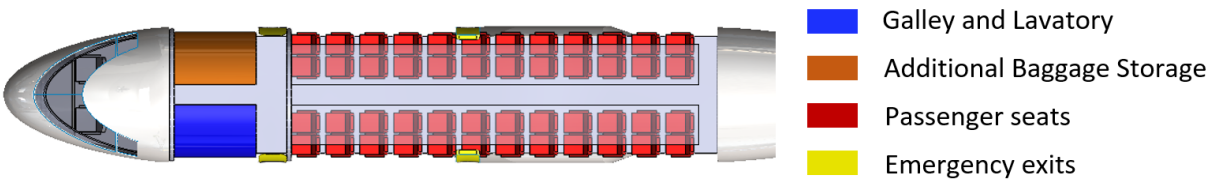

Figure 8.4: Seating plan of the SRP-22

Tail Cone Sizing

The presence of a conical shape at the tail contributes to increasing the fineness ratio of the aircraft's tail section, leading to a lower afterbody drag [20]. Initial length estimations of the tail section (l_t) and the tail cone length (l_{tc}) can be computed by the approximations presented by J. Roskam [25]. From the tail cone geometry, the tail angle of the aircraft is calculated to be 17.1° [24]. A suitable scrape angle (θ_{tc}) of 16.7° also has to be chosen for the aircraft to have a sufficient angle of attack of 5.5°, discussed in Chapter 9, during take-off without the occurrence of tail-strike. Thus, this will comply with **RA-SYS-MSC-3**.

Emergency Exits

Emergency exits are designed to provide means of evacuation in case of an emergency, and to comply with **RA-SYS-SRE-2.2** and EASA CS-25.807. The SRP-22's seating capacity falls under the 40-79 passenger interval, meaning that the aircraft requires at least one Type I exit and one Type III exit equipped for each side of the cabin [20]. Extra fuselage length may be needed as seats cannot be positioned in front of exit doors for ease of emergency evacuation. By inspecting Figure 8.4, one can observe the window seats of the furthest seat row is located seven rows from the nearest emergency exits, which equals to approximately 5.3 [m]. The distance of the same seat from the nearest exit on the opposite site is estimated to be 6.1 [m].

Summary

The fuselage and cabin sizing parameters of the final aircraft are summarized in Table 8.2. A detailed drawing of the cabin cross section is also shown in Figure A.1.

Table 8.2: Initial fuselage and cabin design parameters for the aircraft

Parameters	Values
Number of seats abreast	4
Number of passengers	48
Seat width	0.5 [m]
Seat pitch	0.7 [m]
Standup Aisle Height	1.9 [m]
Aisle Width	0.46 [m]
Fuselage inner diameter	2.8 [m]
Fuselage outer diameter	3.0 [m]

Parameters	Values
Tail scrape angle	17.1 [°]
Thickness of the fuselage	0.21 [m]
Fuselage length	23.9 [m]
Cabin length	11.7 [m]
Cylindrical fuselage length	11.2 [m]
Tail length	8.6 [m]
Tail cone length	9.0 [m]
Nose cone length	3.7 [m]
Cockpit length	3.7 [m]

8.2. Wing Planform and Propulsion Placement

The initial wing planform is designed based on the wing surface area (S_w), and taper ratio (λ). The wing surface area is taken from the wing loading diagram and the taper ratio is assumed from literature [19]. For the thickness to chord ratio ($\frac{t}{c}$), the aircraft design Mach number is low enough to lead us to a $\frac{t}{c}$ of 0.18. However, the wings in the design are empty and receive no bending relief due to fuel, a higher thickness to chord ratio of 0.21 is chosen to increase the MOI Section 9.1. The equations used to calculate the required planform parameters are presented by R. Vos and J.A. Melkert [26].

Table 8.3: Initial wing planform geometry

S_w [m^2]	b [m]	c_r [m]	c_t [m]	t/c [-]	MAC [m]	y_{MAC} [m]
59.9	26.8	3.1	1.4	0.21	2.3	5.9

The placement of the propulsion system and its energy source greatly affect the center of gravity location and should therefore be determined carefully. The electric propellers are used as sized in Section 12.6. A big propeller (and electric motor) will be placed under each wing, relatively close to the fuselage. In addition, a smaller propeller will be placed under each wingtip, to reduce lift-induced drag [27]. To allow for propeller clearance, a **high-wing configuration** is chosen. The LH2 tank will be placed in the aft, of which the design will be elaborated upon in Section 10.2. The fuel cell will be placed here as well, such that the hydrogen can be converted quickly after leaving the tank. Hereafter through wiring, the electricity will be used to power the motors.

8.3. Center of Gravity Estimations

Center of gravity estimations is conducted to scale the surface area and the lever arm of the empennage design. The center of gravity calculations is conducted by a combination of class I weight estimations and class II weight estimation. The fuselage, wing, empennage system, and fixed items weight fraction with respect to maximum takeoff weight fractions are shown in Table 8.4.

Table 8.4: Weight fractions with respect to MTOW and longitudinal placement [28]

	Weight fractions	Longitudinal placement
Fuselage	0.12	$0.4 \cdot x/l_f$
Wing	0.11	$0.4 \cdot x/\bar{c}$
Propulsion	0.07	$-0.2 \cdot x/\bar{c}$
Empennage	0.07	$0.9 \cdot x/l_f$
Fuel Tank and fuel cell	0.09	$0.64 \cdot x/l_f$
System + others	0.18	$0.4 \cdot x/l_f$

Based on the method discussed by R.Vos and J.A. Melkert [28] for the center of gravity calculation, the location of the LEMAC (x_{LEMAC}) is 11.5 m and the location of the center of gravity (x_{cg}) of the operational empty is 12.3 m. The most forward and aft center of gravity of the aircraft will be discussed in Section 15.1.

8.4. Empennage Design

The empennage consists of the horizontal- and vertical tail. The empennage needs to provide trim, stability, and control. The surface areas, S_{h} and S_{v}, of the horizontal- and vertical tail respectively are determined using approximate volume fractions. A.J. Kundu states that the ratio between the horizontal tail- and wing area should be in the range of 0.25 to 0.35 [29]. From the Design Option Tree (DOT), the most promising tail designs have been selected as a result of the performed trade-off [30]. Based on the propulsion system (propeller) and wing placement (high), a **T-tail configuration** was chosen. With this configuration, the design has a more efficient horizontal tail (due to less downwash effect), lower complexity and lower weight.

The horizontal stabilizer of the T-tail introduces a bending moment in the vertical tail, which results in an increase in its structural weight. Nevertheless, the horizontal stabilizer of a T-tail is more efficient, as it is less affected by downwash by the wing. Therefore, the surface area of the horizontal tail can be relatively lower, thus decreasing its structural weight. Nonetheless, the separated airflow, created at a high angle of attack results in a deep stall possibility at the horizontal stabilizer. This was taken into account during the airfoil selection.

Parameter Estimations

In order to calculate the design parameters of the empennage, the tail volume, the aspect ratio, and the taper ratio were estimated. Furthermore, the tail arm was determined. This is constrained by the fuel tanks and the aft fuselage. The estimation of the horizontal and vertical tail volume is based on Roskam tail sizing estimations for regional turboprop aircraft [25]. A higher tail volume will result in a larger tail. The horizontal stabilizer is more efficient for a T-tail, which means that the horizontal tail volume coefficient can be reduced.

The benefits of the aspect ratio, A, of the tail are relatively similar to that of the wing. A higher aspect ratio results in an increase in generated lift, combined with a higher structural weight. The horizontal stabilizer of the T-tail should have a low A, in order to relieve the bending moment in the vertical tail. Nonetheless, a higher A could reduce the vortex-induced downwash, resulting in an earlier stall, and especially relevant at low speed combined with high altitude. The aspect ratio values are estimated from Roskam [25].

Further tail sizing parameters can then be determined, using the estimated surface area of the horizontal- and vertical tail. The equations for this purpose are similar to the wing planform equations [28]. The initial estimate for the tail planform sizing is presented in Table 8.5. This will be reiterated in Chapter 15.

Other Design Considerations

Other parameters adding to the stability can be considered. These are generally used in the case of a small vertical tail area. These improve the lateral-directional stability of the aircraft. A dorsal fin can be added after sizing the vertical tail. It improves the efficiency of the vertical tailplane at high angles of attack of yaw. Using a dorsal fin would mean that the control speed can be reduced during takeoff operation. Furthermore, the central fin can be attached, which would prevent lateral instabilities at high speed. The three basic options, relating to the tail setting configurations, are a fixed, adjustable, and all-moving horizontal stabilizer. These increase with complexity, and chances of failure. Considering the nature of the aircraft that is being designed an adjustable tail will be used.

Table 8.5: Initial parameters empennage

	Horizontal tail	**Vertical tail**
Tail arm [m]	11	9.6
Surface area [m^2]	10	13
Span [m]	6.4	4.2
Root chord [m]	1.8	4.3
Tip chord [m]	1.4	2.1
Sweep angle [°]	0 (at 3c/4)	26 (at LE)

8.5. Undercarriage design

The main purpose of the landing gear is to provide a suspension system during taxi, takeoff, and landing. It is designed to absorb and dissipate the kinetic energy of landing impact, thereby reducing the impact loads transmitted to the airframe [31].

The process of designing the undercarriage starts with determining the number of tires of the nose- and main wheels, followed by the size and pressure of these. Once these values are obtained, the landing gear is to be placed following a given set of angular and positional constraints.

Furthermore, the landing gears have a brazing system accounted for, an anti-skid braking system with a deceleration of 0.50g during roll-out on a dry surface. These will be made from carbon being 40% lighter than conventional brakes and offering a significant deceleration improvement from 0.45g to 0.50g [32]. Moreover, the anti-skid braking system consists of a control unit relating the hydraulics and pressure input from the pilot and the temperature and speed sensors on the wheels, resulting in compliance with requirement **RA-SYS-UCG-1**. The final dimensions and locations of the main and nose landing gear are presented in Table 8.6 and Table 8.7 respectively.

Tire Sizing

The methodology used to size the undercarriage is presented during the Aerospace Design System Engineering Elements lectures presented by the Delft University of Technology [28]. The choices of the number of wheels, configuration, and dimensions directly depend on the runway conditions on which the aircraft will operate. One could define this aircraft as a CS25 regional turboprop. For this type of aircraft, the number of wheels for the nose gear is two [28].

It can be assumed from data from similar aircraft, the load classification number (LCN) will be around 19. The tire pressure is, therefore, equal to 586 KPa or 85 PSI [28].

Table 8.6: Tire sizes

Wheel type	Outer diameter [m]	Inner diameter [m]	Thickness [m]	Number [-]
Main Wheel	0.836	0.406	0.247	4
Nose Wheel	0.343	0.152	0.108	2

Undercarriage Positioning

The requirements **RA-SYS-UCG-2.1**, **RA-SYS-UCG-2.2**, **RA-SYS-UCG-3** relating to undercarriage positioning are proven in this section. Firstly it must be noted that the origin of the x, y, and z coordinates is located at the symmetric center of the fuselage at the nose. The scrape- and tip-back angles are driving for the location of the main landing gear. Whilst the moment equilibrium is used to determine the position of the nose landing gear. In order to comply with the overturn angle requirement of 55°, wingtip tip over, and engine tip over the spanwise position of the main landing gear is be determined.

The lateral nose wheel position is driven by the minimum force in ground turning, determined using moments. The z-location is chosen to be the same as that of the main landing gear, resulting in a deck angle of 0°.

Table 8.7: Final landing gear dimensions

X_{mlg} [m]	Z_{mlg} [m]	h_{mlg} [m]	X_{nlg} [m]	y_{mlg} [m]	Z_{nlg} [m]
13.4	2.26	0.75	4.2	1.75	2.26

8.6. Freighter conversion

To meet the design objective **RA-OBJ-3**, the SRP-22 aircraft shall be convertible to a freighter aircraft. To allow for cargo placement the cabin interior furnishing will be removed and the floor will be reinforced. The operational empty mass of the freighter configuration is calculated by subtracting the furnishing mass as estimated in Chapter 7 and by adding 10% to the fuselage mass which accounts for the floor reinforcement. To calculate the cargo mass capacity, the same fuel mass as the standard passenger configuration is added and this sum is subtracted from the maximum takeoff mass, resulting in the operational empty mass and cargo mass found in Table 8.8.

Table 8.8: Mass overview of the SRP-22 freighter configuration

Mass	Value	Unit
$MTOM_{freighter}$	18650	[kg]
$OEM_{Freighter}$	11930	[kg]
M_{cargo}	6030	[kg]
M_{fuel}	683	[kg]

The cargo-hold dimensions are shown in Figure 8.5. The cargo-hold can fit five LD3 containers[1] with dimensions 2.01m by 1.55m by 1.63m with a maximum total mass of 6000 kg. A large cargo door with dimensions 2.95m by 1.8m will be be added to front part of the cargo-hold to load and unload the cargo pallets. The payload range diagram of the SRP-22 freighter configuration is shown in Figure 16.1b.

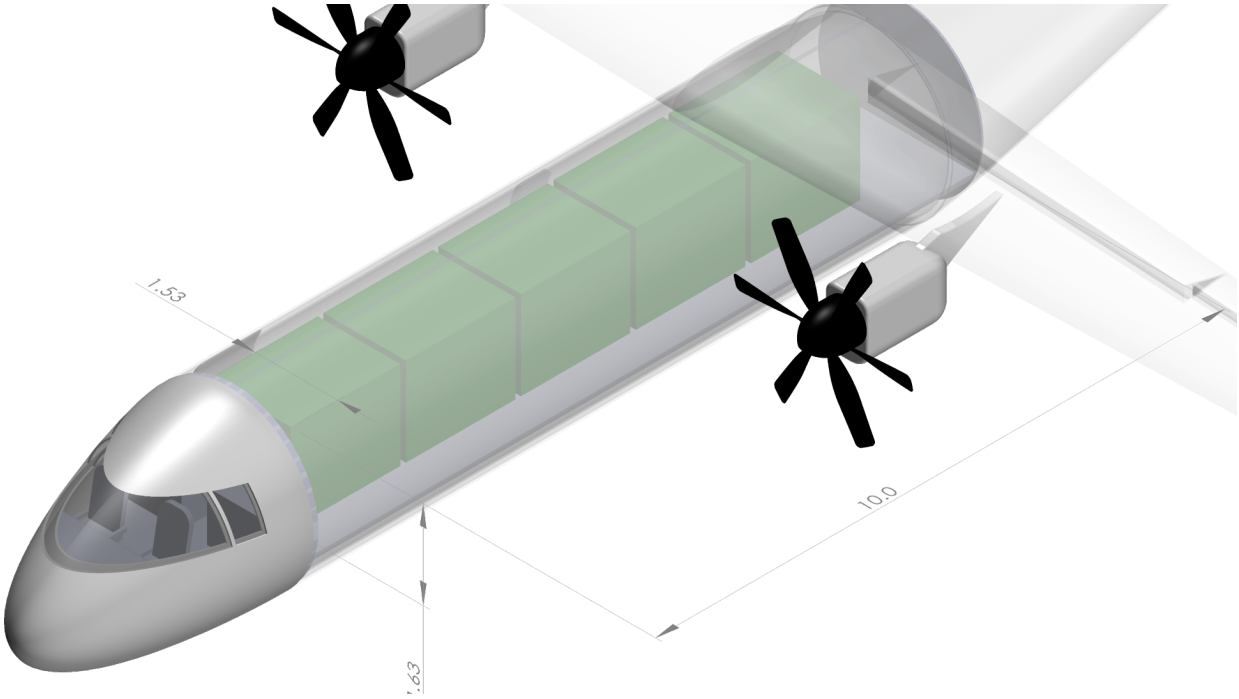

Figure 8.5: SRP-22 Freighter Configuration

[1]URL https://www.air-cargo-products.de/ld3-container.html [cited 31 Jan. 2023]

9 Aerodynamics

The aerodynamic characteristics of an aircraft are critical to its design as it provides insight into the limits of performance and how to enhance it. At this phase of the design, some key decisions on the airfoil selection, wing and drag characteristics and the High Lift Device Design (Section 9.1, 9.2 and 9.3) is done, which are crucial to flight.

9.1. Airfoil Selection

Selecting the airfoil is a process of making compromises. The chosen airfoil should encompass the best of five qualities. Namely, its thickness-to-chord ratio, maximum lift coefficient, stall behavior, and lift and drag characteristics.

Table 9.1: Criteria for Airfoil Selection

Parameter	Desired value
t/c	Higher for structure. Lower for Aerodynamics
Stall characteristics	Gradual
$C_{l_{max}}$	Highest
(C_l/C_d)max	Highest
C_l at (C_l/C_d)max	Highest (closest to cruise CL)
Drag bucket - C_l range	Largest

Airfoil Tradeoff

To choose the most ideal airfoil for the design, it is necessary to perform a tradeoff between some airfoils based on the important criteria that impact the performance and design of the aircraft. Airfoil data from five airfoils, one NACA 5-digit and four NACA 6-digit airfoils are presented in Table 9.2 for a Reynolds number of $1 \cdot 10^6$ [1]. Table 9.3 is the final tradeoff table which uses the percentage change relative to the maximum value to grade the various airfoils. Zero (no deviation from the ideal) is the best possible score in the tradeoff and the lowest score represents the best possible choice.

Table 9.2: Airfoil data used for tradeoff (Re = $1 \cdot 10^6$) [1]

Criteria	NACA 23018	NACA 63(3)618	NACA 64(3)618	NACA 63(4)421	NACA 64(4)421
t/c	0.18	0.18	0.18	0.21	0.21
Stall characteristics	Abrupt	Gradual	Gradual	Gradual	Gradual
$C_{l_{max}}$	1.54	1.55	1.5	1.4	1.37
(C_l/C_d)max	90	133	136	120	123
C_l at (C_l/C_d)max	1.2	1.23	1.24	1.17	1.19
Drag bucket-C_l range	1.3	1.4	1.3	1.73	1.64

Table 9.3: Airfoil deviation from ideal criteria values used for tradeoff

Criteria	Maximum	NACA 23018	NACA 63(3)618	NACA 64(3)618	NACA 63(4)421	NACA 64(4)421
t/c	0.21	14.3	14.3	14.3	0	0
$C_{l_{max}}$	1.82	15.4	14.8	17.6	23.1	24,7
(C_l/C_d)max	136	34	2.3	0	12	9.3
C_l at (C_l/C_d)max	1.2	2.3	1.5	0	6	4.6
Drag bucket-C_L range	1.8	25.7	20	25.7	0	6.3
	Total	91.7 %	52.8 %	57.6 %	41.0 %	44.9 %

With the lowest deviation from the ideal score, NACA 63(4)421 is chosen for its overall good aerodynamic performance, along with the high t/c ratio which increases the second area MOI and hence benefits the wing design. Table 9.4 presents some basic parameters of the chosen airfoil, taken from wing tunnel data [33].

Table 9.4: Wing airfoil parameter

Parameter	Value
t/c	0.21
$C_{l_{max}}$	1.5
C_{l_α}	5.99 [1/rad]

Tail Plane Airfoil

For vertical tails, a symmetric airfoil is chosen mainly due to aircraft symmetry. For horizontal tails, an airfoil is chosen such that it provides good lift performance at positive and negative angles of attack, as well as having a high C_L- α slope and generates lift with minimum drag and pitching moment. Furthermore, the tailplane must be clear of any compressibility effects from the wing (lower flow Mach number), which is achieved by having an airfoil thinner than the wing [25] .

The airfoil chosen for both the horizontal and vertical tail is the NACA 0012 as it satisfies the above requirements for both tail surfaces. Its characteristics are shown in Table 9.5, taken from wing tunnel data [33].

Table 9.5: Tail airfoil parameter

Parameter	Value
t/c	0.12
$C_{l_{max}}$	1.6
C_{l_α}	5.73 [1/rad]

9.2. Wing Aerodynamic Characteristics

The lift and drag characteristics are computed based on the aircraft's mission profile and wing planform. The airfoil C_l- α curve is plotted based on wind tunnel data [33] and the C_L- α curve is computed based on the DATCOM method [34].

The parasite drag (or zero-lift drag) is estimated using the component build-up method, which adds the contributions of the fuselage, wing, empennage and nacelles (and flaps/landing gear for take-off/landing) to the zero-lift drag (C_{D_0}) [19]. The lift-induced drag is calculated using the calculated lift coefficient and the change in Ostwald efficiency factor(e) due to flaps being implemented for takeoff and landing configurations [4]. The wing-tip propellers in the design lead to a reduction in total drag, and therefore a 10 % reduction in drag is taken into account [27]. According to T. Sinnige this is still a conservative estimate, but is chosen as such as no specific flight data for the aircraft is available at this stage.

The aerodynamic parameters in clean configuration are described in Table 9.6 and plotted in Figure 9.3. Furthermore, the lift coefficient distribution (clean) over the span of the wing is given in Figure 9.1.

Table 9.6: Aerodynamic parameters

Parameter	Value	Parameter	Value
$(C_L/C_D)_{max}$	20.5	C_L at $(C_L/C_D)_{max}$	0.78
$C_{L_{Des}}$	0.63	$(C_L/C_D)_{Des}$	20
$C_{L_{max}}$	1.35 (clean) | 2.4 (flaps)	α_{Des}	4 [deg]
C_{L_α}	5.63 [1/rad]	C_{D_0}	0.021
α_{stall}	14.6 [deg]		

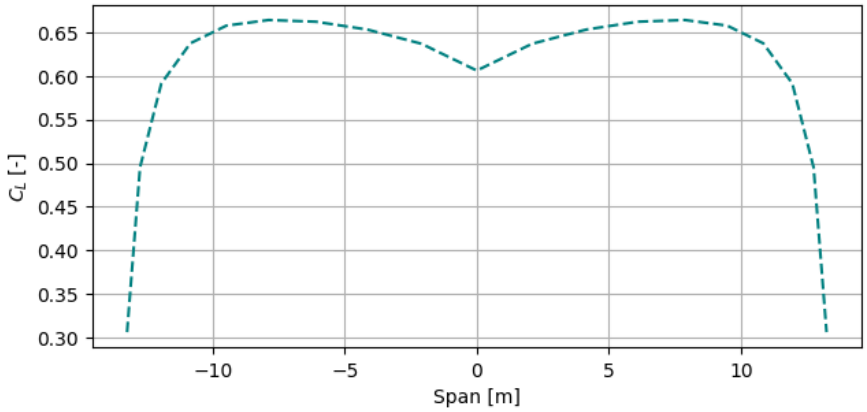

Figure 9.1: Local lift distribution over wing

9.3. High Lift Device Design

The $C_{L_{max.clean}}$ of the wing is stated to be 1.35 as discussed previously, however from the wing loading diagram the design constraint of $C_{L_{max}}$ is 2.4. Hence, the use of high-lift devices with a design ΔC_L of 1.05 is required. The method of designing the high-lift device follows the process presented by F. Olivero [35].

Trailing edge and leading edge high-lift devices are considered while designing the high-lift devices, however, to decrease the weight, mechanism complexity, and maintenance cost, leading-edge high-lift devices are not used. The design choice for the trailing edge high lift device is chosen based on reducing the weight of the high lift device and the mechanism complexity. Hence, the lowest c_f/c and $c^{'}$/c design option is chosen. The high lift device choice characteristics are shown in Table 9.7.

Table 9.7: High Lift Device Design Choice Characteristics

Variable	Value	Variable	Value
Max ΔC_L	1.05	Maximum Deflection	40 [deg]
Flap starting location	1.5 [m]	Flap ending location	7.37 [m]
Flap type	Double Slotted Flap	Swf/S	0.62
c_f/c	0.34	$c^{'}$/c	1.18

For the design choice the retraction mechanism will use the six bar mechanism [36]. The dimensions of the high lift devices could be seen in Figure 9.2.

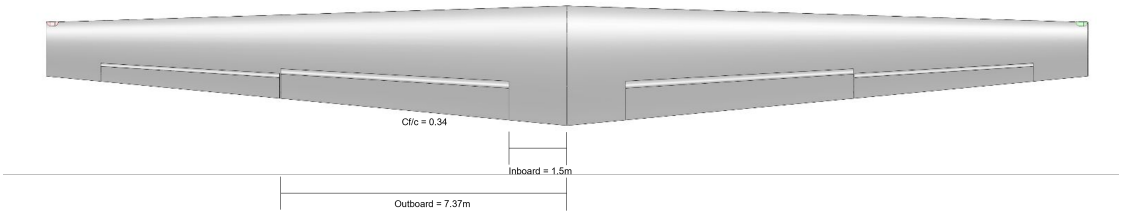

Figure 9.2: High Lift Devices Dimensions

The effect of high lift devices on the lift and drag characteristics of the wing is shown in Figure 9.3 and Table 9.8.

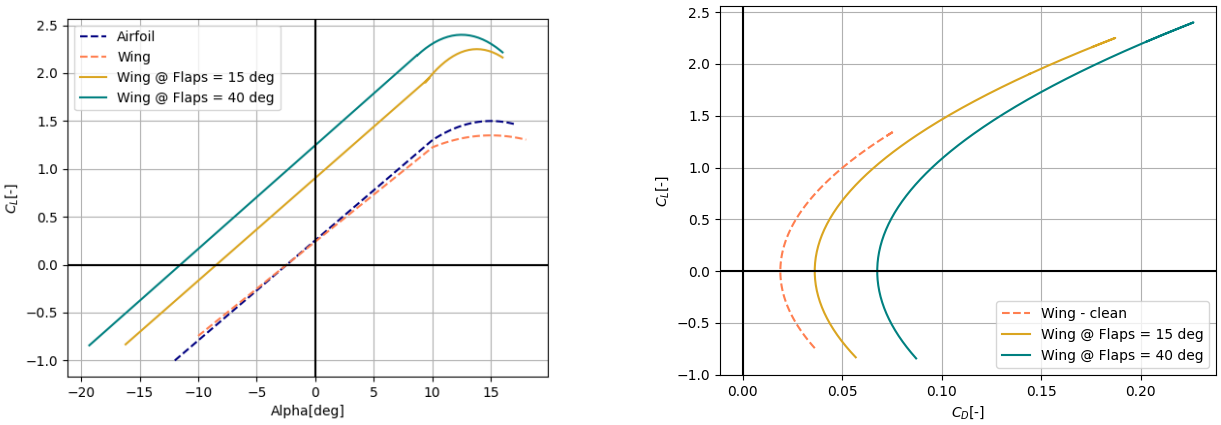

(a) Lift curve

(b) Drag polar

Figure 9.3: Lift and Drag Characteristics

Table 9.8: Effect of High lift Devices on Aerodynamic Parameters

Parameter	Value	Parameter	Value
$C_{D_{0_{f,\ 40deg}}}$	0.075	$C_{D_{0_{f,\ 15deg}}}$	0.04
$C_{L_{max_{f,\ 40deg}}}$	2.4	$C_{L_{max_{f,\ 15deg}}}$	2.25
$(C_L/C_D)_{Max_{f,\ 40deg}}$	11.6	$(C_L/C_D)_{Max_{f,\ 15deg}}$	15.2
C_L at $(C_L/C_D)_{Max_{f,\ 40deg}}$	1.6	C_L at $(C_L/C_D)_{Max_{f,\ 15deg}}$	1.1

The sensitivity of high lift device sizing with regards to a decrease in $C_{L_{max\ clean}}$ has been evaluated. In the situation that the $C_{L_{max\ clean}}$ of the wing is lower than 1.3, a double slotted flaps will still be feasible, however the c_f/c will increase to 0.4. The increase of c_f/c still deem feasible as it is still within the margin within the hinge line and the trailing edge of the wing. Additionally, the likelihood of the $C_{L_{max\ clean}}$ to further decrease is unlikely, as the $C_{l_{max}}$ value is conducted by wind tunnel testing.

[1] http://airfoiltools.com/

10 Structures & Materials

Designing the airframe structure is one of the most difficult and detailed phases of aircraft sizing. This chapter aims to provide an overview of the initial wing box design together with the integration of the empennage, fuselage and hydrogen storage tank. Finally, a material selection is made for the main components of the aircraft, mainly focusing on cost and sustainability.

10.1. Airframe Design

Wing

To be able to approach the wing box structure, the span was split into nine sections to simulate taper. This gives a general approximation of the required components to be able to sustain the loads. The spars are assumed to be placed at 0.15 and 0.6 chord length. From an initial analysis of the loads acting on the wing the top flange of the front spar is assumed to be critical, thus driving the design. In order to size the wing box structure, the loads on the wing need to be determined. In Table 10.1 the maximum loading is determined by comparing the load factor at OEM and at MTOM together with the loading diagram in Section 16.2. These load factors are from the gust and maneuver envelope, Figure 16.2. Thus by taking the ultimate loads as the design load, the structures are sized such that the design complies with requirement **RA-SYS-SRE-4**.

Table 10.1: Maximum Wing Loading

	MTOM	OEM
Load Factor	2.64	3.25
Total Load	483 [kN]	407 [kN]

To calculate the bending moment distribution, the lift generated by the wing and its structural weight are considered as well as the weights of the engines. The lift is modelled as ten point loads along the half-span derived from the lift distribution. The weight of the wing structure is also modelled as ten point loads at the same location as the lift point loads. The magnitude of these loads are scaled based on the chord length over the span and such that the total weight of all points combined is equal to the structural weight estimation. The weight of the inner and outer engine are added to the nearest wing weight point load. The resultant bending moment is then computed for the 10 points along the half-span using Figure 10.1:

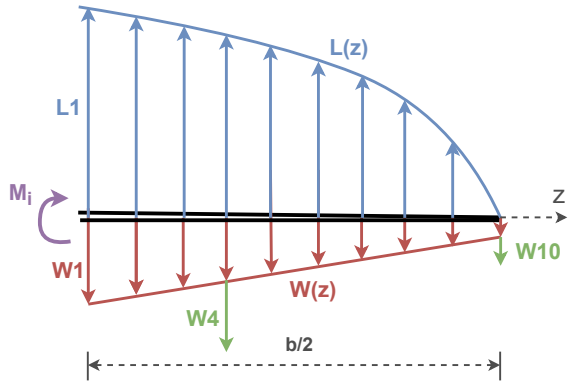

Figure 10.1: Free body diagram of the half-wing with the considered loads (not to scale)

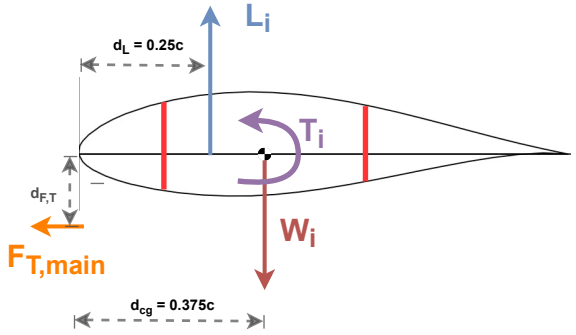

Figure 10.2: Free body diagram of the wing cross section at the main engine with the considered loads (not to scale)

$$M_{\mathrm{i}}(z) = (L_{\mathrm{i}} - W_{\mathrm{i}}) \left(\frac{b}{2} - z_{\mathrm{i}} \right) \tag{10.1}$$

$$W_{\mathrm{i}}(z) = D_{\mathrm{i}}(z)(z_{\mathrm{i=1}} - z_{\mathrm{i}}) \tag{10.2}$$

The resulting diagram can be found in 10.3. The shear force diagram is obtained by taking the derivative of the bending moment diagram. To calculate the torque distribution, the center of gravity is assumed to be on the center line of the wing cross section and in the midpoint between the front and aft spar. The lift along the span and thrust of the inner engine are considered, where the lift is assumed to act on quarter chord, and the perpendicular distance from the thrust vector to the center line is obtained from the SRP-22 technical drawing, found in Figure A.4. The torque is then calculated for all ten points using Equation 10.3 (where c_{i} is the local chord.) and plotted in Figure 10.3.

$$\begin{aligned} z_1 \leq z_{\mathrm{i}} \leq z_4 \qquad & \qquad z_4 \leq z_{\mathrm{i}} \leq z_{10} \\ T_{\mathrm{i}} = F_{\mathrm{T,main}} \cdot d_{\mathrm{F,T}} + 0.125 c_{\mathrm{i}} \cdot L_{\mathrm{i}} \qquad & \qquad T_{\mathrm{i}} = L_{\mathrm{i}} \cdot 0.125 c_{\mathrm{i}} \end{aligned} \tag{10.3}$$

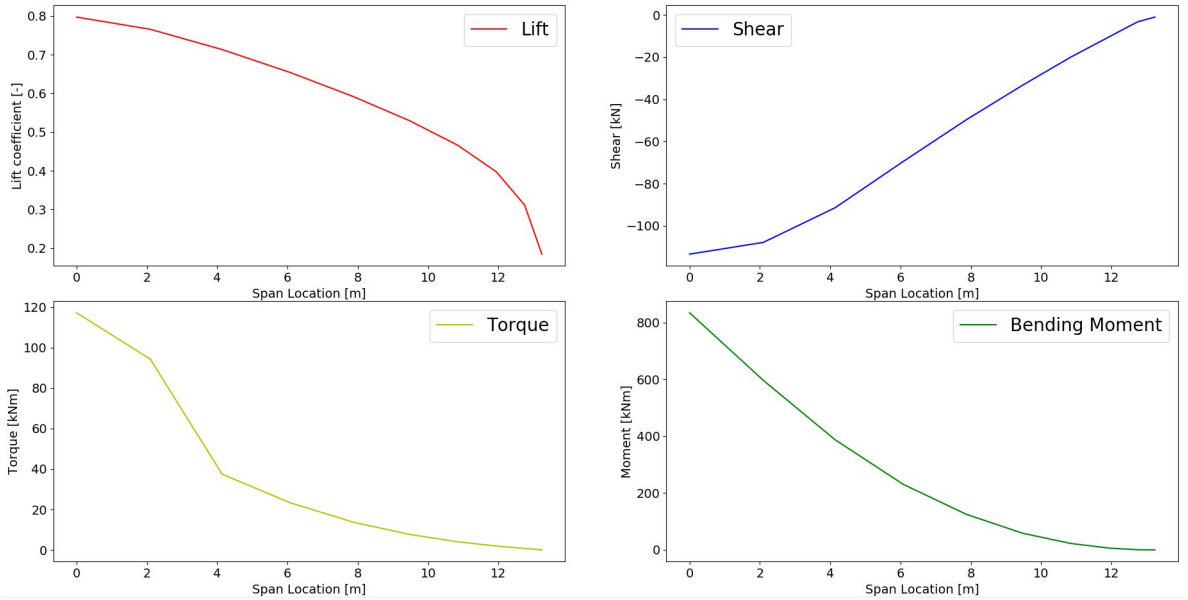

Figure 10.3: Loading diagrams of the wing over the half span

For the structural wing design 2024-T3 aluminium alloy was used[6]. This has a density of 2840 kg/m^3, tensile yield strength of 352 MPa, shear yield strength of 285 MPa, E modulus of 73.1 GPa and a poisson's ratio of 0.33. Next, using the moment diagram in Figure 10.3, the required second area of inertia could be determined, such that the yield strength would not be reached in the skin (assuming safety factor 2.0). From this the spar, assuming an I beam shape, could be sized. The spar height and width tapers with the chord length, whereas the thickness for the web and flange are assumed to be constant. A general overview of the height, width and thickness of all components in the wingbox are presented in Table 10.2.

Table 10.2: Wing Structure Components

	Thickness [mm]	**Height**	**Width**
Front Spar	Web = 8.0 Flange = 10.0	0.17 $\cdot ch_{\mathrm{l}}$	0.25 $\cdot sp_{\mathrm{h}}$
Aft Spar	Web = 8.0 Flange = 10.0	0.15 $\cdot ch_{\mathrm{l}}$	0.25 $\cdot sp_{\mathrm{h}}$
Ribs	3.0	$0.18 \cdot ch_{\mathrm{l}}$	$0.45 \cdot sp_{\mathrm{h}}$
Stringers	2.0	2.0 [cm]	2.0 [cm]

The ch_l stands for the chord length at a certain wingspan and the sp_h the spar height at a certain wingspan. Most components were scaled by fitting them into the airfoil and assumption by literature. The web and flange thickness were calculated by the taking the required second area of inertia, deducting the skin second area of inertia and thus resulting in the required spar second area of inertia. Optimizing this shape for second area of inertia/weight and shear results in a web thickness of 10.0 mm and 12.0 mm for the flanges. Next, using Equation 10.4 the rib spacing could be calculated. due to the simplified approach of the wingbox in nine section, the spacing does not perfectly align along the span. The results can be found in Table 10.3.

$$b = \sqrt{\sigma \cdot \frac{\pi^2 \cdot E_{\mathsf{Al}}}{(1-v^2)} \cdot t_{\mathsf{skin}}^2} \tag{10.4}$$

Finally, the stringer pitch could be determined. This spacing has the same inconsistency due to the simplified wing box approach. By applying Equation 10.5 the spacing can be calculated, using $K_{\mathsf{c}} = 6.32$ due the b/t ratio as found in "Airframe stress analysis and sizing" page 610 [37]. The results can be found in Table 10.3 and a cross-sectional view in Figure 10.4.

$$b = \frac{t_{\mathsf{skin}}}{\sqrt{\frac{\tau}{K_c \cdot E_{\mathsf{Al}}}}} \tag{10.5}$$

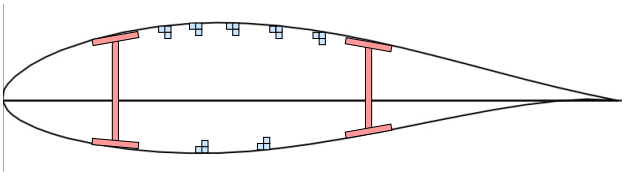

Figure 10.4: Airfoil Cross-section with Stringers at Spanwise Location $9.4m$

Due to the wing not having any bending relief due to fuel storage in the wing, the wing weight is expected to be higher that of aircraft that store fuel in the wing. Using the data from Table 10.3 the weight of the wing box is estimated to be **1265 kg**. Using the relation from the Journal of Aerospace eq. 56 [38], the wing box weight and total wing weight are related with a factor 1.73, resulting in an estimated total wing weight equal to **2188 kg**

This is just below the estimate from the Class II weight estimation using Torenbeek's method in Chapter 7 [20]. However, the estimation of the wing structure is not optimized, as this would require a detailed design.

Table 10.3: Skin Thickness, Rib and Stringer Spacing of the Wing Box

Spanwise Loc. [m] from the Root	**Skin Thickness [mm]**	**Rib Spacing [m]**	**Stringers [-] Top Flange**	**Stringers [-] Bottom Flange**
0.0	3.0	0.44	25	14
2.1	2.5	0.45	25	14
4.1	1.7	0.63	25	13
6.0	1.0	0.72	25	11
7.8	1.0	0.84	22	10
9.4	1.0	1.02	18	7
10.8	1.0	1.27	13	2
11.9	1.0	1.6	6	-
12.7	1.0	-	2	-
13.2	1.0	-	-	-

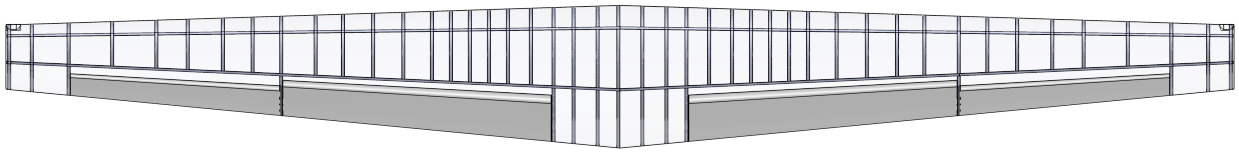

Figure 10.5: Wing Structure Design Overview

Fuselage

The initial part of structurally designing the fuselage structure is determining the load cases and determining the ultimate load. for the loading analysis, the weight, gust, symmetrical horizontal tail deflection, rudder deflection, and side slip are considered. From this analysis, it was concluded that the skin at the top of the fuselage would be the most heavily loaded in compression, caused by maximum horizontal tail control surface deflection force, maximum gust loading at OEM and the weight of the empennage considering no cabin pressurization. By applying the method in "Aircraft Fuselage Design Study"[39], a maximum moment of $1.1 \cdot 10^6$ Nm was determined.

The fuselage structural design was mainly done for bucking of the fuselage skin. The skin thickness was set at 2.5 mm. The surface area of a stringer was assumed to be $2.3 \cdot 10^{-4}$ m^2, deducted from the stringer dimensions of a KC-135[5]. Through an iterative process of increasing the number of stringers to be able to not reach the aluminum alloy yield strength (safety factor 2.0) and optimizing for buckling, done with Equation 10.4. This resulted in a fuselage stringer pitch of 0.18 m.

For the frames, a similar approach was applied as for the ribs in the wing structure. This requires an estimate of the maximum torsion. This torsion is caused by rudder deflection, slide slip, and weight when the aircraft is at a bank angle. This caused torsion of $43 \cdot 10^3$ Nm. By using Equation 10.5 the frame spacing was determined to be 0.53 m.

Finally, around the windows, doors, and emergency exits reinforcement is necessary due to the cut-outs. In Figure 10.6 a general overview of the stringer and frame spacing is presented together with the reinforced area around a window. For the entire fuselage structural layout, Appendix A should be consulted.

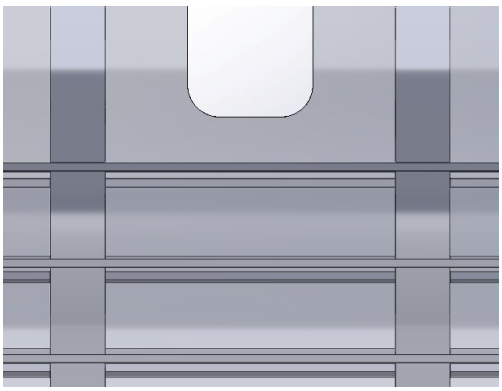

Figure 10.6: Fuselage Structural Layout Showing Frame and Stringer Pitch

Empennage

The empennage structural design methodology is similar to that of the wing. The detailed structural design was not performed for the empennage, as it was deemed to be of little importance for the conceptual design. The most important aspect was the integration of the empennage spars into the fuselage around the hydrogen storage tank, as seen in Figure 10.7.

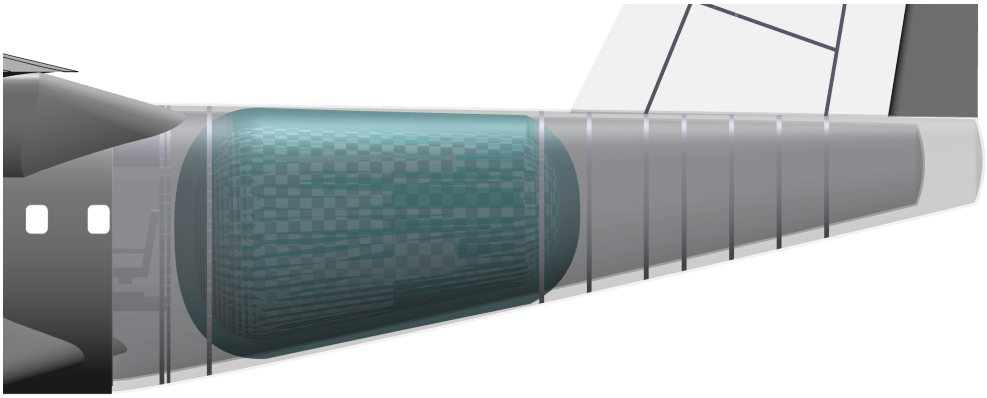

Figure 10.7: Empennage structural integration

It becomes clear that the empennage spars enter the fuselage structure aft of the entire hydrogen storage structure. Therefor, it is assumed that the empennage can be integrated into the airframe in a conventional manner.

Undercarriage

The landing gear is one of the most critical components in an aircraft, and an undercarriage collapse can be critical upon landing or takeoff. It is therefore important to size the struts according to the possible loads and forces that are to be endured, as these bear most of the loads upon landing and braking. Upon braking, the main landing gear strut bears a force of 1.5 times the static load whilst the nose landing gear bears a force of 0.2 times the static load

Thus, struts should be made of a durable, resistant material which is at the same time lightweight and inexpensive. Assuming the struts have a circular cross section, and are of cylindrical shape, the following equation may be used to calculate the stress to be endured by the struts:

$$\theta_{\text{strut}} = \frac{F_{\text{y}}}{A} + \frac{M \cdot R}{I} \tag{10.6}$$

A viable option could be the use of Titanium 10Al-2Fe-3V, which has a large safety factor, whilst still having the lowest value of maximum stress and deflection developed, which avoids structural failures.

10.2. LH2 Storage Tank

The tank designed to store the liquid hydrogen is made with a carbon fibre reinforced polymer (CFRP). The implementation of CFRP is currently being researched and first prototypes have been presented, showing the feasibility of this technology[1]. CFRP has a density of about 1800 kg/m^3, a yield strength of 550 MPa and a thermal conductivity of 0.3 W/m$\cdot$ K [40] [2] [3]. From multiple studies into the implementation of hydrogen tanks into aircraft, it is determined that an aft-placed storage tank is the best option for a regional aircraft [41]. Moreover, a choice must be made between an integral or non-integral tank. An integral tank is generally heavier as it is load-bearing, but requires less volume in the fuselage [42]. The decision was made to have a aft-mounted integral tank in the tail cone.

Pressures and Forces

To be able to integrate the tank into the aircraft an overview of the forces acting on the structure is provided. The loads during flight are considered to be the weight of the empennage, part of the fuselage aft of the tank and the forces caused by the control surfaces on the empennage. For simplicity the tank is uniformly designed for the ultimate load that it must be able to transfer. The ultimate load is on the tank is near the top and bottom of the tank, mainly due to bending and torsion. During a pull-up manoeuvre will cause the weight aft of the tank to create a large bending moment. The weights of the empennage and fuselage are determined using the statistical group weights method from Raymer [19]. the c.g. location of the tail cone is assumed to be 1/3 (that of a hollow cone) of the fuselage length aft of the tank. The horizontal and vertical tail planes both have their c.g. at 0.4 of the chord length. For the loads caused by the lift of the

tail plane and control surfaces, the analysis estimates a force of about 96 kN on the horizontal tail surface. This combined with bending caused by weight results in a moment around the lateral axis of 560 kN· m.

After determining the tank thickness necessary to carry the forces acting on the aircraft, the thickness accounting for the pressure differnces can be computed. Table 10.4 shows the different pressures accounted for during tank design.

Table 10.4: Pressures used for Tank Design

Filling	Venting	Cruise	Hydrostatic	Ultimate △Pressure
1.2 [Bar]	3.0 [Bar]	0.3 [Bar]	0.2 [Bar] [43]	2.9 [Bar]

Next the thickness of the outer shell can be determined. The thickness required for the bending load is calculated using the equations in chapter 6, Mechanics of Materials [44]. The thickness for the pressure difference is calculated using Equation 10.7:

$$t_{\text{pres}} = \frac{\Delta P_{\text{max}} \cdot r_{\text{shell}}}{\sigma \cdot e_{\text{w}}} \tag{10.7}$$

e_{w} is the safety factor of 0.8 used for pressurized tanks [41]. The overall thickness, taking a safety factor of two, is equal to 5.6 mm. This thickness is for the entire tank, as the caps are ellipsoids with a radius ratio of 2:1, is equal for the conical part and caps. The ellipsoid cap shape is chosen due to its weight en shape characteristics which are beneficial for the integration of the tank [45].

Fuselage Integration

To structurally integrate the tank, carbon fiber composite rods are used to connect the tank with the aluminium fuselage airframe. Connecting these materials can cause corrosion, but can be mitigated using solid state welding [46]. As the CF composite rods have a low thermal conductivity, equal to the storage tank, it conducts little heat the aluminium fuselage structure into the tank. The rods are connected to the tank such that they act as a truss structure. The rods and tank will be surrounded by insulation material, which is covered with a thin layer of composite skin such that the fuselage has a smooth surface. The integration of the hydrogen storage tank can be found in Figure 10.8

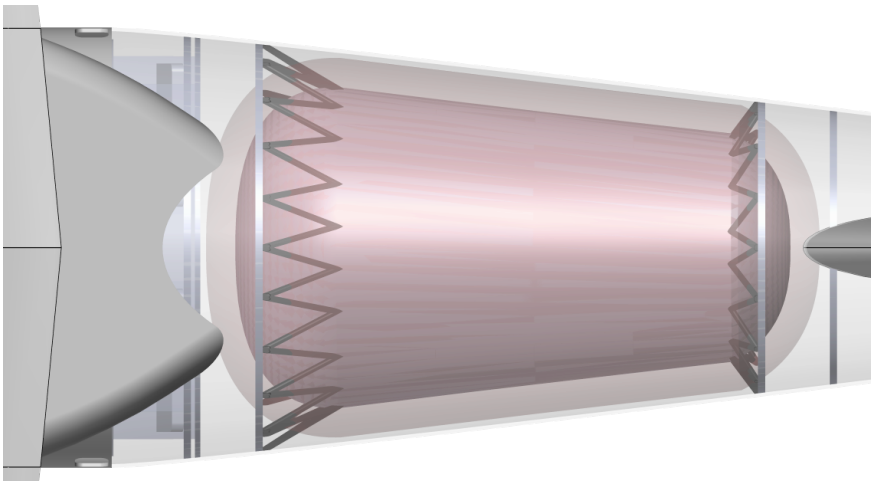

Figure 10.8: Top view of LH2 Storage Tank Fuselage Integration

Thermal

For the insulation of the tank EPS is selected. This material is chosen due to its low thermal conductivity of 0.0037 W/m· K and relatively low density of 26 kg/m^3 [4]. An alternative is insulation by MLI. This new insulating technology using a vacuum is determined not to be favorable for the application in aircraft due to its catastrophic failure nature and its constant servicing to maintain the vacuum [47]. Moreover, it is generally heavier than EPS for the same thermal resistance, but less voluminous. As this technology is not

readily available and much more complicated than using EPS, for this conceptual design it was discarded.

Determining the insulation thickness is an iterative process, depending on the allowed heat flow into the tank. If too much heat gets into the tank it will cause excess boil-off, increasing the pressure in the tank. Using the allowed boil-off rate for the propulsion system from Chapter 12, the allowed heat flow can be determined, resulting in a required thickness of 13 cm. However, this is not considering the thermal conductivity of the structure connecting the tank to the fuselage and other unforeseen heat flow. Therefor a safety factor of 1.5 is applied, ultimately resulting in a thickness of 20 cm.

Tank Weight and Geometry

The tank is sized to fit into the tailcone of the aircraft. This requires the tank to taper at approximately the same rate as the outer skin of the fuselage, angle of 14°, as can be seen in Figure 10.8. A general overview of the geometry of the tank, together with the weight estimation are presented in Table 10.5, The tank is designed to carry 683 kg of hydrogen, needing a volume of 9.9 m^3 (including a 3% margin).

Table 10.5: LH2 Storage Tank Weight and Geometry

	Thickness [mm]	Diameter [m]	Length [m]	Mass [kg]
Front Cap	5.6	2.27	0.57	98
Aft Cap	5.6	1.16	0.29	291
Conical Section	5.6		2.7	48
Complete Tank	5.6		3.56	437

Each section mass is including the insulation mass. The gravimetric index, defined as $\frac{m_{\text{tank}}}{m_{\text{fuel}}}$, of the tank (without insulation or regulation systems) is estimated to be 0.64, relatively inline with the reference composite tank design[1]. Moreover, a tank divider is included such that the tank is split into two tanks, necessary to comply with CS-25 regulations. Adding frames, stringers, insulation and environment control subsystems would likely increase the total mass significantly, resulting in a gravimetric index of 1.4-1.8 [48]. For the aircraft design a gravimetric index of 1.4 was selected for the entire storage system, resulting in a total tank mass of 956 kg.

10.3. Materials

The material selection for SRP-22 are chosen for optimal performance and by taking the following requirements and design objectives into account:

RA-TOP-COS-1: The aircraft shall have a maximum asking unit price of 31 million USD.

RA-OBJ-1: Minimize the environmental impact of the entire aircraft life-cycle.

RA-OBJ-2: Minimize the usage of hazardous materials.

Airframe

Aluminium alloy 2024-T3 is chosen for the majority of the airframe, for its high strength-to-weight ratio, high fatigue resistance, excellent toughness and high maturity with regards to manufacturing in aerospace applications. Moreover, it has very high recyclability. The use of composites in the airframe has been omitted due to lower recyclability, higher cost and more complex manufacturing process.

Landing gear and pylons

Titanium alloy 10Al-2Fe-3V is used for the landing gear and pylons, since these components contain critical load paths, making this high strength titanium alloy very suitable. It also has excellent corrosion resistance and high recyclability. Titanium 10Al-2Fe-3V is more expensive and more difficult to fabricate than Aluminium alloy 2024-T3, therefore is chosen to use this material exclusively for these components.

Hydrogen tank

The rationale for the material selection for the hydrogen storage tank are described in Section 10.2. EPS is fully recyclable, while carbon fiber reinforced plastic (CFRP) is currently not commonly recycled industrially.

However, extensive research is conducted on its recyclability with promising methods as a result. It is therefore assumed that by the end of the lifetime of the first SRP-22 aircraft, CFRP is 90% recyclable.

Miscellaneous

The propulsion system is mostly composed of off-the-shelf products as described in Chapter 12. Electric motors and other electric systems are mostly composed of metals such as steel and copper that have high recyclability. Fuel cells in addition also contain precious metals, which are already recycled up to 90% currently. The cabin interior will be fully composed of recycled materials, such as thermoplastics and recycled fabrics.

This material selection results in an overall End-Of-Life recyclability of at least 91%. An overview of selected materials can be found in Table 10.6, and a visualization of the main structural materials is presented in Figure 10.9.

Table 10.6: Materials used in SRP-22

Component	**Principal material**	ρ **[kg/m^3]**	σ_y **[MPa]**	m **[kg]**	**Fraction of OEM [%]**	**Recyclability [%]**
Airframe				**8300**	**66**	**92**
Fuselage, wing, empennage	Al 2024-T3	2780	345	6800	54	93
Landing gear, pylons	Ti 10Al-2Fe-3V	4650	1170	1500	12	90
Hydrogen tank				**950**	**7.6**	**92**
Tank structure and integration rods	CFRP	1800	550	800	6.4	90
Insulation	EPS	26	-	150	1.2	100
Miscellaneous				**3000**	**24**	**97**
Cabin interior	Thermoplastics and fabrics	-	-	1000	8.3	100
Fuel cells	Steel, precious metals	-	-	800	6.4	95
Electric motors, electronics, avionics	Copper, steel	-	-	1200	9.6	95
Total				**12250**	**98**	**91**

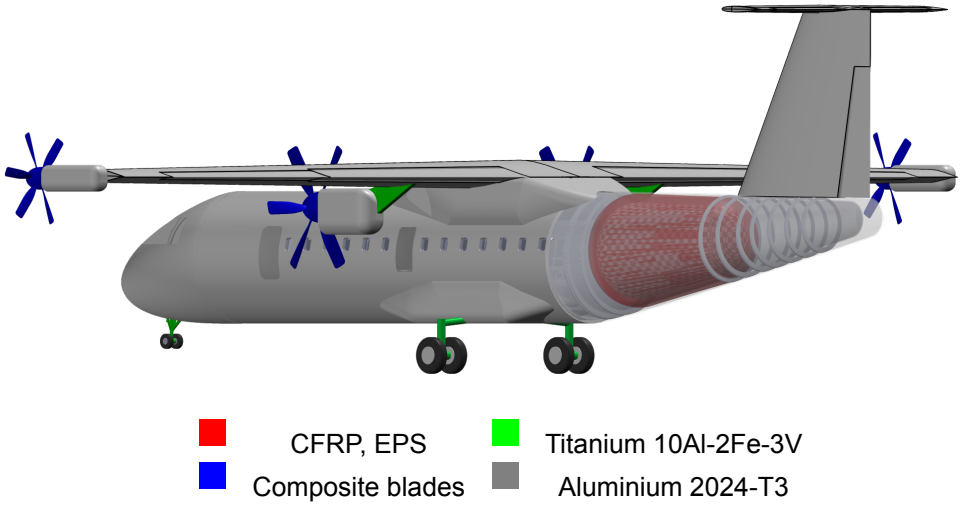

Figure 10.9: Materials used in the airframe, propellers and tank of the SRP-22

Lightning Protection

As dictated by requirement CS 25.581, **RA-SYS-SRE-3** in the requirement list, the aeroplane must be protected against the catastrophic effects from lightning. This can be shown by designing the components in such a way that the strike does not endanger the aeroplane.

Firstly, the skin around the cabin and interior compartments is designed with a metallic mesh which provides an additional layer of protection, conducting electricty through the exterior protecting the passengers, crew, and avionics. This not only prevents damage to the structure but also prevents the buildup of electric current in any one area. Additionally, areas that are more prone to receive lightning strikes are further protected with the following features:

1. **Wire Bundle Shields**: This especially protects the avionics and flight control system, which could be easily destroyed by a lightning strike and cause critical damage. Special shield protection is installed in wiring such that no damage occurs
2. **Static Dissipators**: These are metallic pieces connected electrically to the frame of the aircraft, with spikes or needles on the end. It is housed in a fiberglass rod to insulate it from the airplane. Because the spikes concentrate the electric charge around them, and they are connected to the airframe, they allow the airplane to dissipate any static electricity it may build up out into the air. If lightning does strike the plane, the electricity will go through the dissipator and not through the airplane by reducing the electric field to below lightning-collection levels, within the protected area.

[1]URL https://newatlas.com/aircraft/hypoint-gtl-lightweight-liquid-hydrogen-tank/ [cited 13 Jan. 2023]
[2]URL https://www.christinedemerchant.com/carbon_characteristics_heat_conductivity.html [cited 13 Jan. 2023]
[3]URL https://www.chemeurope.com/en/encyclopedia/Carbon_fiber.html [cited 13 Jan. 2023]
[4]URL https://omnexus.specialchem.com/selection-guide/expanded-polystyrene-eps-foam-insulation [cited 18 Jan. 2023]
[5]URL https://www.researchgate.net/figure/Dimensions-of-stringer-and-frame-for-the-KC-135-fuselage-panel-dimensions-in-inches-1_fig6_253689277 [cited 19 Jan. 2023]
[6]URL https://asm.matweb.com/search/SpecificMaterial.asp?bassnum=MA2219T851 [cited 19 Jan. 2023]
[7]URL https://www.appropedia.org/Composites_in_the_Aircraft_Industry [cited 20 Jan. 2023]
[8]URL https://aviation.stackexchange.com/questions/81661/materials-usually-used-in-dorsals-fins-specifically-in-the-atr-72 [cited 20 Jan. 2023]

11
Electrical Systems

The aircraft's electrical systems are one of the most important systems in an aircraft. This includes the exterior lighting, anti-icing, anti-rain and anti-fog systems, autopilot and of course the electrical block diagram.

11.1. Lighting System

Exterior Lighting

The lighting of an aircraft is a key system. External lights are required for safety purposes as they are used to alert the personnel working around the aircraft in low light hours. They also allow aircraft identification in flight, and some lights also help the pilots to navigate the aircraft on the ground and help to view certain structures of the aircraft. According to EASA - SERA regulations, these are the following lights needed by the aircraft, which will be applied to the aircraft, in order to comply with **RA-SYS-SRE-1**.

1. **Anti Collision Lights**
   (a) **Beacon**: In normal operations, these red flashing lights located in the fuselage belly and horizontal stabilizer are used during ground and flight operations.
   (b) **Strobes**: Located in the wingtips and below the tailcone, these very bright synced flashing lights are only used upon line-up and takeoff
2. **Navigation Lights**: Made to be able for an observer to identify the aircraft's direction, these consist of three lights; the port, or left wingtip which should be red. the starboard, or right wingtip which is green and a white rear tailcone light.
3. **Landing Lights**: These are integrated in forward part of the sponson belly, provide enough light for night landing without glare / halation for pilots.
4. **Taxi Lights**: These help the pilot to navigate during airport taxiing, located in the nose landing gear strut.
5. **Take-Off lights**: These are also located in the nose landing gear strut, and have longer beams.
6. **Logo Lights**: Placed on horizontal stabilizer, these illuminate the company logo and attract attention towards the aircraft.
7. **Wing Engine inspection Lights**: Located in the fuselage, these light up the engines and wings without excessive glare

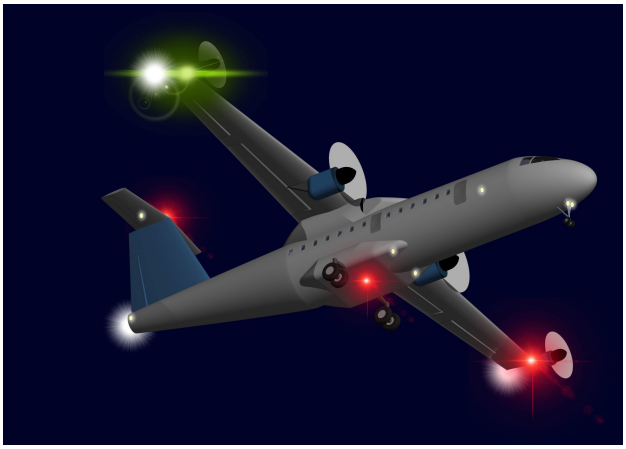

Figure 11.1: All Relevant Exterior Lights

11.2. Anti-Icing, Anti-Rain and Anti-Fog systems

It is expected that the SRP-22 also operates under challenging conditions such as ice, heavy rain, and fog. Consequently, special systems to alleviate the effect of these conditions have to be designed.

Anti-Icing System

In order to prevent the accumulation and formation of ice in critical aircraft systems an anti-icing system may be used. The formation of ice can have catastrophic consequences such as degradation of flight performance, malfunction of critical systems, and even result in accidents.

The SRP-22 is equipped with Electro-Impulse de-icing systems, which operate by delivering mechanical impulses to the surfaces on which ice has formed, such as the wing leading edge, and vertical and horizontal tailplane. These impulses are generated by electromagnetic coils which can be installed on these surfaces. Additionally, a thermal electric system can also be implemented in order to prevent ice formation on other critical systems such as pitot tubes, stall vanes, and total air temperature probes. Thus, complying with **RA-TOP-SRE-3**.

Anti-Rain and Anti-Fog System

When flying through severe rain it is quite possible that rain accumulates on the windshields and thus pilot visibility is severely reduced. In order to avoid this, a simple windshield wiper is installed on the windshield exterior, as well as rain repellent adhesives on the wiper paths.

Additionally, under certain humidity conditions, fog can form on the inside and outside of the windshield. In order to avoid this, special electrical wiring is installed inside the windshield material.

11.3. Autopilot

When the autopilot is engaged, the Autopilot servo provides inputs to the yaw, roll, and pitch to the rudder, aileron, and elevator. Additionally, just like in the Cessna Citation II, the autopilot commands may be overridden at any time by the pilots.

Additionally, being an irreversible flight control system, the control surfaces are not directly linked to the controls. Meaning that at the flight controls, the aeroforces at the surface cannot be felt. In this case, there is a hydraulic power control unit in between the actual surface and the cockpit controls, as depicted by Figure 13.3

Regarding the navigation, the autopilot may also be used to set a given heading, speed, vertical speed, and altitude as well as set to follow a certain route. Additionally, in order to comply with **RA-TOP-SRE-2.1** research in the necessary instruments and equipments will be performed for day and night rules. Furthermore, research on the landing requirements for the instrumentation for the IFR compliance will be done with respect to requirement **RA-TOP-SRE-2.2**.

11.4. Electrical Block Diagram

All the above systems that require electricity discussed in Chapter 12, Chapter 20 and Chapter 11 are shown in the electrical block diagram Figure 11.2.

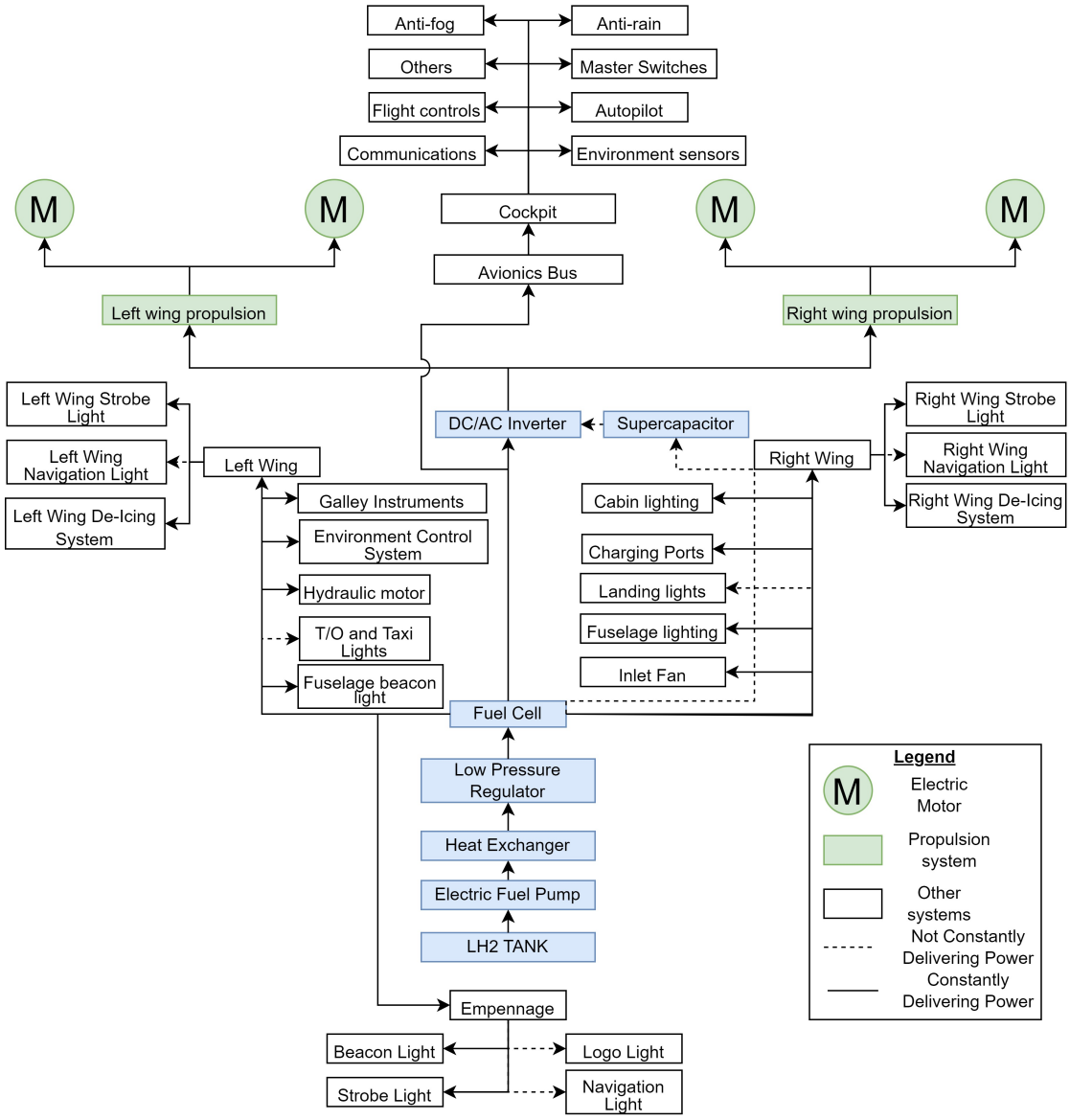

Figure 11.2: Electrical Block Diagram of the SRP-22

12
Propulsion

Together with the design of the liquid hydrogen storage tank, the propulsion system is where the bulk of the innovation of the SRP-22 lies. The purpose of this section is to design, size, and select multiple components that will propel the aircraft from take-off to landing and through its cruise altitude and velocity while maintaining net greenhouse emissions at zero during all phases of operation. To do this, a fuel cell powertrain is sized and selected, along with the design of the air inlets, motor configuration, and propeller sizing.

12.1. Power Requirements

To size the propulsion system accordingly, it is necessary to have an overview of the power consumption of the aircraft. The power estimations are split it up into multiple components.

Propulsion Shaft Power

The shaft power is sized based on the maximum power required to take off, as this is the limiting factor. This is derived from the design Power-to-weight ratio through the following equation, giving a maximum value of approximately 2395 kW.

$$P_{\text{p}} = \frac{W_{\text{TO}}}{W/P_{\text{Des}}} \tag{12.1}$$

Cabin Electrical Power

Due to the limited information openly provided by aircraft manufacturers, it is hard to estimate the power consumption of in-flight systems. As a first, generic estimate, the following values are used:

- Environmental Control System: 24 kW
- Cabin lighting (cockpit, galley, aisle, bathroom, seat belt, and individual reading lights) [49]: 20 kW
- Galley instruments (oven, hot beverage maker, water heater, air chilling unit) [50]: 9.5 kW
- Charging ports [1]: 4 kW
- Inlet fan (Equation 12.3): 1 kW

This is brings the total cabin electrical consumption to an approximate value of 60 kW. As a reference, the total power consumption of the aircraft would hypothetically peak when the aircraft delivers maximum propulsive power, all cabin lights are on, cabin heating is on, and all charging ports are in use. This brings the peak required power to approximately 2455 kW.

12.2. Fuel Cell

The central focus of the propulsion system revolves around a proton-exchange membrane fuel cell, which is an electro-chemical device that extracts electricity from a redox chemical reaction [51] - to produce:

$H_2 + \frac{1}{2} O_2 \longrightarrow H_2O$ with biproducts heat and extracted electricity

Based on the aforementioned characteristics as well as power requirements, the fuel cell chosen is the Horizon VLS-III series Liquid-Cooled Stack [2], which has the following characteristics:

Table 12.1: Horizon VLS-III Characteristics and Configuration

Parameter	Value	Unit
Rated power	250	[kW]
Number of cells	500	-
Cell voltage (avg.)	0.7	[V]
Operating temp.	70-85	[°C]
Min. low temp. start	< 30	[°C]
Dimensions (l · w · h)	837 · 552 · 266	[mm]
Efficiency	0.67	-
Mass	80	[kg]
Number of stacks chosen	10	-
Total available power	2.5	[MW]
Total weight	800	[kg]
Total volume	0.123	[m^3]

12.3. Air Inlets

The air inlets provide a source that conducts atmospheric air for use as a reactant in the fuel cell, as well as to pressurize the aircraft cabin. The general architecture of the inlets is portrayed in Figure 12.1.

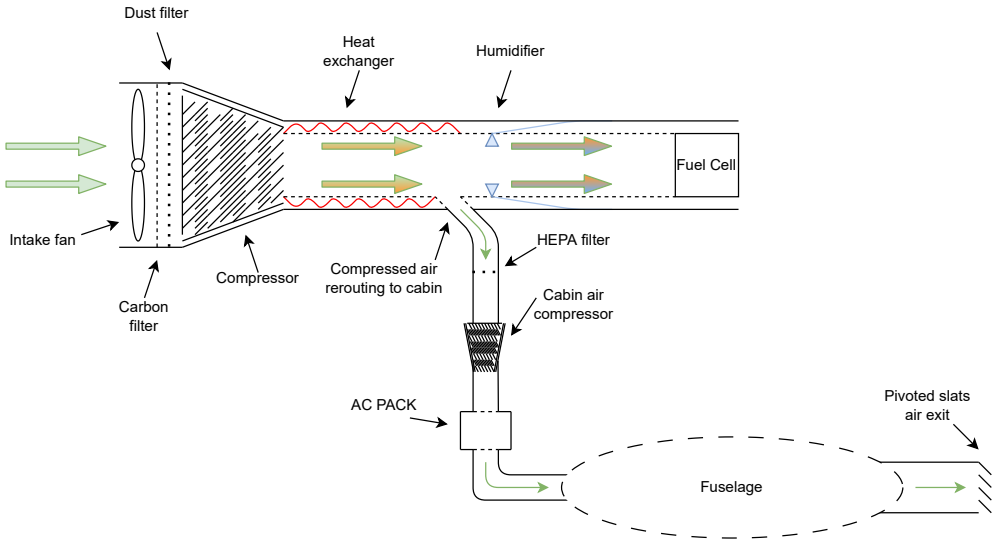

Figure 12.1: General Inlet Architecture (not to scale) [own work]

Cabin Pressurization

CS-25 regulations state that each compartment must have enough fresh air (but not less than 0.28 m^3/min.) per member (section AMC 25.831) [1]. Assuming a cabin air density equal to an altitude of 2000 m (ρ = 1.007 kg/m^3), an airflow of 0.282 kg/min. must be provided per occupant, thus totaling 0.24 kg/s for the entirety of the cabin.

Oxygen Fuel for Fuel Cell

The oxygen content required to power the fuel cell is calculated through the following [21]:

$$\dot{m}_{O_2} = \frac{M_{O_2} \cdot P}{n \cdot F \cdot V_{cell}} \tag{12.2}$$

where M_{O_2} is the molar mass of oxygen, P is total power required (followed from Section 12.1), n is the number of electrons per mole involved in the reaction, F is the Faraday constant, and V_{cell} is the individual

cell voltage. However, the mass flow must be adjusted to compensate for the concentration of oxygen in the ingested air, as well as the oxygen stoichiometric ratio in the reaction:

$$\dot{m}_{\text{air}} = \frac{\dot{m}_{\text{O}_2} \cdot \lambda_{\text{O}_2}}{g_{\text{O}_2}} \tag{12.3}$$

where λ_{O_2} is the oxygen stoichiometric ratio (taken from [52]), and g_{O_2} is the mass fraction of oxygen in air. This gives a required air flow of 6.88 kg/s.

Inlet Sizing

The inlet is designed so that - only during ground operations - fans are required to be in operation to ensure sufficient air. The inlets are integrated as protrusions on the fuselage. To calculate the inlet area, the mass flow rate formula is used. However, due to the position of the inlets near the fuselage, the free stream velocity of air cannot be used due to interference with the boundary layer. It is necessary to therefore calculate an average velocity of air based on the protrusion of the intake with respect to the boundary layer. To minimize an increment of drag, the protrusion of the inlet is sized to be the thickness of the boundary layer. The average flow velocity for a given protrusion ratio can be calculated by integrating the 1/7-power law velocity profile [3] [53]:

$$V_{\text{avg}_{\text{BL}}} = \int_0^h V_\infty \cdot \left(\frac{y}{\delta}\right)^{\frac{1}{7}} = \frac{7}{8} \cdot V_\infty \cdot \left(\frac{h}{\delta}\right)^{\frac{8}{7}} \tag{12.4}$$

Using a protrusion ratio of 1 $\left(\frac{h}{\delta}\right)$ and a free stream velocity equal to the lift-off true airspeed, the average boundary layer velocity can be used to calculate the inlet area through the aforementioned mass flow equation, to give a total required area of 0.3 m^2.

The final inlet design is composed of two separate inlets - one on each side of the fuselage, placed on the sponsons directly perpendicular to the free stream flow, each with an area of 0.15 m^2. The inlets are traditional scoops (as opposed to the commonly used NACA ducts), as minimize pressure losses inside the inlet, requiring less pressurization for cabin use.

To calculate the power required to run the fan, the required mass flow at sea-level is computed (10.5 kg/s per inlet), and the dynamic pressure difference across the fan is computed (based on lift-off speed, 35 Pa) to give a total power required of approximately 400 W. Thus, the total maximum power required to run both inlet fans is of 800 W.

The sensitivity of number of stacks chosen with regards to the increase of total cabin and inlet fan power has been evaluated. For the number of stacks to remain the same as discussed in Table 12.1, the maximum total cabin and inlet fan power is 105 kW, which represents to approximately 73% increase in total cabin and inlet fan power than estimated. Hence, the power requirement is deemed acceptable.

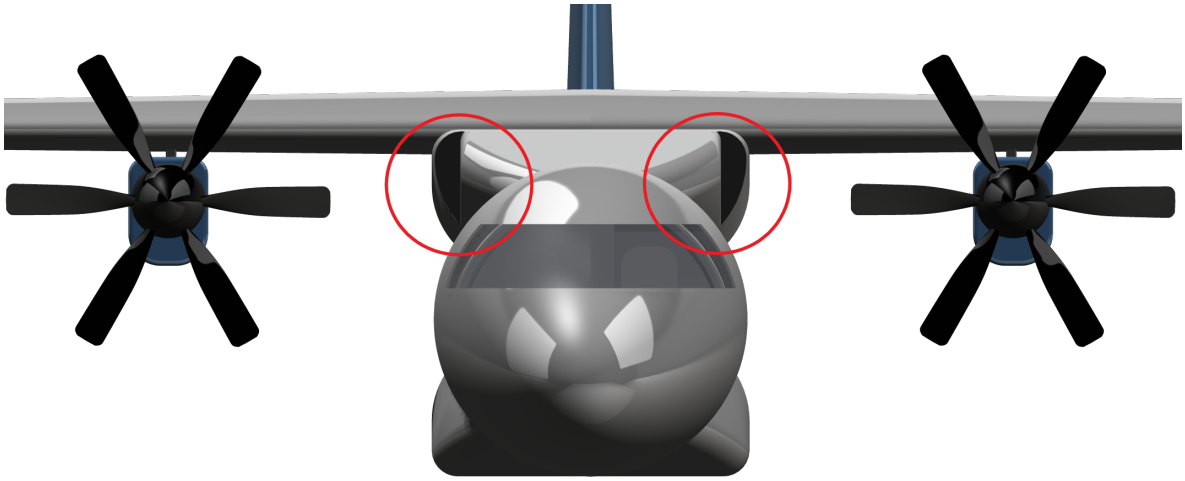

Figure 12.2: Inlet Positioning and Size

12.4. Electric Motor

The propulsion system is distributed across four motors - two inboard and two wingtip-mounted - to benefit from the aerodynamic advantage of wingtip-mounted propellers, while maintaining a low level of maintenance and complexity, and allowing for a relatively easy control of the aircraft under a one-engine-inoperative condition. According to [27], wingtip propellers can attenuate wingtip vortices when the motors counter-rotate the direction of the vortices, which is statistically quantified in a minimum of 17% total drag reduction for this specific aircraft in cruise conditions.

The two inboard motors are sized to provide 80% of the total power, while the two outboard propellers are sized to provide the remaining 20%. Based on the peak power aforementioned in Section 12.1, the electric motors are selected.

Electric Motor Selection

The wingtip-mounted motor chosen is the H3X HPDM-250 [4], which has the following characteristics:

Table 12.2: H3X HPDM-250 Characteristics

Parameter	Value	Unit
Peak power	250	[kW] (for 30 s)
Continuous power	200	[kW]
Continuous torque	95.5 (direct) and 640 (6.7:1 gearbox)	[Nm]
Cruise system efficiency	0.957	-
Mass	13	[kg]
Operating temp.	-40 to 60	[°C]
Max. operating altitude	FL350	-
Volume	0.009	[m^3]
Integrated DC-AC inverter?	Yes	-

The inboard motor selection is of greater complexity because current market options offer either low-power solutions (<250 kW), or high-power solutions (>2.8 MW). However, H3X offers the alternative of custom-made motors ranging from 30 kW to 30 MW [5]. As such, choosing a custom-made motor is the most viable and economically feasible solution. This motor shall provide 958 kW of power, while maintaining the operating temperature ranges, maximum operating altitude, and integrated DC-AC inverter solutions of the HPDM-250.

12.5. Supercapacitor

A supercapacitor is connected to the fuel cell as an alternative means of delivery of power to the motor. The supercapacitor is - under normal conditions - not used to provide any power. However, it is a redundancy mechanism in case there is a malfunction with one or multiple fuel cell stacks. The supercapacitor is sized to temporarily provide the maximum power output of one fuel cell stack, should there be a loss of fuel cell power during the peak-power flight phase. The supercapacitor selection is based on the required capacitance [6]:

$$C = \frac{I_{backup} \cdot t}{V} = \frac{I^2 \cdot t}{P_{FC}} \tag{12.5}$$

where I is the current produced by one fuel cell stack, t is the running time of the supercapacitor, and P_{FC} is the power produced by one fuel cell stack. The running time of the supercapacitor is preset to be the time it takes from the aircraft at standstill to reach V_2.

As such, the supercapacitor selected must be able to deliver a capacitance of 74 F, over a voltage difference of 350 V. To achieve this, smaller supercapacitors can be stacked to produce the desired voltage difference. However, the bigger the stack, the greater the voltage imbalance between individual supercapacitors, which can lead to a supercapacitor having a greater voltage than the rated voltage [7].

To limit this effect, two supercapacitor stacks are designed to work in parallel (one for each set of motors), with a capacitance of 74 F, but a voltage difference of 175 V.

12.6. Propeller Design

Propeller Sizing

The two different motors require two different propeller sizes for their corresponding power. The propeller diameter is calculated through a statistical first estimated provided by [19]:

$$D_p = 0.55 \cdot \sqrt[4]{\frac{P_{TO}}{1000 \cdot n}} \tag{12.6}$$

where P_{TO} is the maximum shaft power of the aircraft (aforementioned in Section 12.1), and n is the number of engines. This results in a diameter of 3.03 m for the two inboard propellers, and 2.15 m for the two wingtip-mounted propellers.

Number of Blades

The number of blades on each propeller was determined through a comparison study with the reference aircraft [30], as well as by blade efficiency comparison and noise generation.

While a theoretical blade limit does not exist, it is precautionary to keep the number below eight - eight blades translates into a basic fan, which can be ducted to reduce noise and tip losses [9]. Furthermore, a single blade propeller is not possible due to the excessive vibrations caused. As such, it is ideal to maintain the number between two and eight blades. Assuming a constant propeller diameter for all options, it is observable that adding more blades to a propeller increases the thrust generated. Propeller efficiency decreases due to the incremental generation of drag. Incrementing the number of blades reduces the blade-tip vortex noise [54].

It is concluded that the design number of blades is of six blades per propeller. This is because, although the propeller efficiency slightly decreases, the propeller is still able to generate significantly more thrust, and a reduction in noise emissions. This is supported by the fact that a majority of the reference aircraft also have a six-blade design.

Braking

Due to the nature of the propellers, reverse thrust is not a possibility for this aircraft. For landing, braking must be achieved through an alternative method. Apart from conventional disk brakes used on the undercarriage, by including a variable-pitch mechanism, the propellers' pitch can be set to negative values (beta-position), to reverse the direction of the airflow and generate reverse thrust, without changing the rotational direction of the propellers [8].

Furthermore, an additional propeller brake system is installed on the main inboard propellers, which allow the propeller to lock in place while still letting the motor turn. As such, the motors can be used as auxiliary power units without generating thrust, in order to power the aircraft for ground operations [55].

12.7. Propulsion System Architecture

To summarize the powertrain components, an overview of the propulsion system architecture is provided in Figure 12.3.

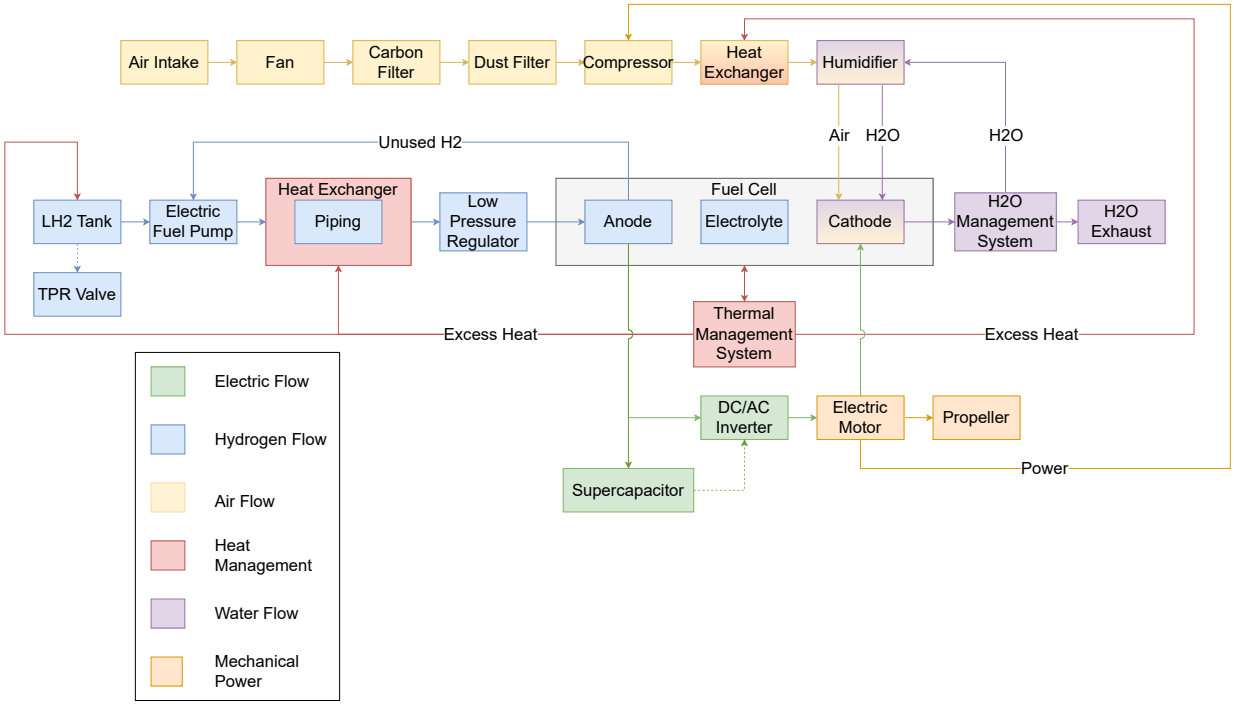

Figure 12.3: Propulsion System Architecture Block Diagram

[1]URL https://www.seatmaestro.com/guide-to-laptop-power-ports-on-planes [last accessed 20-01-2023]
[2]URL https://www.horizonfuelcell.com/%E5%89%AF%E6%9C%AC-%E5%89%AF%E6%9C%AC-vls-ii [last accessed 18-01-2023]
[3]URL https://www.tec-science.com/mechanics/gases-and-liquids/boundary-layer-and-dimensionless-similarity-parameters/ [last accessed 19-01-2023]
[4]URL https://h3x.docsend.com/view/q28n79niiqbj59kn [last accessed 19-01-2023]
[5]URL https://www.h3x.tech/#custom [last accessed 19-01-2023]
[6]URL https://www.powerelectronicsnews.com/ebook-may-21-4-choosing-the-right-supercapacitor-for-your-application/ [last accessed 20-01-2023]
[7]URL https://www.analog.com/en/design-notes/voltage-balancing-techniques-for-series-super-capacitor-connection-for-max3888689.html [last accessed 25-01-2023]
[8]URL https://dronesgator.com/how-many-blades-for-a-drone-propeller/ [last accessed 20-01-2023]
[9]URL https://www.aopa.org/news-and-media/all-news/2017/march/pilot/turbine-reverse-thrust [last accessed 23-01-2023]

13
Aircraft Integration

The first part of this chapter focuses on the creation of a pleasant and safe environment in the cabin for the passengers. Therefore, the air needs to be appropriately managed, which will be significantly different considering the use of electric propellers rather than air-breathing engines. The regulation of waste, water, and food supply will be undertaken. Furthermore, the regulatory system for the fuel and hydraulic system is laid out, whilst a representation of the hardware and software system is presented for the entire aircraft. Finally, the information flow software for the cockpit is presented.

13.1. Environmental Cabin Control

The interior cabin environment is of utter importance, especially considering the passenger experience. Ensuring a nice temperature, comfortable pressurization and fresh air ventilation increases passenger satisfaction and thus is desired by the customer.

Air

In general, the air required for air circulation is obtained from the air-breathing engines, where the air is compressed and cooled before mixing with internal re-circulating air. It is then supplied to the passenger cabin and cockpit by the environment control system. However, as electric propellers do not breathe air, an inlet should be placed along the fuselage in order to provide both fresh air and provide fresh oxygen to be used by the hydrogen fuel cells.

Once the external air has been obtained from the inlet, it is sucked and compressed and this bleed air is then supplied into the cabin mixed with recirculating filtered air. This re-used air is passed through several filters including HEPA filters to remove any unwanted gases, vapors, fumes as well as bacteria, viruses, and particles.

Additionally, from previous studies and statistical data it is given that the optimal cabin temperature inside the cabin should be in the 18 to 24-degree range. Thus, the air mixture is heated to those temperatures before being supplied to the passenger cabin, through several air diffusers which are located alongside the cabin as well as in individual controls above each seat, allowing every passenger to customize their temperature as well as ensuring a fresh air circulation at all times.

Given that the SRP-22 has a cruising altitude of 28,000 feet, a pressurized cabin is required. Typically, commercial aircraft cabins are pressurized to keep an inner atmosphere that resembles that of 6,000 to 8,000 feet, which is still comfortable for passengers as it only decreases oxygen levels in the blood by 4%[1].

Waste, water, and food supply

Regarding comfort, the water and waste system is designed to provide water for galleys and lavatories. Fresh water is stored and distributed while a different system deals with wastewater. That system includes a thoughtful engineering method to dispose of the different wastes that could occur during the flight.

The lavatory waste collection system consists of a vacuum lavatory, which makes use of the pressure differential between the cabin interior and exterior to pump the waste out of the lavatory and into the waste tank. Additionally, water is also added to flush the toilet. This water is mainly wastewater obtained from the sink water as well as possible residual water produced by the fuel cell. Once on the ground, the waste tank will be emptied by a truck.

Potable water is supplied to the aircraft by ground trucks and is stored in a special tank. This is mainly used in the galley in order to make coffee, tea, and other drinks.

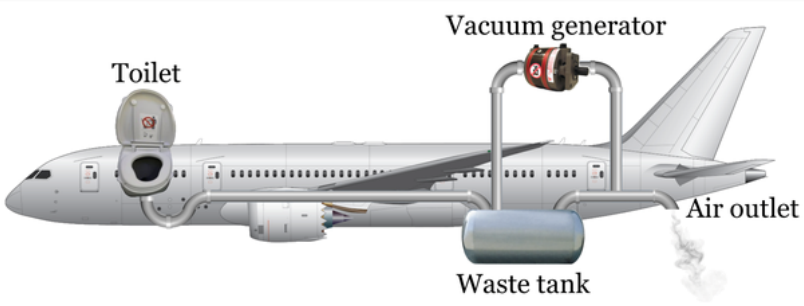

Figure 13.1: Representation of different parts of the water and waste system [56]

Additionally, the waste and water system also consists of a water tank pressurization system that pressures the water tank and air dealing with the tank (including air compressor, pressure regulator filter, and pressure relief valve).

The aircraft galley is to be located in the front of the aircraft, next to the service door which allows for easy access to catering and ground services.

13.2. Fuel and Hydraulic System

The integration and relation between the hydrogen fuel cell and generated electricity to power the electric propellers are presented in the following section. Alongside the design of the hydraulic system that will supply fluid to different control systems.

Fuel system layout

The main layout of the hydrogen fuel system is presented in Figure 13.2. The blue arrows represent the hydrogen that is fed from the hydrogen tank onto the fuel cell with the help of a compressor and valve. The output of the fuel cell is an electric current which is fed into the four electric propellers

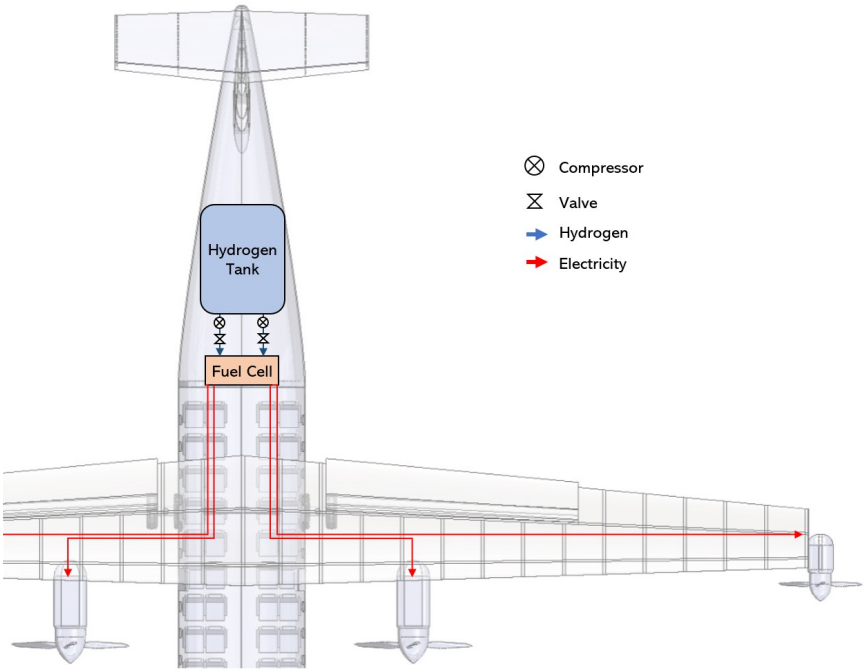

Figure 13.2: Representation of the fuel system

Hydraulic system layout

Generally, the functions of the hydraulic system vary from one aircraft to another, but typical functions of this system are to provide hydraulic power to the actuators which at the same time are in charge of moving the primary flight control systems such as ailerons, rudder, and elevator, as well as move secondary flight controls like flaps, trim, and speed brakes. Additionally, the hydraulic system is also in charge of extending and retracting the landing gear and ground steering.

The SRP-22 has two hydraulic systems, namely the green and blue systems. Each system is designed to supply fluid to different parts. The layout for the hydraulic system is presented in Figure 13.3.

1. **Reservoir**: Located behind the main gear, it provides hydraulic fluid to both systems (green and blue)
2. **Electric green & blue pump**: Powered by the aircraft, the objective of these is to increase the speed of the fluid flow to different parts.
3. **Accumulator**: Where the pressurized fluid is stored until it is sent to specific components.
4. **Cross feed valve**: This valve connects both green and blue systems

The blue system is designed to supply fluid to the propeller brake, spoilers, flaps, the nose wheel steering, parking, and emergency brake, via the emergency accumulator. The green system supplies the main landing gear retraction and extension systems as well as the normal, parking, and emergency brakes.

The hydraulic system is to be located inside the landing gear sponsons, making use of empty space and also being quite close to relevant systems such as landing gear and brakes which reduces the pipe length.

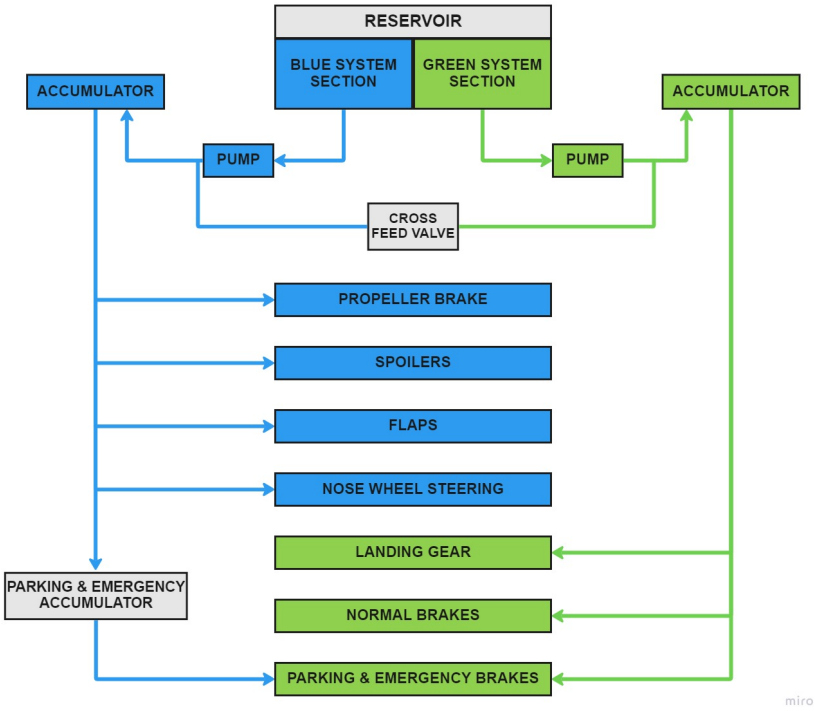

Figure 13.3: Representation of the hydraulic system layout

When designing the complex system the following design guidelines are taken into account: firstly, all lines and components are easily accessible for maintenance and repair. Additionally, The hydraulic lines are routed such that no critical hydraulic lines are close together. This way, in case a catastrophic failure occurs not all hydraulics, would be affected at the same time.

13.3. Hardware & software block diagram

The hardware and software block diagram show the overall flow of systems in the aircraft. Figure 13.4 is aimed at providing a general overview of how systems are interconnected. In this block diagram, only the propulsion system is depicted in detail. Therefore, in later stages, the hydraulics, cabin equipment, and communications systems should be worked out in more detail to show the flow of information back to the cockpit.

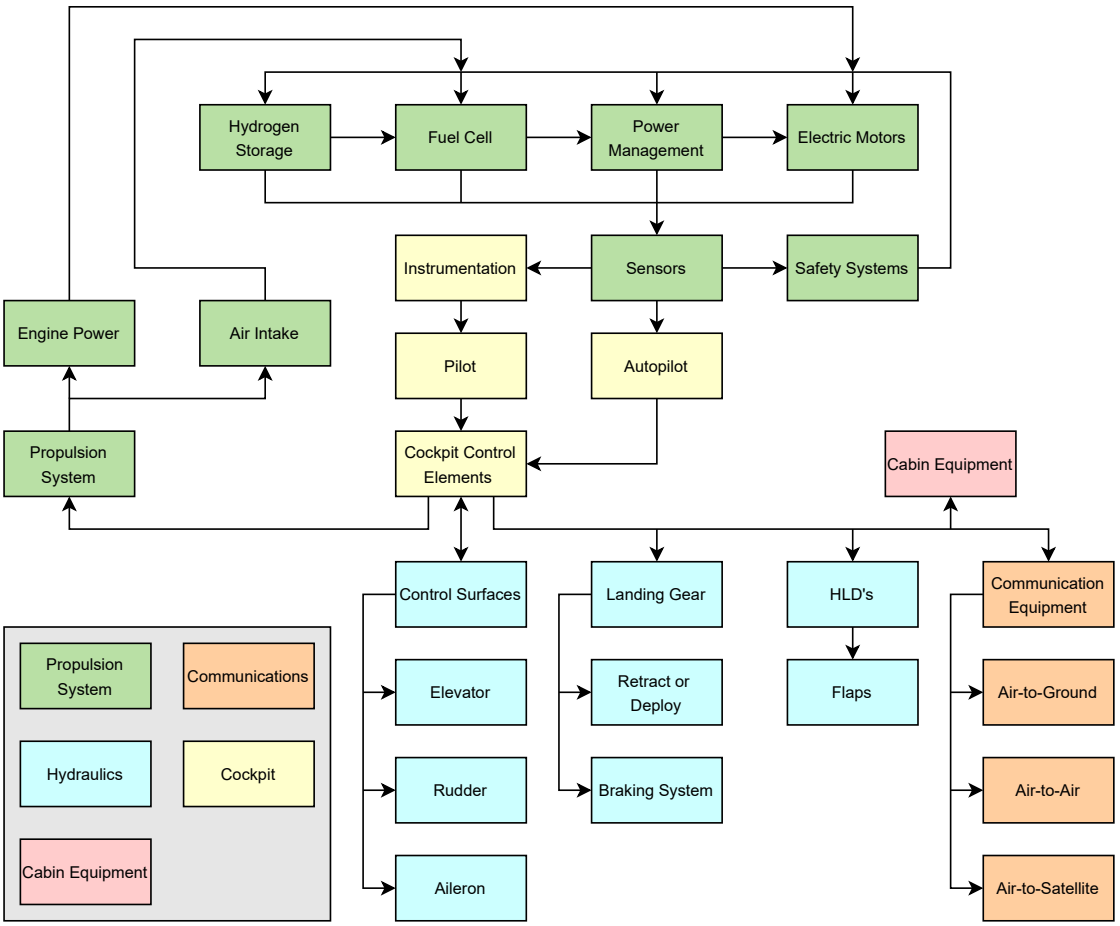

Figure 13.4: Hardware & Software Block Diagram

13.4. Data Handling Block Diagram

The data handling block diagram shows how data is collected, processed, and finally used in the aircraft. Figure 13.5 shows a smaller branch in the diagram, which shows how the main aircraft parameters such as speed, altitude, position, and navigation data are fed onto the cockpit

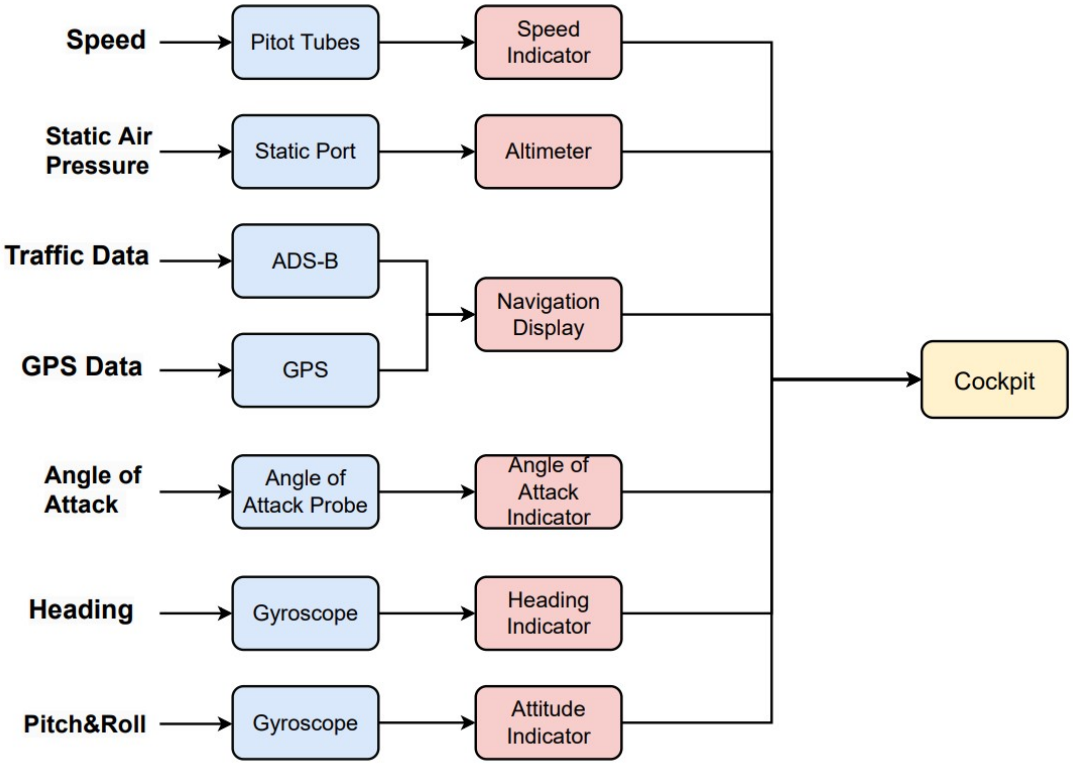

Figure 13.5: Data handling block diagram

[1]URL https://aerospace.honeywell.com/us/en/about-us/blogs/why-do-aircraft-use-cabin-pressurization#:~:text=What%20is%20the%20cabin%20pressure,6%2C000%20to%208%2C000%20feet%20high. [Cited 20 Jan. 2022]

14
Production Plan

In this chapter, the production plan of the aircraft is assessed. A lean thinking approach is taken during the production process, which will ensure the reduction of waste while procuring the materials, manufacturing all needed parts throughout the assembly, and during the final step of integration, taking into account human resources and transportation when necessary. A lean methodology is an approach in which materials, economics, human factors, and other resources are set up such as to maximize the outcome of a desired event while minimizing waste.

14.1. Manufacturing

The first step is the procurement of all necessary materials. For the SRP-22, this includes raw materials such as titanium, aluminum, and composites, followed by the procurement of other miscellaneous parts, such as stringers, ribs, rivets, spars, and skin panels.

Once the necessary materials are procured, the manufacturing processes are established. A lean manufacturing philosophy will be taken into account throughout the entire process. A large number of parts will be manufactured in-house, using different manufacturing methods, while there will be some components that will already be manufactured and procured from external manufacturers, such as the electric motors, propellers, fuel cells, electronic systems, etc. Long delivery time of ordering off-the-shelf products will have to be accounted for when the production schedule of the aircraft is planned, in order to prevent delays to aircraft assembly.

14.2. Assembly

The assembly of the SRP-22 is generally similar to the one adopted for other conventional turboprop aircraft. The process resembles a line production that streamlines the manufacturing process by allowing a number of complex sub-assembly to be accomplished outside the main assembly line simultaneously before being simply connected to the rest of the aircraft.

The assembly starts with parts manufacturing and parts acquisition. Next, the tail cone and the nose cone are assembled and subsequently joined with the cylindrical fuselage assembly. At the current stage, the tail cone sub-assembly will already have included the hydrogen tank, thermal insulation, and fuel cells. In the next step, the empennage of the aircraft is assembled and attached to the tail cone section of the fuselage. At the same time, the first stage of wing construction also started, as the primary structures of the wing (spars, ribs, stringers, and skin panels) are being assembled. Once the wing is constructed, the sub-assembly continues with mounting the HLDs and ailerons and the product is then mounted onto the fuselage. Next, the main undercarriage and powerplant subsystems are fabricated and attached to the main assembly. To finalize the process, cabin items are installed and the livery is painted. Figure 14.1 provides an illustration of the order in which the aircraft will be assembled.

Multiple checks must be carried out during the production process, and after delivery of the product, in order to ensure the final product will perform as intended, as well as to guarantee operational safety. These checks can be performed through inspection of the parts produced and non-destructive evaluation used to detect defects on the materials of the product. Ultrasonic testing may be employed to investigate laminate separation and/or voids in parts manufactured with composites [57].

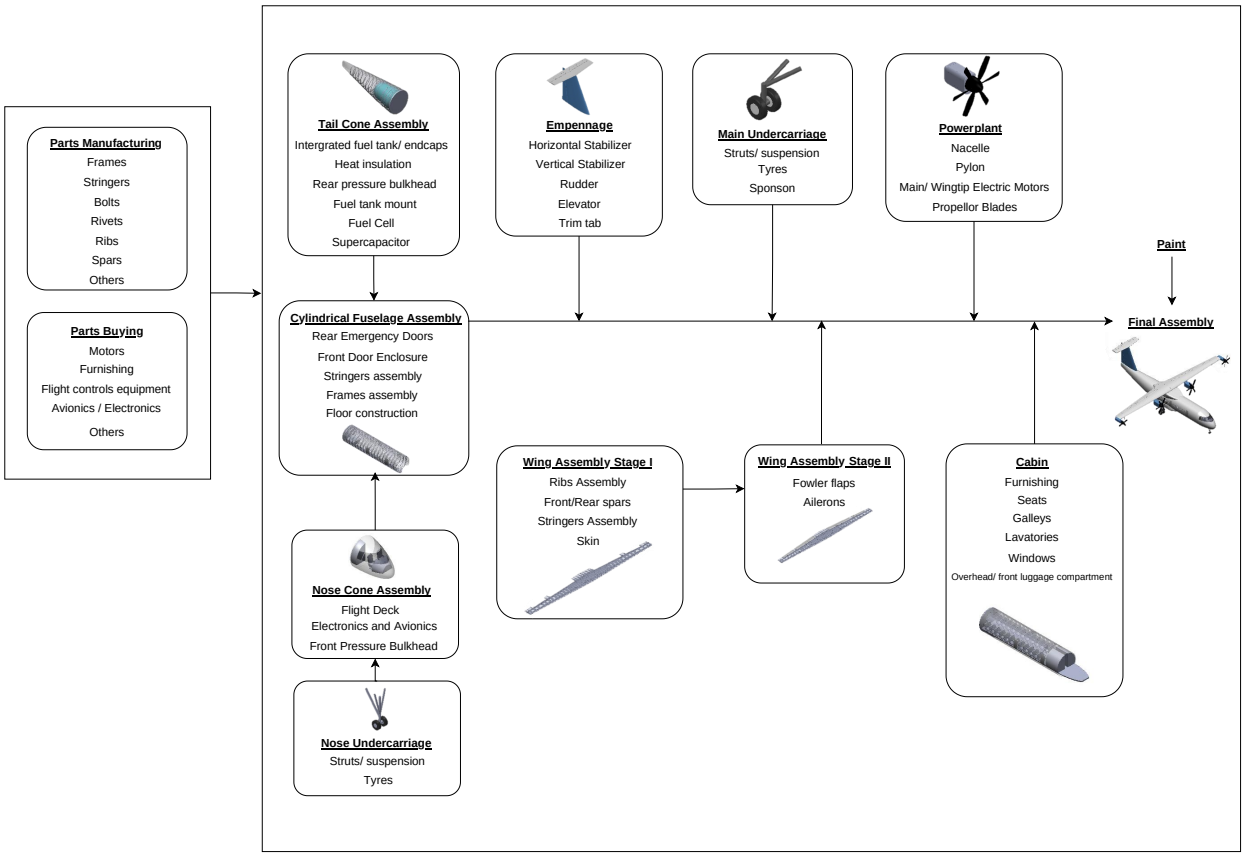

Figure 14.1: Assembly sequence chart of the SRP-22

15 Stability and Control

In order to adhere to the requirements set, the static and dynamic stability has to be analyzed, in longitudinal, directional, and lateral directions. For this purpose, an analysis of the aircraft balance has been performed. Furthermore, the control surfaces located on the wing and the tail for rotations in the vertical, lateral, and longitudinal axis are designed.

15.1. Loading Diagram

To analyse aircraft balance, the loading diagram of the aircraft is constructed and the most forward and most aft c.g are determined. By loading the cargo, passengers and fuel sequentially and then in alternative orders, the resulting loading diagram can be seen in Figure 15.1. The most front c.g. is found to be located at approximately **11.7 m** from the nose of the aircraft (0.08 MAC), whereas the most aft c.g. is located when the aircraft is at its OEM. The most aft c.g. can be found at **12.7 m** from the nose (0.47 MAC). The most front c.g. is chosen at MZFM rather than from the blue line from loading passengers, as the cabin crew can be ordered to load the passengers such that no issues arise.

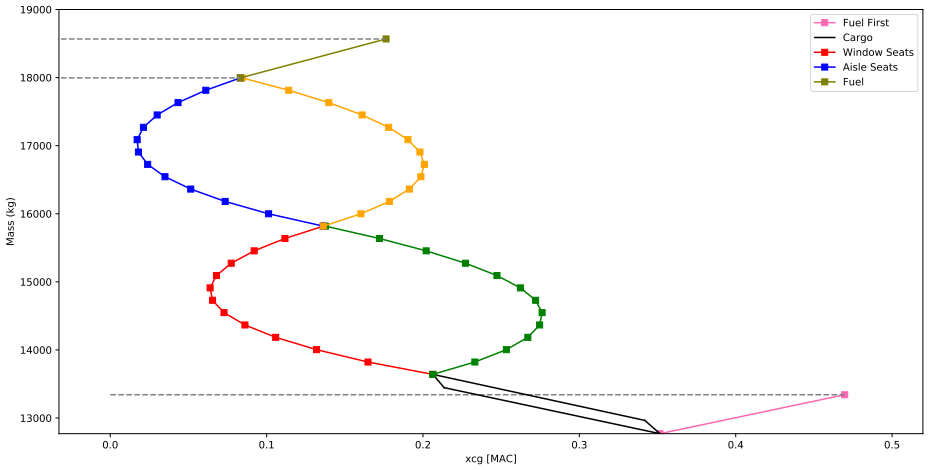

Figure 15.1: Loading diagram

15.2. Longitudinal Static Stability and Control

Requirement **RA-SYS-MSC-2** refers to static stability and control along the longitudinal, lateral, and directional axes. The previously sized and positioned horizontal tail is evaluated for longitudinal stability and control. The critical condition for stick fixed static stability is during cruise, whilst for the trimming of the aircraft, the critical condition is during landing, with the flaps full out. The scissor plot presented in Figure 15.2 shows the compliance of the horizontal tail sizing to longitudinal stability and control, as stated in **RA-SYS-MSC-5**. A safety margin of 0.05 MAC with respect to the front and aft c.g. as obtained from the loading diagram (Figure 15.1) is taken into account in the c.g. range. Resulting of this, the S_h/S ratio has been evaluated to be equal to 0.17. Longitudinal static stability states that:

$$x_{np} > x_{cg_{aft}} \tag{15.1}$$

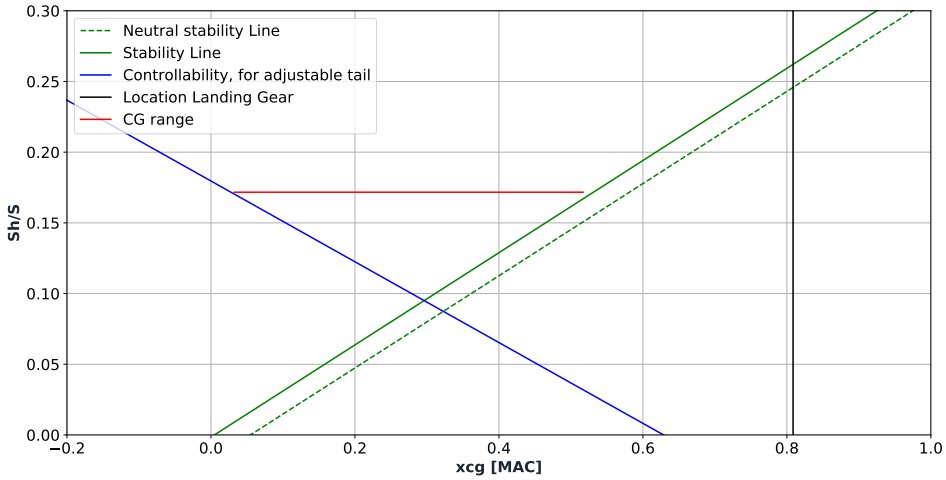

Figure 15.2: Horizontal tail sizing with longitudinal stability and control

15.3. Stability Derivatives and Requirement Compliance

In order to check compliance with the static stability requirements **RA-SYS-MSC-10**, **RA-SYS-MSC-11**, and **RA-SYS-MSC-12** the lateral, and longitudinal stability derivatives of the aircraft are computed based on the methodology in [25]. The lateral static stability derivatives, their requirements and compliance are presented in Table 15.1 and the longitudinal stability derivatives are presented in Table 15.2.

Table 15.1: Lateral and directional stability derivatives and requirements

With respect to	Derivative	Value	Requirement for stability
Sideslip angle	C_{Y_β}	-1.1	<0
	C_{l_β}	-0.06	<0
	C_{n_β}	0.09	>0
Roll rate	C_{Y_p}	-0.13	<0
	C_{l_p}	-0.51	<0
	C_{n_p}	-0.087	<0
Yaw rate	C_{Y_r}	0.46	>0
	C_{l_r}	0.29	>0
	C_{n_r}	-0.18	<0

Table 15.2: Longitudinal stability derivatives

With respect to	Derivative	Value
Airspeed	C_{X_u}	0
	C_{Z_u}	-1.27
	C_{m_u}	0
Angle of Attack	C_{X_α}	0.39
	C_{Z_α}	-5.63
	C_{m_α}	-1.70

With respect to	Derivative	Value
Acceleration along top axis	$C_{X_{\dot{\alpha}}}$	0.45
	$C_{Z_{\dot{\alpha}}}$	0.29
	$C_{m_{\dot{\alpha}}}$	-0.17
Pitching velocity	C_{X_q}	0
	C_{Z_q}	-6
	C_{m_q}	-17

The maneuverability requirement about the X_B-axis, can be quantified using the steady rolling flight requirement, stated in Equation 15.2 [58]. The value for the non-dimensional roll rate has been found to be 0.151, thus meeting requirement **RA-SYS-MSC-6**.

$$\left(\frac{pb}{2V}\right)_{\text{max}} = -\frac{C_{\text{l}_{\delta_a}}}{C_{\text{l}_\text{p}}} \cdot \delta_\text{a} > 0.07 \tag{15.2}$$

Note that the static longitudinal stability requirement is met, as C_{m_α} is negative. Furthermore, the static longitudinal stability requirement is met, as C_{m_α} < 0, relating to **RA-SYS-MSC-9**. The aircraft moment coefficient dependent on the angle of attack is calculated by summing the contribution of the wing and of the horizontal stabilizer [59]. Figure 15.2 and Table 15.1 demonstrate that the static stability and control requirement **RA-SYS-MSC-2** is met.

15.4. Control Surface Design

In this section, the aircraft control surfaces elevator, aileron, and rudder are designed. The control system is controlled through a mechanical-powered hydraulic system. At the end of the section, a summary of all control derivatives is given.

Elevator design

The longitudinal stability and equilibrium of the aerodynamic moment about the center of gravity are driving the sizing of the horizontal tail and the elevator, as well as the hinge moment. The backup in case of failure of the control system will be through manual reversion, using a reversible control system, using a natural feel for the force exerted on the elevator through the stick. The elevator would then be controlled using a push-pull rod system. The control stick is then linked through cables, that are linked to pulleys to the push rod at the elevator. The elevator control force is presented in Figure 15.5, and considering the high nature of the elevator control force, a shielded horn has been designed. The sizing is done by force equilibrium and will decrease the hinge moment derivative due to deflection significantly [58]. The methodology used to size the elevator is presented in the [59] and [32]. The requirement for trim stick force stability, $\frac{dF_\text{e}}{V} > 0$ is met, as can be visualized in Figure 15.5, thus complying with requirement **RA-SYS-MSC-8.1**. From the equations for the elevator deflection angle over angle of attack and velocity it can be deduced that trim stability is obtained, when the signs of $C_{\text{m}_{\delta_e}}$ and C_{m_α} are both negative. In Table 15.3 it has been calculated that the sign of the elevator efficiency is indeed negative whilst in Table 15.2, presented in Section 15.3, the C_{m_α} has been calculated. The respective values for compliance of **RA-SYS-MSC-8.2** and **RA-SYS-MSC-8.3** are presented in Table 15.3. The final values for the geometry of the elevator and trim tab are presented in Table 15.4 and Table 15.5, and are visualized in Figure 15.4.

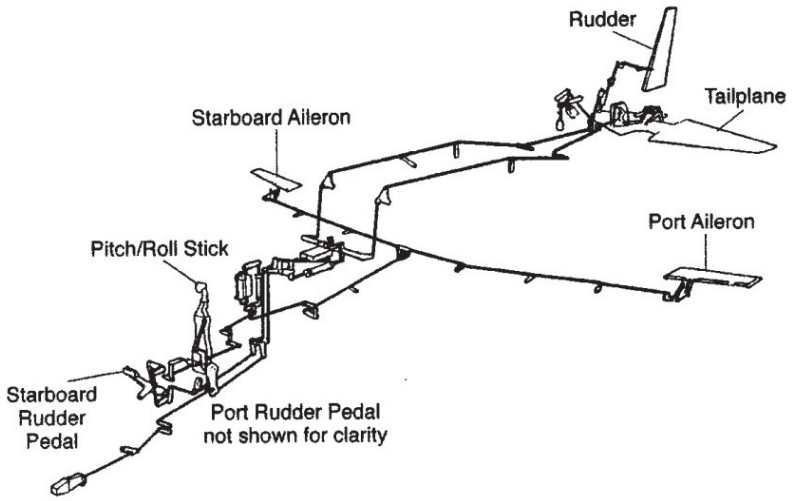

Figure 15.3: Example of a human mechanical powered system [59]

Table 15.3: Requirements for the elevator sizing

	Value	Requirement
Hinge moment derivative due to deflection [59]	-0.072	$Ch_\delta < 0$
Elevator efficiency [59]	-1.11	$Cm_{\delta_e} < 0$

Table 15.4: Sizing parameters for the elevator on the horizontal tail

Parameters	Values	Units
S_e	1.35	[m^2]
$C_{\text{e}_{tip}}$	0.42	[m]
$C_{\text{e}_{root}}$	0.54	[m]
b_e	2.6	[m]

Table 15.5: Sizing parameters for the trim tab on the horizontal tail

Parameters	Values	Units
S_tab	0.65	[m^2]
$C_{\text{tab}_{tip}}$	0.295	[m]
$C_{\text{tab}_{root}}$	0.35	[m]
b_tab	2.0	[m]

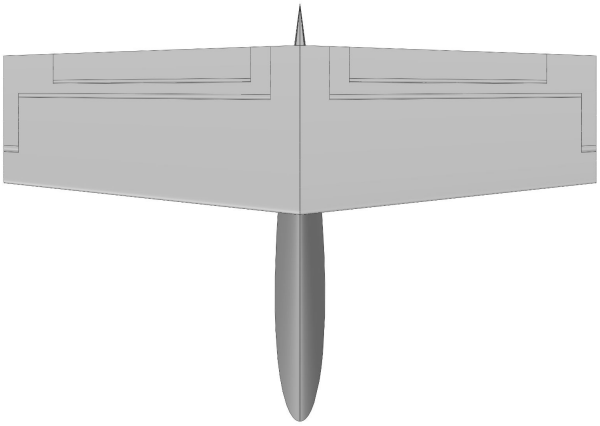

Figure 15.4: Elevator, trim tab, and horn design

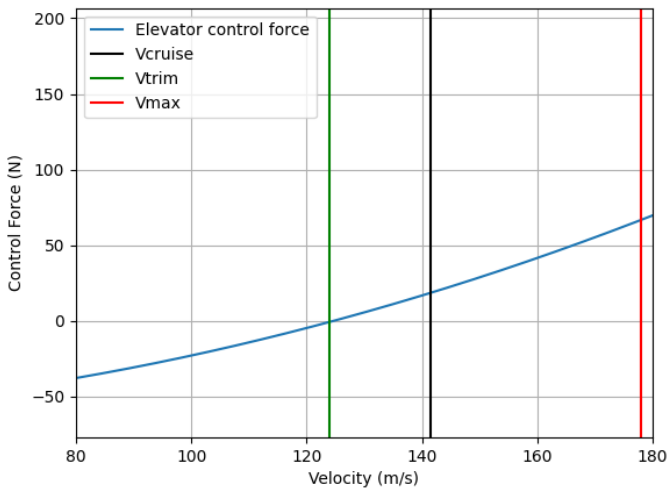

Figure 15.5: Trim stick force stability curve

Vertical tail and rudder design

In order to adhere to **RA-SYS-MSC-7** the vertical tail has been resized. The vertical tail can be sized for its most critical requirement, which in a multi-engine transport aircraft is for a One Engine Inoperative situation upon takeoff [60]. Where it is assumed that the pilot performs the corrective measure of cutting off the opposite wing tip engine, to reduce the yawing moment. This can be done by taking moments about the z-axis of the aircraft, as the thrust asymmetry generated by the engine inoperative will produce a yawing moment which should be counteracted by the vertical tailplane force. The vertical tailplane force is defined as in Equation 15.3 and the moment equilibrium by Equation 15.4.

$$Y = \frac{1}{2}\rho V^2 S C_{Y_{\delta_r}} \delta_r \tag{15.3}$$

$$T_L y_T = Y l_v \tag{15.4}$$

Where T_L is the thrust asymmetry y_T is the lateral distance from the resultant to the centerline and l_v is the distance from the aft center of gravity to the aerodynamic center of the vertical tail. The moment of the vertical tail is a function of aircraft geometry, sideslip angle, aileron deflection, and rudder deflection. However, it is assumed that in this flight condition, there is no sideslip angle and the aileron is not deflection. The effect of a sideslip angle is shown in Section 25 As such, from the required moment to be counteracted by the vertical tailplane due to the thrust asymmetry one can calculate the required vertical tailplane force.

Using equation Equation 15.3 one can then compute the vertical tail area needed for the most critical requirement. As shown in Table 15.6. A 14 m^2 tail will provide sufficient force at a nine degree rudder deflection in order to counteract the thrust asymmetry moment.

Once the vertical tail area is calculated, the next step is to calculate the rudder dimensions and size.

As mentioned in [60] , the most critical flight condition when sizing the rudder for a multi-engine (wing placed) transport aircraft is the asymmetric thrust caused by a One Engine Inoperative Condition. Following the method presented in [60] the ratio of chord lengths between the vertical tail and the rudder may be obtained. Then, the rudder span, tip chord, root chord and other geometric aspects are derived with the use of simple Aspect Ratio, and Area equations. The final rudder dimensions are shown in Table 15.7 and visualized in Figure 15.6.

Table 15.6: Sizing parameters for vertical tail

Parameters	Values	Units
S_v	14	[m^2]
b_v	4.3	[m]
$C_{v_{tip}}$	2.1	[m]
$C_{v_{root}}$	4.2	[m]

Table 15.7: Sizing parameters for tail rudder

Parameters	Values	Units
S_r	2.2	[m^2]
b_r	3.0	[m]
$C_{r_{tip}}$	0.46	[m]
$C_{r_{root}}$	0.93	[m]

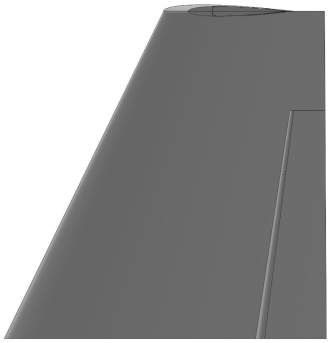

Figure 15.6: Rudder and vertical tail design

Aileron design

SRP-22 is considered a class II aircraft in which the roll performance of the SRP-22 shall have a steady roll of the aircraft at level flight to a bank angle of 45° in 1.4 seconds in all flight phases, **RA-SYS-MSC-4**. The most critical stall speed of the aircraft is during takeoff, in which the stall speed at takeoff is $50\,\mathrm{m\,s^{-1}}$. The c_a/c ratio of 0.30 was taken so that a 10% chord margin was used between the rear spar and the leading edge of the aileron. As the c_a/c ratio is 0.30, hence the aileron effectiveness for the chord ratio is 0.52 [60]. Additionally, all possible design options for ailerons are using differential ailerons, which minimizes the adverse yaw effect. The method of designing the aileron follows the process presented by F. Olivero [35]. The design choices got the aileron are shown in Table 15.8 and in Figure 15.7.

Table 15.8: Aileron design choice

Parameters	Values
Inboard aileron location	$7.4\,\mathrm{m}$
Outboard aileron location	$12.0\,\mathrm{m}$
c_a/c	0.30
$\delta a_{\text{up,max}}$	25°
$\delta a_{\text{down,max}}$	19°
Steady roll rate	$32.3^\circ\,\mathrm{s^{-1}}$
Time to bank 45°	$1.39\,\mathrm{s}$
Aileron type	Differential aileron

Figure 15.7: Aileron design

Control derivatives

The control derivatives for the deflection of the control surfaces (aileron, rudder, and elevator) are given below in Table 15.9, which were computed using the method described in Roskam [25].

Table 15.9: Control derivatives for aileron, rudder, and elevator

With respect to	Derivative	Value	Sign convention [58]
Aileron deflection	$C_{Y_{\delta a}}$	0	0
	$C_{l_{\delta a}}$	-0.39	< 0
	$C_{n_{\delta a}}$	0.01	> 0
Rudder deflection	$C_{Y_{\delta r}}$	0.25	> 0
	$C_{l_{\delta r}}$	0.03	> 0
	$C_{n_{\delta r}}$	-0.09	< 0
Elevator deflection	$C_{X_{\delta e}}$	0	
	$C_{Z_{\delta e}}$	-0.24	

15.5. Dynamic Stability and Control Analysis

The requirements **RA-SYS-MSC-13**, **RA-SYS-MSC-14** relate to dynamic stability and are proven in this section. This includes an analysis of the aircraft response to different aircraft motion in symmetric and asymmetric conditions as well as the dynamic directional stability based on the aileron.

For dynamic stability, the main criterion for dynamic stability is that all real parts of the complex eigenvalues are negative. Furthermore, the aircraft is designed to comply with the Level I stability requirements from MIL-F-8785C for a Class II aircraft for Category B flight phase.

The lateral and longitudinal stability derivatives presented in the section above are used to find the eigenvalues for the asymmetric and symmetric flight motions respectively. The symmetric motions that have been analyzed are the short period (sp) and phugoid motion (ph), for the asymmetric case the aperiodic roll (r), Dutch roll (d), and spiral (s) are investigated.

The requirement compliance for the symmetric and asymmetric motions are listed in Table 15.10. The damping ratio, natural eigenfrequency, and roll mode time constant of the motions are calculated using the eigenvalues. The eigenvalues of the symmetric and asymmetric motions have been determined analytically and are plotted in Figure 15.8 and 15.9 respectively [59][32].

Table 15.10: Compliance of the symmetric and asymmetric motion towards stability

Motion	Parameter	Value	Requirement [58]
Short period	ζ_{sp}	0.95	$0.30 \leq \zeta_{sp} \leq 2.00$
Phugoid motion	ζ_{ph}	0.179	$\zeta_{ph} \geq 0.04$
Aperiodic roll	T_r	0.74 [s]	$T_r < 1.4$ [s]
Dutch roll	ζ_d	0.16	$\zeta_d \geq 0.08$
Dutch roll	$\zeta_d \omega_{n_d}$	0.18	$\zeta_d \omega_{n_d} \geq 0.15$ [rad/s]
Dutch roll	ω_{n_d}	1.2	$\omega_{n_d} \geq 0.4$ [rad/s]
Spiral motion	T_{2_s}	36 [s]	T_{2_s} > 20 [s]

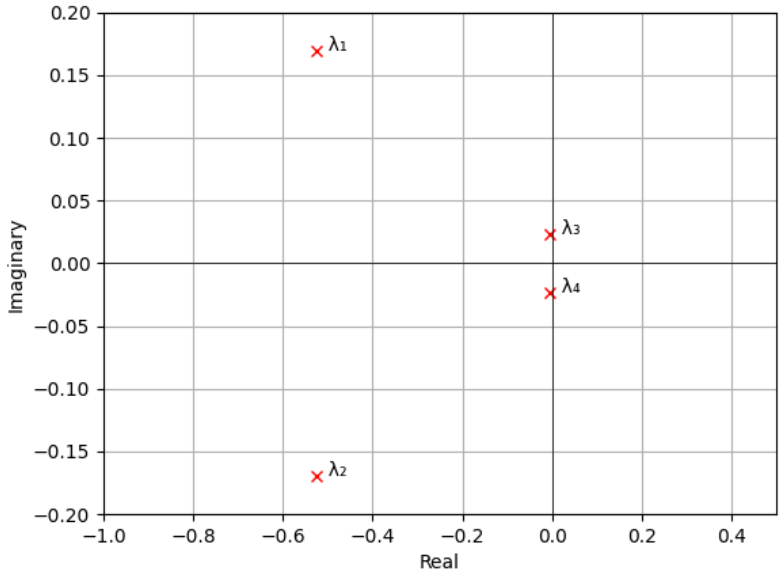

Figure 15.8: Eigenvalue requirement compliance for symmetric motions: short period (λ_1 and λ_2) and phugoid (λ_3 and λ_4)

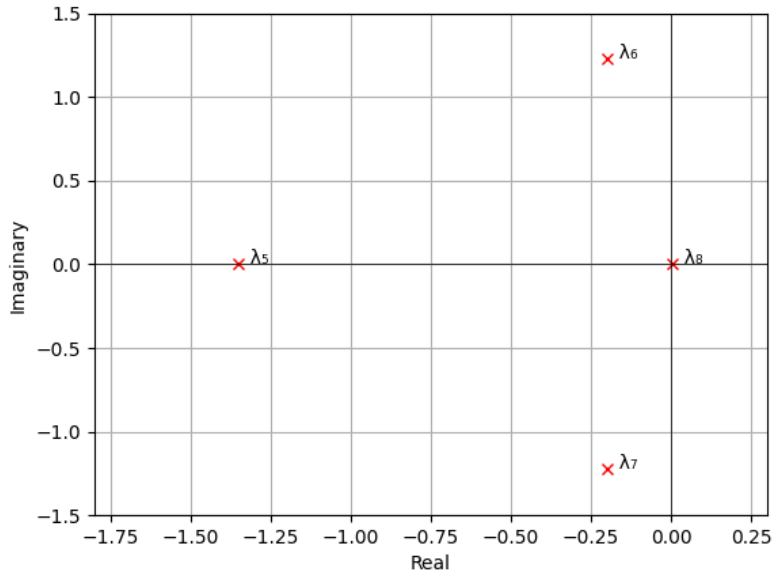

Figure 15.9: Eigenvalue requirement compliance for asymmetric motions: aperiodic roll (λ_5), Dutch roll (λ_6 and λ_7), and spiral (λ_8)

The criterion for aircraft departure characteristics is based on dynamic directional stability. The requirement for the Lateral Control Departure Parameter (for Aileron Alone) is presented in Equation 15.5, this has been calculated to be equal to 0.088. From this analysis, it can be concluded that the aircraft fulfills **RA-SYS-MSC-15**.

$$LCDP = C_{n_\beta} - C_{l_\beta} \frac{C_{n_{\delta\alpha}}}{C_{l_{\delta\alpha}}} > 0 \tag{15.5}$$

16
Flight Performance

The goal of flight performance is to show the capabilities of the aircraft in flight. This includes transportation capabilities, climbing, takeoff and landing performance, and banking. Furthermore, the loading factors the aircraft will have to be able to sustain during flight are determined. Combining all of the flight performance characteristics results in a general overview of the overall mission.

16.1. Payload Range Diagram

A payload range diagram is generated in order to show the transportation performance of the aircraft. The diagram represents the range at two important design points - the design payload (Point B) and ferry range (Point C). The payload is taken to serve 48 passengers, with a mass of 200 lbs and the luggage mass as defined in the requirements. The diagrams shown in Figure 16.1a was constructed for the SRP-22 using the Breguet range equations [4]. The range at design payload is found to be equal to 1020 nmi, sufficing the range defined in the requirement **RA-TOP-PER-2**. A detailed overview of all points can be found in Table 16.1. The total fuel mass, presented in the table takes into account the contingency fuel, and necessary fuel for divergence, thus meeting requirement **RA-SYS-SRE-5**.

The payload range diagram for the SRP-22 freighter configuration is shown in Figure 16.1b. Due its lower operational empty mass the ferry range is slightly higher.

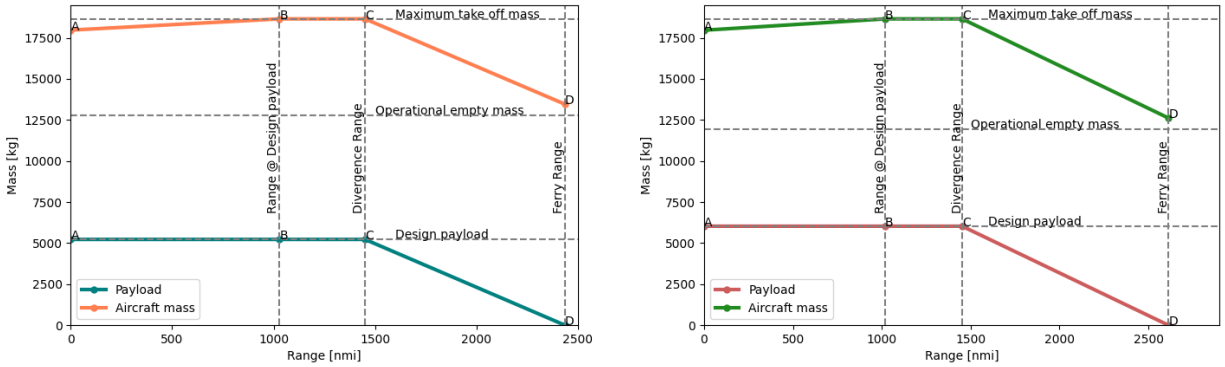

(a) Conventional configuration

(b) Freighter configuration

Figure 16.1: Payload Range Diagrams

Table 16.1: Points on Payload Range Diagram

Aircraft mass [kg]	Payload mass [kg]	Fuel mass [kg]	Range [nmi]
OEM + Payload mass	Design payload	0	0
MTOM	Design payload	Trip fuel	1020
MTOM	Design payload	Total fuel mass	1450
OEM + Total fuel mass	0	Total fuel mass	2440

16.2. Gust and Maneuver Load Diagram

The ultimate load factor the aircraft would have to be able to sustain is determined. The load factor is the ratio between the lift generated by the aircraft and its weight. CS-25 regulations specify that two overlaying plots be constructed to obtain the entirety of the flight envelope, named a V-n diagram as it relates the structural load limits of the aircraft to its velocity. The velocities that are used for the construction of the diagram are defined in

- $V_S = 60.5$ [m/s] (Stall speed)
- $V_C = 141.5$ [m/s] (Design cruise speed)
- $V_D = 158.7$ [m/s] (Design diving speed)
- $V_A = 97.2$ [m/s] (Design maneuvering speed)
- $V_B = 117.6$ [m/s] (Design speed for maximum gust intensity)

Note: all velocities are given in EAS.

Maneuverability

The maneuver diagram is constructed at the aircraft's three main operating altitudes, namely sea level (FL000), cruise altitude (FL280), and loiter altitude (FL195). This last one is defined as such because it is the boundary between low and high operating airway structures, and is the theoretical limit at which pilots can fly under visual flight rules. For each altitude, the limiting load factors are calculated based on the stall speed, cruise speed, and dive speed, as well as the limits imposed by CS-25. The limiting load factors are plotted for both clean configuration and with flaps deployed.

Gust Loads

The gust diagram is constructed for three aircraft weights (namely operating empty weight, operating empty weight with maximum fuel, and maximum take-off weight), based on CS-25 requirements for gust velocities, gust gradient distances, and flight profile alleviation factors. The changes in load factor are calculated and plotted at the design speed for maximum gust velocity, cruise speed, and dive speed. It was concluded that the most extreme case derives from the operating empty weight at FL000, since this is the one with the highest changes in load factor.

Flight Envelope and Ultimate Load Factor

The gust diagram at operating weight and gust diagram at maximum take-off weight were overlapped with the maneuver diagram at maximum take-off weight, both at the limiting case of FL000, to obtain the flight envelope, as seen in Figure 16.2. As a result, the maximum load factor is 3.25, while the minimum load factor is -1.25. As stated in CS-25 regulations, *"Unless otherwise specified, a factor of safety of 1.5 must be applied to the prescribed limit load which are considered external loads on the structure,"* with which the ultimate load factors may be calculated:

- $n_{ult_{max}}$ = 3.25 · 1.5 = 4.875
- $n_{ult_{min}}$ = -1.25 · 1.5 = -1.87

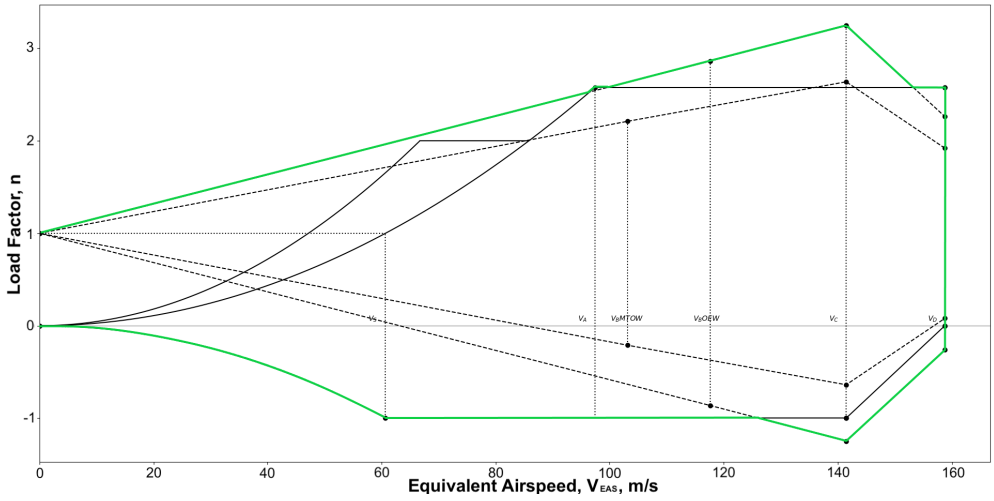

Figure 16.2: Complete Gust and Maneuver Envelope

16.3. Optimum Velocity

Using Chapter 15 of Ruijgrok, it was found that for maximum endurance, the ratio $\frac{C_L^3}{C_D^2}$ should be maximized [61]. This ratio was found with $C_L < 1.0$, in order to avoid stalling conditions. This resulted in a C_L of 0.98. When using it to solve for velocity in the lift equation, the optimum velocity to fly at FL280 was found to be equal to 213 KTAS [61]. As this is below the required minimum cruise speed, this was not considered a viable option. When solving for density rather than velocity, it was found that at optimum altitude to fly at 275 KTAS was FL400. The summary of the results can be found in Table 16.2.

Table 16.2: Optimum Flight Velocities

Case	V_{TAS} [kts]	ρ [kg/m]^3	Altitude [FL]
Min. cruise altitude	213	0.49	280
Opt. altitude $V_{cr_{min}}$	275	0.31	400

16.4. Bank Angle

To comply with **RA-SYS-MSC-1.1**, a bank angle performance analysis was performed. Using eq. 12.2-3 from Ruijgrok [61], the power required to perform a 40° bank angle turn can be calculated. Furthermore, due to the bank angle, the vertical lift will decrease. To compensate this loss of lift, the angle of attack must be increased. This was done using eq. 12.1-13.

Table 16.3: 40° Bank Angle Turn Analysis

Power Available	2.44 $\cdot 10^3$ [kW]	Vertical Lift Cruise	1.83 $\cdot 10^5$ [N]	AoA Cruise	3.9 [°]
Power Required	2.26 $\cdot 10^3$ [kW]	Vertical Lift 40° Turn	1.40 $\cdot 10^5$ [N]	AoA 40° Turn	6.6 [°]

From Table 16.3 it is clear that sufficient power is available. The 1.40 $\cdot 10^5$ N vertical lift generated during the turn is not sufficient to overcome the weight of the aircraft. Therefore, as shown, the angle of attack shall be increased to 6.6° to overcome this. By doing so, the altitude can be maintained while banking without stall occurring (from Figure 9.3). Furthermore, note that the lift during cruise as shown in Table 16.3 is calculated with V_{cr} equal to 275 kts and the design C_L, hence requirement **RA-TOP-PER-3.1** is met.

16.5. Flight Profile

The flight can be divided into three phases: climb, cruise and descent. In addition, climb and descent can be divided into more phases, such as approach for example. The overall mission profile (Figure 16.3) describes all phases that are determined. For both the climb and descent phases the velocity is given in constant KIAS. The KIAS of the final climb phase and first descent phase are chosen as such that at cruise altitude the velocity is effectively equal to the cruise velocity, which is given in KTAS. The descent is performed under a constant glide angle of 4.5°.

The takeoff field length has been calculated for the critical case as defined by requirement **RA-TOP-PER-4.1.2**. The method for runway length and air length as defined by R. Vos was used [4]. This led to a runway length of 855 m, a length of 305 m to fly over the 50 ft obstacle, and hence a total takeoff length of 1160 m. As this is satisfied, this also holds for the less critical situation defined in requirement **RA-TOP-PER-4.1.1**.

Furthermore, the landing field length is calculated to be equal to 1125 m for the most critical case, per CS-25 and the method as defined by R. Vos [1] [4], thus complying with **RA-TOP-PER-4.2.1** and **RA-TOP-PER-4.2.2**. For this, $C_{LFL} = 0.45$ and $V_{SR0} = 50$ m/s. According to CS-25 regulations, the velocity during approach (at the 50 ft obstacle) may not be smaller than $1.23V_{SR0}$ [1]. This means the velocity shall have a minimum of 61.5 m/s. When solving the lift equation at landing weight (assumed 0.97$\cdot$ MTOW) for C_L with this minimum velocity, this results in a C_L of 1.55 at 5000 ft landing altitude, which is achievable (from Figure 9.3. As 61.5 m/s (120 kts) is below 141 kts, the approach speed is well below category C and hence requirement **RA-TOP-PER-3.2** is met.

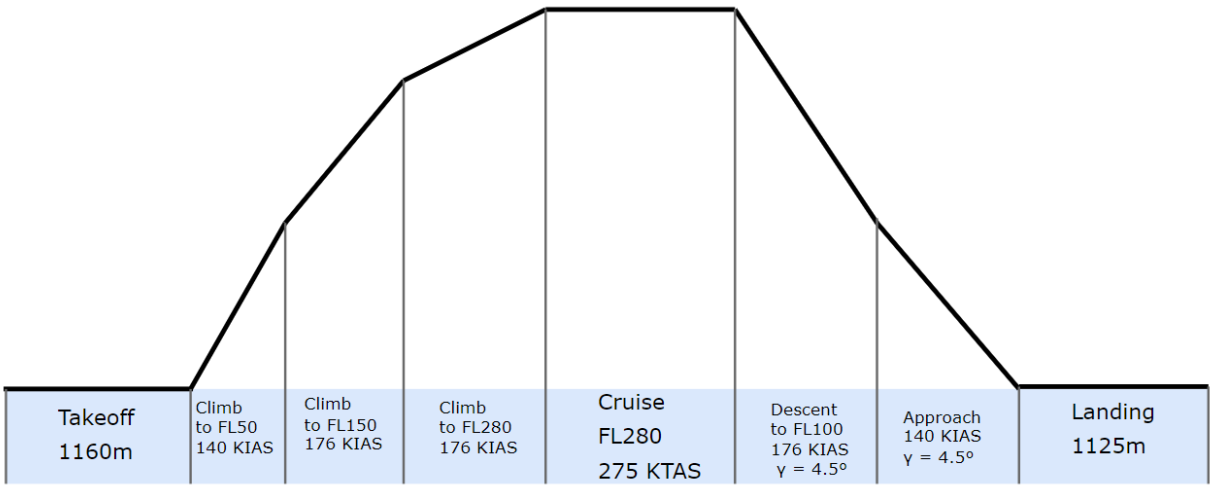

Figure 16.3: Mission Profile

The climb phase has a variable ROC depending on the power required at every instance. Furthermore, the aircraft is constantly accelerating to fly at constant IAS, as the TAS does change with altitude. In addition, the aircraft shall accelerate to enter a new climb phase, until finally the cruise level at FL280 is reached. The detailed climb profile has been worked out and is shown in Figure 16.4. The horizontal distance of the climb is equal to 74.5 nmi with a climb time of approximately 20.3 minutes. The climb profile shows compliance with requirements **RA-SYS-MSC-1.2**, **RA-TOP-PER-5.1**, and **RA-TOP-PER-5.2** respectively.

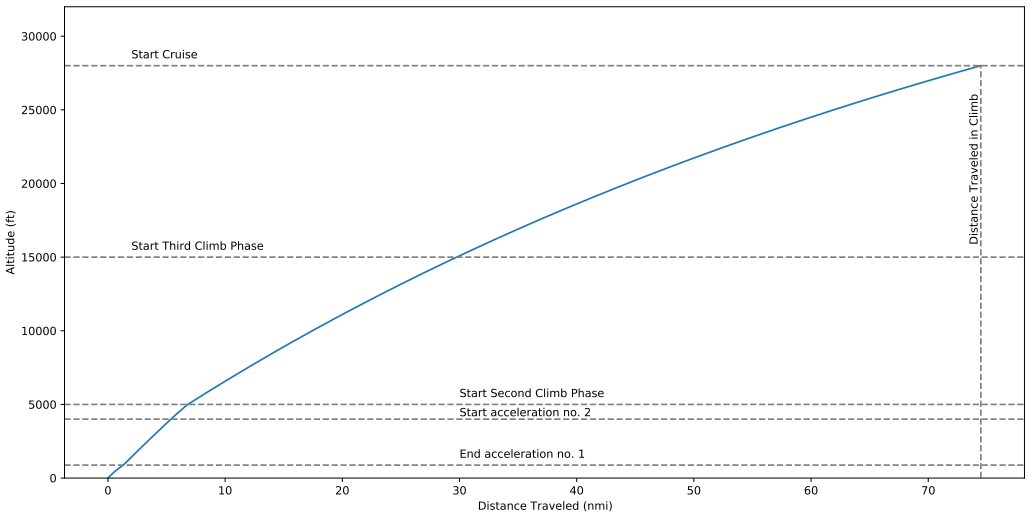

Figure 16.4: Climb Profile

16.6. Different Mission Profiles

The maximum attainable velocity can be calculated by setting $P_a = P_r$ for the respective altitude. At FL280, this results in a maximum attainable velocity of 336 KTAS for the current design C_L. The difference in consumed energy by flying at the maximum velocity with respect to the minimum cruise speed is 50.7% and hence is disregarded. Next, the difference in energy consumption between flying at FL280 with the minimum cruise speed and at FL400 as found in Section 16.3 is computed. When climbing to FL400 whilst adjusting the mission profile such that the cruise velocity remains 275 KTAS, the distance spent in cruise is found to decrease. In addition, the energy consumption decreases. The results are given in

Table 16.4. Note that the only difference in the mission profile would be that a constant speed of $\approx$ 140 KIAS is maintained for both climb and descent. Furthermore, the length of the phases increases a little as the cruise altitude changes to FL400. However, since the maximum operating altitude of the electric motors is FL350 (Section 12.4), flying at this altitude is infeasible.

Table 16.4: Difference in energy consumption of different flight levels

Variable	FL280	FL400	Percentage Difference
Cruise Distance	1650 [km]	1525 [km]	-7.6%
Energy Consumption	15,410 [MJ]	13,960 [MJ]	-9.4%

16.7. Critical Climate Takeof

As per objective **RA-OBJ-7**, the goal is to have proper performance in hot and high climates. To quantify this, an altitude of 7600 ft with a temperature of 40° is taken, which is where the A380 tested for their hot and high performance [3]. Next, using the one-engine inoperative case equation for required takeoff power as given by R. Vos [4], the W/P ratio is computed. As this condition was limiting in the design of the power train, the obvious outcome is that there is too little power available. However, if C_{L2} is increased by 12% to 2.1 which according to Figure 9.3 is achievable, the power required is around 2.44 MW. As the electric motors do not suffer from any power lapse, the SRP-22 has a big advantage over aircraft containing air-breathing engines, as the peak power remains 2.44 MW as per sea level. Furthermore, it is found that the distance to clear the obstacle is equal to 244 m, which means a climb angle of 3.5° shall be achieved. When computing the maximum achievable climb angle at these conditions, it is found that a climb angle up to 8.5° can be reached, easily complying with the aforementioned required climb angle.

[1] https://www.h3x.tech/ [cited 20 Jan. 2023]

[2] https://www.researchgate.net/figure/Typical-propeller-efficiency-curves-as-a-function-of-advance-ratio-J_fig3_281946347 [cited 20 Jan. 2023]

[3] https://www.geaerospace.com/press-release/jv-archive/gp7200-powered-a380-completes-high-altitude-and-hot-weather-testing[cited 31 Jan. 2023]

17
Technical Budget Breakdown

In the early phases of aircraft design, a technical budget was assigned to quantify a value for each key technical parameter of the design [30] and a contingency was assigned to the same. At this phase of the design, this budget is reviewed to check the accuracy of the parameters, which were budgeted.

Range

The first budget to be assessed is the maximum range of the aircraft. The maximum range of the aircraft has a direct effect on the airlines' business model. As a top-level requirement **RA-TOP-PER-2**, the new aircraft shall have a design range of 1000 nmi. This is similar to the regional turboprop aircraft in the market. Therefore, a range budget of 1000 nmi is adopted for the design. For the final design of SRP-22, the range is 1450 nmi, this is the outcome when taking maximum fuel mass and a range of 1020 nmi. taking only the necessary trip fuel mass.

Cruise Speed

For the cruise speed, the top-level requirement **RA-TOP-PER-3.1** states that the aircraft shall have a minimum cruise speed of 275 kts. This is comparable to similarly sized turboprop regional passenger aircraft. Therefore, the cruise speed budget is set at 275 kts. This is also the final value of cruise speed for the SRP-22.

Runway Field length

Determination of the runway field length budget for both take-off and landing is given as requirements **RA-TOP-PER-4.1.1**, **RA-TOP-PER-4.1.2**, **RA-TOP-PER-4.2.1**, **RA-TOP-PER-4.2.2** that the aircraft shall have a maximum field length of 1370 m. Thus, a budget of 1370 m is set. Additionally, the SRP-22 has a 1160 m take-off field length and a 1370 m landing field length.

Mass

Maximum Takeoff Mass Minimizing the weight of an aircraft is a subject of paramount importance as an increase in weight in one component often resulted in a weight increase in another component, commonly known as the 'snowball effect'[20]. The rapid mass estimation method is applied where the component weight of an aircraft is determined by relating it in terms of a fraction given in a percentage of the maximum takeoff mass (MTOM)[29].

Operational Empty Mass Literature suggested that the OEM typically accounts for 53%-58% in a regional/ short-haul aircraft. This is cross-checked with the OEM obtained by taking the average of said parameter of 13 reference aircraft. It can be seen that from both methods, the OEM accounts for around 58% of the aircraft's weight. Thus, for the preliminary estimation of the OEM fraction, a value of 58% is set. The maximum takeoff weight and the OEMs of the reference aircraft are tabulated in Table 17.1, whereas a more detailed estimation of the subsystem level mass fraction of the proposed aircraft is presented in table 17.2.

Fuel mass fraction: Similar to the payload mass budget, the fuel mass budget is also determined by using the rapid mass estimation method. It is suggested that the fuel mass fraction corresponds to 20%-28% of the MTOM in twin-prop regional aircraft whereas, for jet-powered counterparts, the fuel makes up to 22%-30% of the aircraft's total mass[29]. By comparing both values, a preliminary fuel mass fraction of 25% is set for the proposed aircraft.

Payload mass fraction: From literature, it has been suggested that the typical mass fraction of the wing group for a regional aircraft with two shaft engines is 15%-18%. For regional aircraft equipped with two jet engines, the M_{PL} equates to 12%-20% of the MTOM[29]. It is thus decided that for the upcoming regional

aircraft, the payload will account for 17% of the total weight of the aircraft.

Final Values SRP-22 After the class I and class II weight estimations analyzed in Section 7.2 and Section 7.3 respectively, the final MTOM of 18650 kg is determined as seen in Table 17.1, were it can be seen that the OEM is 68% of the MTOM. Note that instead of the rapid estimation method to estimate the OEW percentage contributions, in the class II weight estimations the Raymer method [19] is used and the percentages are defined as in Table 17.2. It can also be seen in conclusion, the final MTOM and OEM of the SRP-22, fall below the previously budgeted values from reference aircraft. Furthermore, the fuel mass turns out to be 4%, which is a much lower percentage, this is due to the fact that hydrogen is used as fuel instead of the conventional Jet A fuel. In addition, the payload mass turns out to be 28%, which turns out to be higher than the budgeted value of 17%, this is due to the fuel mass fraction being 86% lower than the budgeted one, as detailed in the below paragraph.

Table 17.1: MTOM and OEM Relations of Existing Turboprops[62] and SRP-22

Aircraft Model	MTOM [kg]	OEM [kg]	OEM fraction [%]
ATR-42-600	18600	11750	63.2
Dash 8 Q300	19505	11793	60.5
ATR-72-600	22800	13311	58.4
Dash 8 Q400	29800	17819	59.8
Xian MA600	21800	13730	63.0
Saab 2000	23000	13800	60
Fokker F50	20820	13400	64.4
An140	21500	12810	59.6
Average turboprop	**22228**	**13552**	**61**
SRP-22	**18650**	**12770**	**68**

Table 17.2: Estimated Mass Fraction Based on the Rapid Estimation Method[29] and the final SRP-22 values

	REM [%]	SRP-22 [%]	Difference [%]
Fuselage	11	11.8	7.3
Wing	10.5	12.1	15
Empennage	2.5	6.8	172
Undercarriage	4	3.3	-17.5
Powerplant	9.5	11.4	20
System	8.5	11.2	32
Others	16	11.4	-29
OEW	**58**	**68**	**17**
Fuel	25	4	-84
Payload	17	28	65
MTOW	**100**	**100**	

Parameters like Range, Cruise speed etc mentioned above were used are design inputs and therefore have the same value as the budget. Furthermore, a contingency management plan is taken into account for the technical budget, which decreases as the design matures. At this stage of the design, the final configuration has been chosen which is a conventional high-wing and T-tail configuration. The mass is a great contributor to the technical budget breakdown. At the preliminary design stage, a contingency of 20% was taken into account [30]. Since some details of the design have been worked out already, the contingency is decreased from 20% to 10% for further design stage. In addition, parameters like the range, the cruise speed etc are not set to change significantly in further stages of the design taken therefore a contingency factor of 5%.

18
Financial Analysis

The purpose of this chapter is to give insight into the manufacturing and research and development costs for the client. Alongside an analysis of the Return on Investment and break-even point for future marketing. Finally, the operation cost of the SRP-22 program has been established, based on the estimated Direct Operating Cost for different assumptions made for the fuel cell price. All methods within this chapter are discussed by J. Roskam [63] and the cost and price are adjusted for inflation in 2035.

18.1. Manufacturing, Research and Development Cost

The cost of manufacturing is the key influence on the asking price per aircraft, the break-even point, and the ROI. The biggest segment of the manufacturing cost is the production cost, in which fuel cell cost heavily influences the cost. Hence, the effect of the estimated fuel cell price prediction in 2035 will be analyzed. Three different fuel cell prices are taken as a preliminary estimate, one being the current $/kW price of fuel cell stacks, 50% price reduction in current $/kW price of fuel cell stacks, and optimistic fuel cell price by 2035 discussed by Aerospace Technology Institute [64]. The fuel cell prices are shown in Table 18.1.

Table 18.1: Fuel cell price

Types of fuel cell prices	Price [$/kW] (Inflation-adjusted to FY2035, USD)
No price reduction compared to 2022[1]	6,000
50% Price reduction compared to 2022	3,000
Optimistic price[64]	640

As shown from Table 18.1, the difference between the optimistic price of fuel cell and no price reduction fuel cell price is approximately 95%. Due to the great reduction in fuel cell price, the manufacturing cost varies greatly between the different fuel cell prices. The total manufacturing cost of 1,000 aircraft sold is shown in Table 18.2, and the 1,000 aircraft sold analysis is based on the estimate of the SRP-22 program selling 1,000 aircraft stated in Chapter 5.

Table 18.2: Manufacturing cost for different fuel cell prices

Types of fuel cell price	Manufacturing cost [$] (FY2035, USD in millions)
Current fuel cell price	29,500
50% reduction to current fuel cell	21,000
Optimistic price	14,600

As shown from Table 18.2, the difference in manufacturing cost differs by approximately 50%. The manufacturing cost breakdown of each fuel cell price is shown in Figure 18.1.

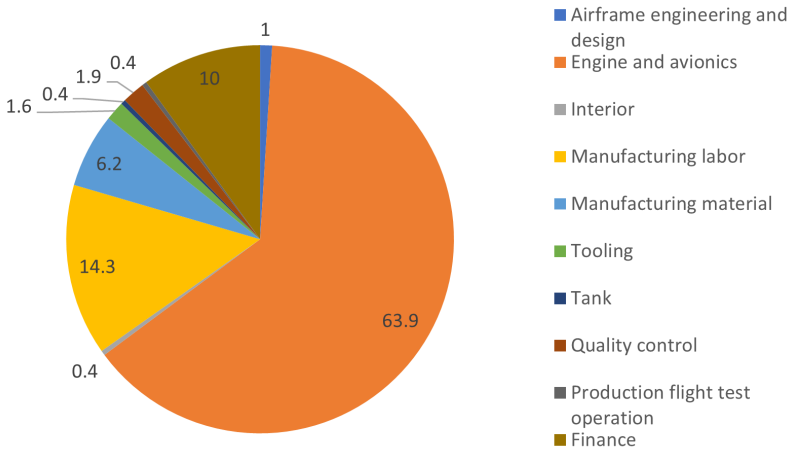

(a) Without fuel cell price reduction

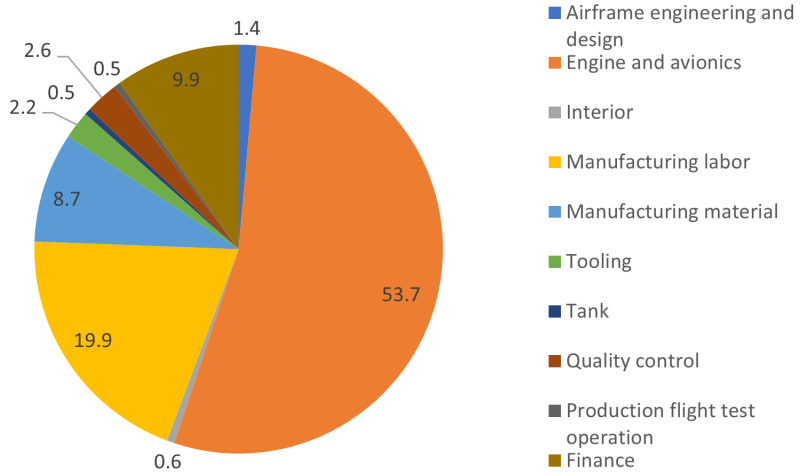

(b) With 50% fuel cell price reduction

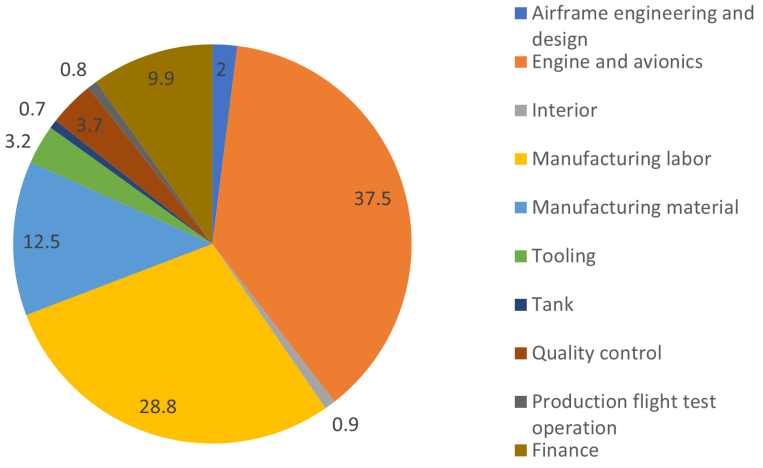

(c) With optimistic fuel cell price

Figure 18.1: Cost breakdown structure for research and development phase

In Figure 18.1, the fuel cell price is incorporated in the engine and avionics price. From the figure, it can be deduced that the fuel cell price greatly influences the cost breakdown of the manufacturing cost. Only when the price is using the optimistic price of fuel cell the engine and avionics price is less than 50% of the total manufacturing cost. Hence, to achieve lower manufacturing costs, the optimistic fuel cell is preferred.

The R&D cost of different fuel cell prices is shown in Table 18.3.

Table 18.3: Research and development cost for different fuel cell prices

Types of Fuel Cell Price	Research and development cost [$] (FY2035, USD in millions)
Current fuel cell price	1,550
50% reduction to current fuel cell	1,510
Optimistic price	1,470

As shown in Table 18.3, the difference between the current fuel cell price and optimistic price R&D cost varies by approximately 5%. To better understand the effect of the fuel cell price influence, the cost breakdown of the R&D phases is illustrated in Figure 18.2.

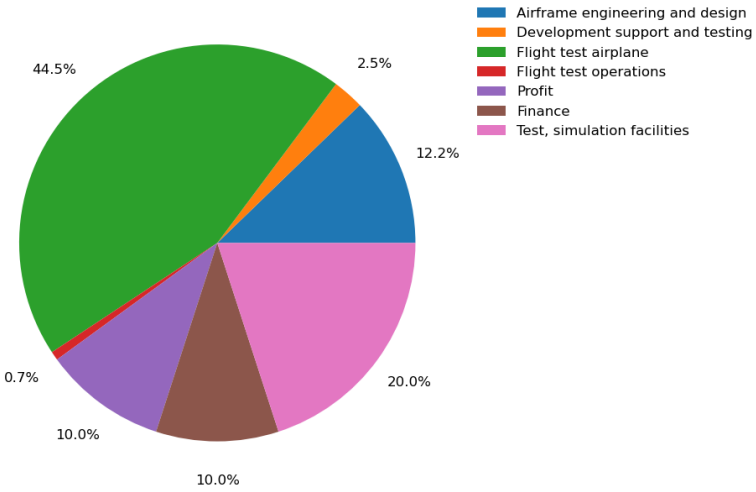

(a) Without fuel cell price reduction

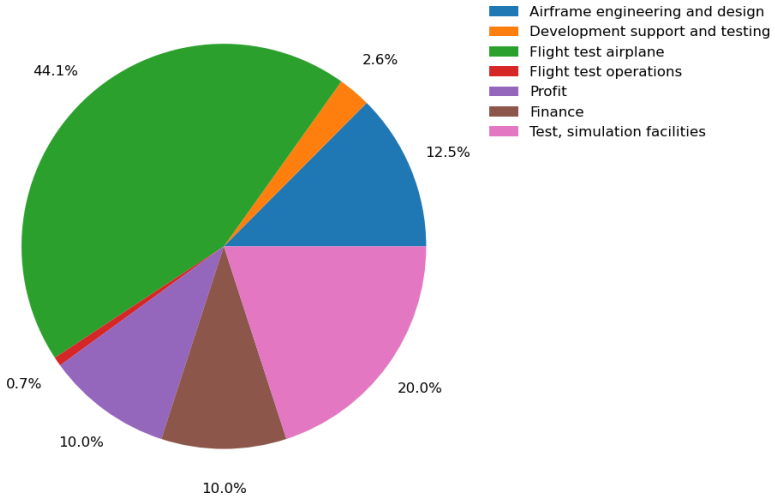

(b) With 50% fuel cell pice reduction

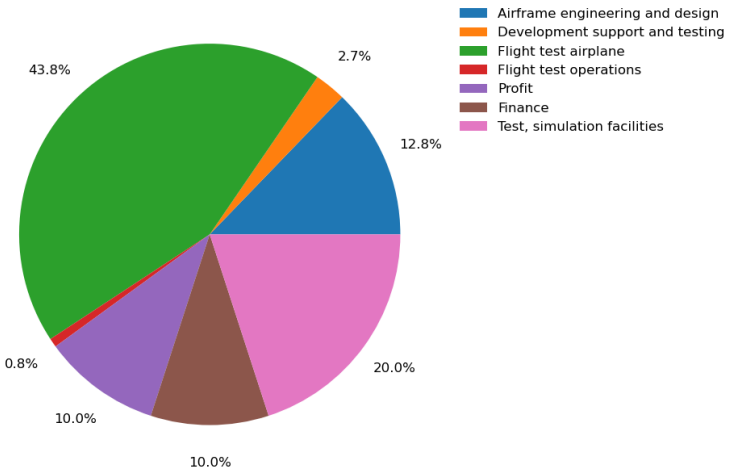

(c) With optimistic fuel cell price

Figure 18.2: Cost breakdown structure for research and development phase

As shown in Figure 18.2 the manufacturing cost of the test aircraft contributes the most to the total cost during the R&D phase, despite the price of the fuel cell. As shown from Figure 18.1 the fuel cell price greatly influences the manufacturing cost, which explains the lower R&D cost for optimistic fuel cell price and the decrease in flight test plane manufacturing cost contribution to the R&D cost.

18.2. Return on Investment and Break-Even Analysis

The Aircraft Estimated asking Price (AEP) could be determined based on the manufacturing cost and R&D cost. The variation of the number of aircraft sold and Aircraft Estimated asking Price with 20% profit margin from manufacturing cost is shown in Figure 18.3.

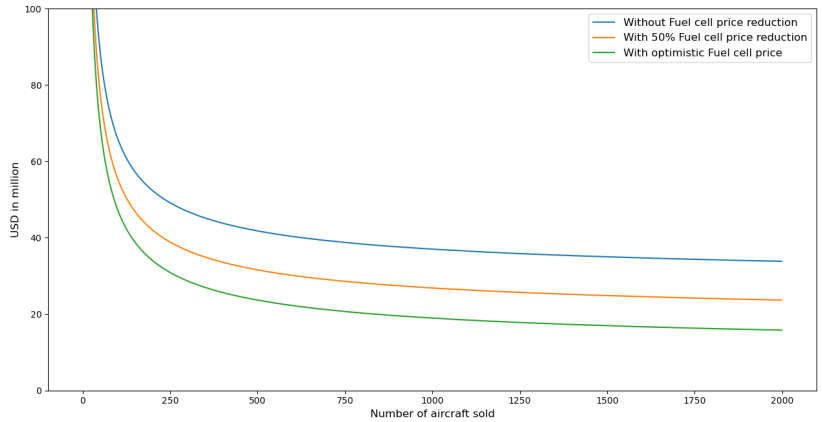

Figure 18.3: Aircraft Estimated asking Price

As shown from the Figure 18.3, the results are proportional to the manufacturing cost and the R&D cost. The AEP for 1000 aircraft sold, the break-even point, and the ROI for 1000 aircraft sold are stated in Table 18.4. From the values it can be deducted that **RA-TOP-COS-1** is met for the three estimated fuel prices for the expected market analysis.

Table 18.4: AEP, break-even point, and ROI

Types of fuel cell price	AEP [$] (FY2035, USD in millions)	AEP [$] (FY2022, USD in millions)	Break-even point (number of aircraft)	ROI
Current fuel cell price	37	31	411	19%
50% reduction to current fuel cell	27	22	502	19%
Optimistic price	19	16	601	18%

As shown from Table 18.4, to achieve the break-even point the earliest the current fuel cell price should be used, and the AEP just meets the market competitiveness discussed in Chapter 5. Whereas in the case of only a 50% reduction of the current fuel cell price by 2035, the AEP is approximately 10 million lower in AEP compared to the asking price discussed in Chapter 5. Whereas in the case of optimistic fuel cell price, despite the lengthy process until the break-even point, the AEP is approximately 50% lower than the asking price discussed in Chapter 5. Hence, the fuel cell price will not hinder the SRP-22 project in terms of AEP. The cost breakdown structure of the SRP-22 program with optimistic fuel cell price is shown in Figure 18.4.

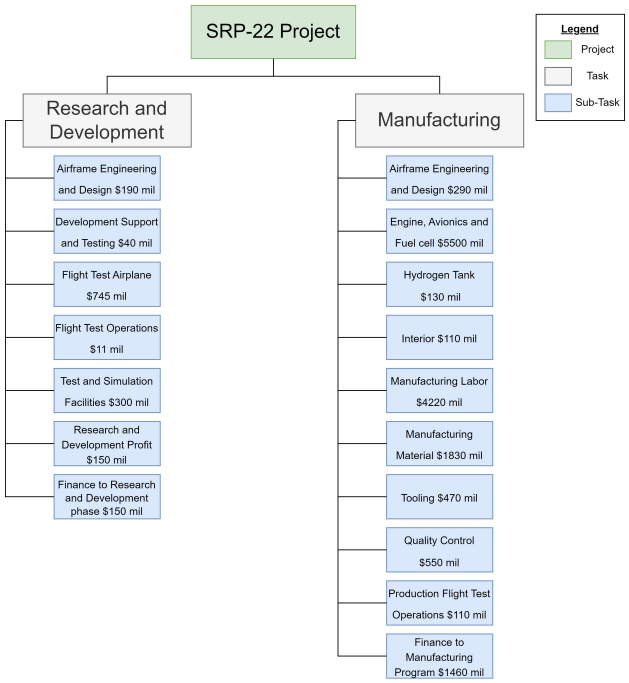

Figure 18.4: Cost breakdown structure of the SRP-22 with optimistic fuel cell price

18.3. Operation Cost

To obtain market competitiveness, the operational cost is analyzed. The Direct Operating Cost (DOC) consists of the flight cost, maintenance cost, depreciation cost, and administration cost. The hydrogen price used to calculate the direct operating cost is $2 per kg^2. All three fuel cell prices are analyzed as the depreciation cost varies greatly due to fuel cell price. The DOC for 500 nmi of different fuel cell prices is shown in Table 18.5.

Table 18.5: Direct Operating Cost for different fuel cell prices

Types of fuel cell price	DOC per seat nmi [$/nmi] (FY2035, USD)	DOC per seat nmi [$/nmi] (FY2022, USD)
Current Fuel cell price	0.26	0.22
50% reduction to current fuel cell	0.22	0.18
Optimistic price	0.19	0.16

As shown in Table 18.5, for the optimistic fuel cell price the 10% reduction in the Direct Operating Cost (in FY2022) requirement **RA-TOP-COS-2** is met as discussed in Section 5.3 with the correction to 2035 using the escalation factor discussed by Roskam [63]. Whereas the Direct Operating Cost for 50% reduction in fuel cell price is comparable to the direct operating cost of the ATR-72. The direct operating cost for no reduction in fuel cell price is comparable to the direct operating cost of the ATR-42. The total operating cost combining direct and indirect operating cost are shown in Table 18.6.

Table 18.6: Total Operating Cost for different fuel cell prices

Types of fuel cell price	Total operating cost per seat nmi [$/nmi] (FY2035, USD)
Current fuel cell price	0.55
50% reduction to current fuel cell	0.46
Optimistic price	0.39

The total operating cost is an important factor for airlines to determine the total program operating cost. For the analysis of total program operating cost, it is assumed a total of 100 airlines are purchasing the SRP-22 based on the routes analysis of SRP-22 in Chapter 5. Furthermore, it is assumed that all airlines purchase 10 aircraft, hence the total program operating cost for airlines is shown in Table 18.7 with the estimate of SRP-22 having a lifespan of 25 years.

Table 18.7: Total Program Operating Cost for different fuel cell price

Types of fuel cell price	Total program operating cost [$] (FY2035, USD, millions)
Current Fuel cell price	4600
50% reduction to current fuel cell	3870
Optimistic price	3290

For the SRP-22 to be considered a successful program and to meet both the aircraft asking price and direct operating cost requirement, the optimistic fuel cell price would be needed. With a 50% reduction in current fuel cell price and no fuel cell price reduction, the program could potentially still be a competitive product due to lower environmental impact, and have comparable direct operating cost to aircraft competitors.

[1]URL https://www.emobility-engineering.com/hydrogen-fuel-cells/ [cited 24 Jan. 2023]

[2]URL https://blogs.worldbank.org/ppps/green-hydrogen-key-investment-energy-transition#:~:text=According%20to%20Bloomberg%20New%20Energy,price%20competitive%20with%20natural%20gas. [cited 24 Jan. 2023]

19 Sustainability

Sustainability is a very important factor when it comes to aviation. Therefore different metrics were used to analyze how sustainable the SRP-22 is. For these a life cycle assessment was done, as well as an Average Temperature Response analysis indicating how much more sustainable the SRP-22 is compared with the ATR42-600. Lastly, the Effective perceived noise was calculated to see whether it complies with noise limit requirements from ICAO.

19.1. Average Temperature Response

The average temperature response (ATR) shows the environmental impact of an aircraft fleet for a certain time in terms of temperature response during flight operations. It is important for sustainability to keep this number as low as possible. The average temperature response is calculated using Equation 19.1. The normalized radiative forcing, RF, is calculated for all emissions during flight, as presented by Proesmans [65]. The calculations of the G-factor are done using the method proposed by [66]. The main input, to be changed, for the average temperature, is the mass flow of the propulsion system.

$$\Delta T(t) = \int_{t_0}^{t} G_T\left(t - t'\right) \cdot \mathrm{RF}^*\left(t'\right) dt' \text{ with } G_T(t) = \frac{2.246}{36.8} \mathrm{e}^{-t/36.8} \tag{19.1}$$

The emissions accounted for when using a hydrogen fuel cell are water vapor emissions and contrails. As these are short-lived emissions, a time horizon of 30 years is accounted for [66]. The graph for the temperature response of the SRP-22 and the ATR42-600 are plotted in Figure 19.1 and Figure 19.2 respectively. Since the ATR of the SRP-22 is significantly lower than that of its counterparts that use kerosene [66], it fulfills the objective of the mission needs statement.

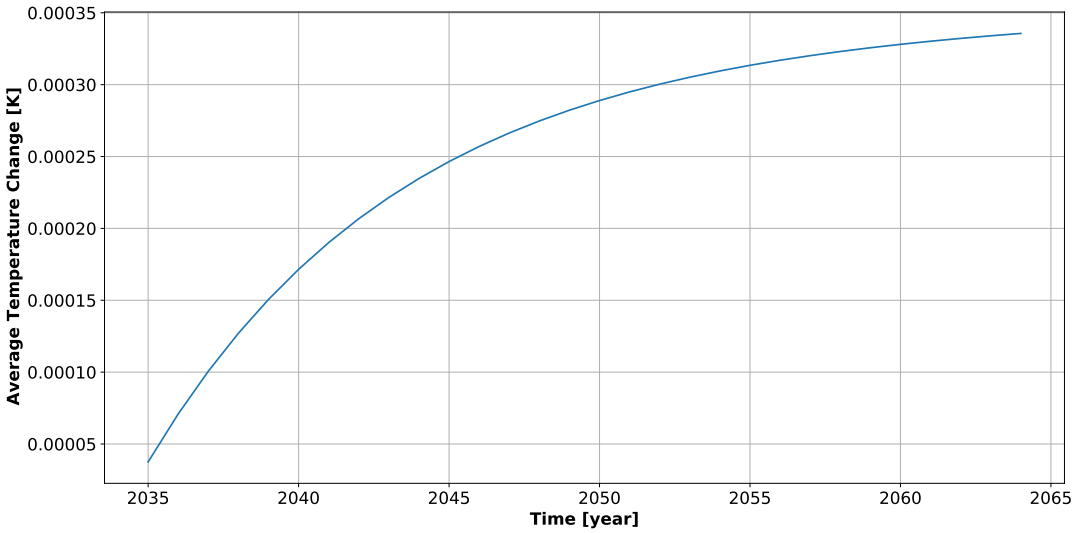

Figure 19.1: Average Temperature Response over 30 years for aircraft fleet of SRP-22

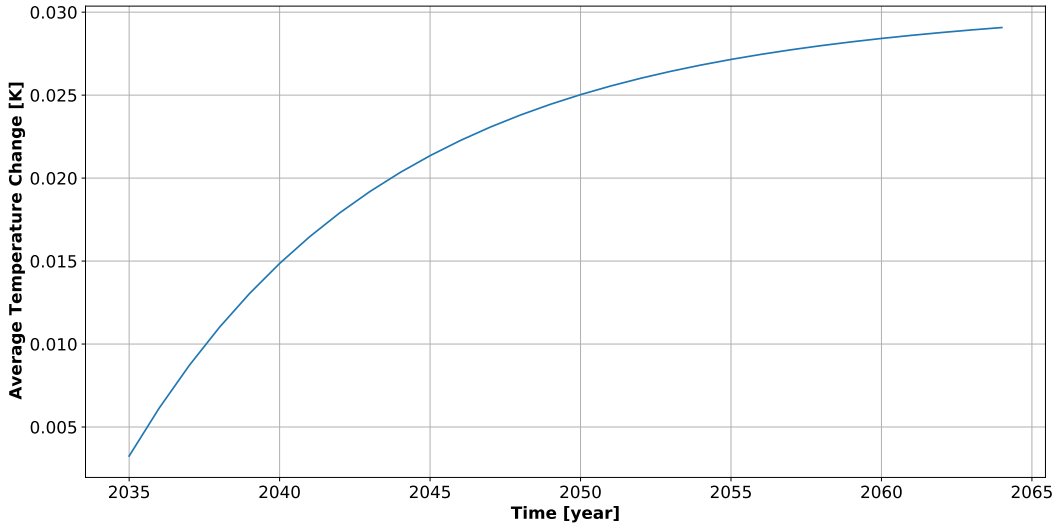

Figure 19.2: Average Temperature Response over 30 years for aircraft fleet of ATR 42

Looking at both graphs above it can be stated that the SRP-22 has an average temperature change lower than the ATR42 by a reduction factor of 80, making it therefore a more sustainable aircraft, thus minimizing climate impact as is stated in the mission need statement.

19.2. Life Cycle Assessment

The environmental assessment is relevant for the entire life cycle. Therefore, the following stages have been defined.

- **Raw material extraction**
  The materials that will be considered for the structure of the aircraft will have to be suitable for sustaining large forces, all while minimizing the environmental impact of the extraction of the raw material and maximizing the durability of the material in the structure. Another part of the raw material extraction is the creation of the energy source that will be used in operations.
- **Manufacturing**
  In the manufacturing stage, different production methods will be considered that can be applied to the various phases in the manufacturing of an aircraft. The manufacturing stage will mainly focus on a sustainable working environment, using green energy sources and minimizing waste, taking a lean thinking approach.
- **Transportation**
  An imperative factor in the design process of an aircraft is transportation. The complex technology of the respective parts creates a necessity for mature technology that can only be found at specific factories, spread across the world. Optimizing the transportation lines for this would optimize sustainability, from both an environmental and economic point of view.
- **Usage**
  The usage of the aircraft entails all operations, including ground and airborne operations. The main objective for minimizing environmental impact during the flight will be related to the reduction of emissions due to propulsion. This reduction in emissions, made possible due to hydrogen propulsion, can be found in Section 19.1
- **Waste disposal**
  The aircraft's after-life can be optimized for environmental reasons by waste reduction. Furthermore, the integration of a circular life cycle will be considered. The SRP-22 is largely constructed using aluminium alloys which are easily recyclable, thus making it more sustainable than its composite counterparts.

19.3. Noise

The noise requirements **RA-TOP-SUS-2.1**, **RA-TOP-SUS-2.2** and **RA-TOP-SUS-2.3** derived from ICAO Annex 16 Volume I state that the maximum noise levels shall not exceed the following:

- At the lateral full-power reference noise measurement point: $\leq$ 94 EPNdB
- At flyover reference noise measurement point: $\leq$ 89 EPNdB
- At approach reference noise measurement point: $\leq$ 98 EPNdB

The lateral, flyover and approach noise certification points are defined by ICAO as shown in figure 19.3. The distance from the flyover point to the aircraft is 640 m, obtained by using the climb profile found in Figure 16.4.

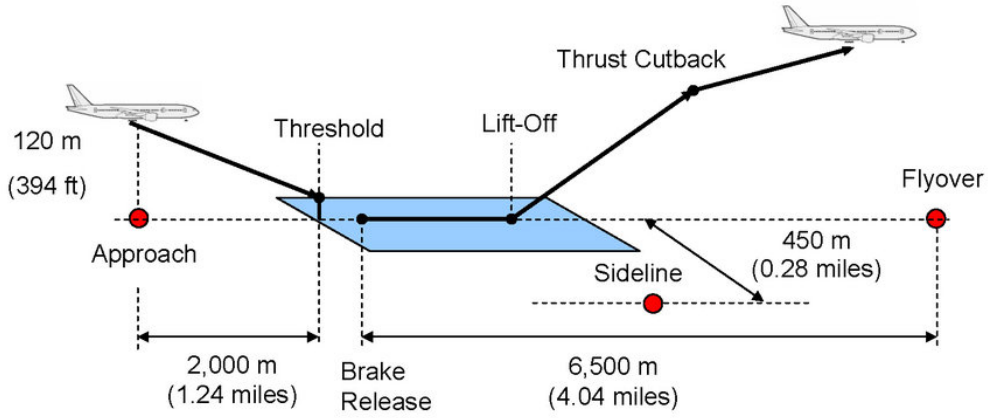

Figure 19.3: ICAO noise certification points [67]

To estimate the noise production of the aircraft, only the largest contributors are assessed. The largest sources of noise of an aircraft are the propulsion system and the airframe, as can be seen in Figure 19.4. The largest noise source of the electric propulsion system are the propellers, whereas the contribution of the electric motors and other mechanical components such as the gearbox are considered negligible in this analysis[68]. The airframe however has a significant impact on the noise emission, especially during approach due to the deployment of the landing gear and high-lift devices. Therefore the noise of the propellers and airframe are both considered.

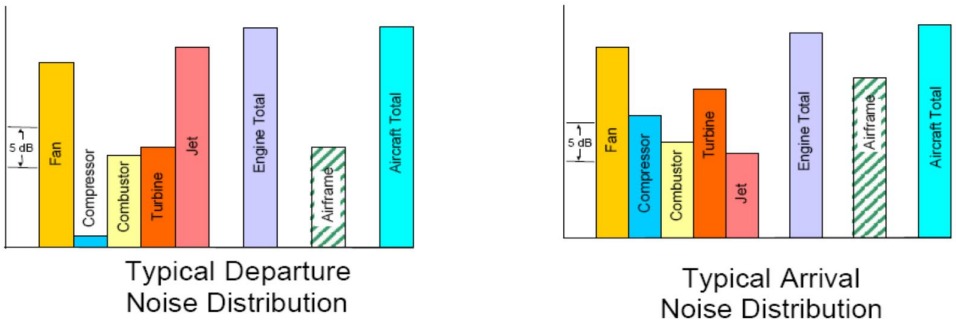

Figure 19.4: Typical noise source breakdown for aircraft [69]

Propeller noise

In order to estimate the noise produced by the propellers of the aircraft, the method presented in [70] is used. Although noise estimation is a complex process, it provides a simple method to give a first order approximation for far-field noise of propellers based on a number of parameters related to the propeller and engine. The parameters that are used are:

Table 19.1: Parameters used for propeller noise estimation

Parameter	Value	Unit	Parameter	Value	Unit
Propeller efficiency	0.8	[-]	Velocity at takeoff	101	[kts]
Number of blades	6	[-]	Velocity at approach	141	[kts]
Blade angle during takeoff	15	[°]	Advance ratio during takeoff	0.6	[-]
Blade angle during approach	17	[°]	Advance ratio during approach	0.85	[-]
Shaft power main engine	1310	[HP]	Rotational frequency main engine	1720	[RPM]
Shaft power wingtip engine	330	[HP]	Rotational frequency wingtip engine	2430	[RPM]
Diameter main propeller	3.03	[m]	Mach number at main propeller tip	0.79	[-]
Diameter wingtip propeller	2.15	[m]	Mach number at wingtip propeller tip	0.79	[-]

For the lateral and flyover case, the takeoff conditions are used. For these cases, the engines are considered to be on the maximum power setting. During approach, 10% of maximum power is assumed. The advance ratio J is chosen such that the engines operate at constant RPM:

$$J = \frac{V_{\text{TAS}}}{n \cdot D} \tag{19.2}$$

Where n is the rotational frequency of the engines in revolutions per second. The advance ratio can be adjusted by changing the propeller blade angle, which can be seen in Figure 19.5.

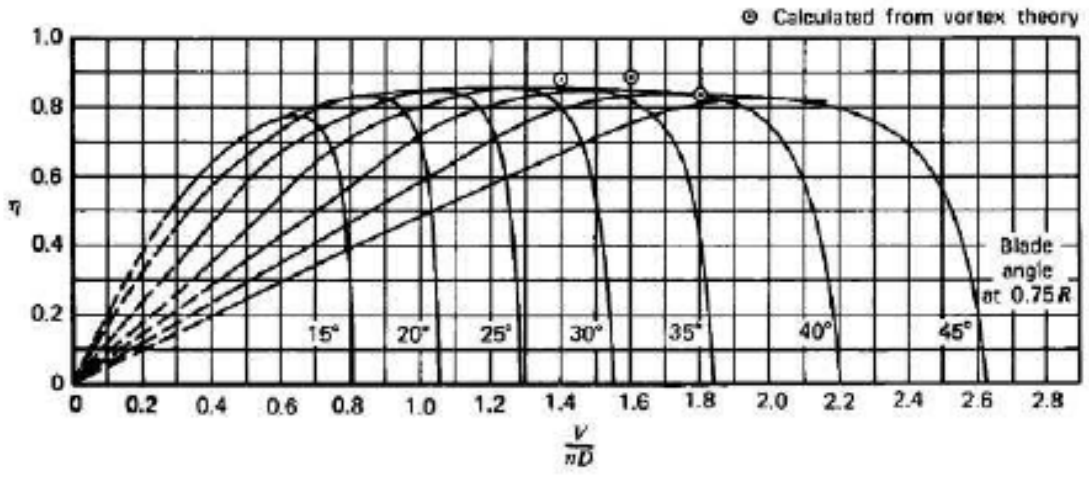

Figure 19.5: Typical propeller efficiency curves as a function of advance ratio J[71]

The resulting noise levels in EPNdB for the main propellers and wingtip propellers are combined using Equation 19.3 to obtain a total noise estimate for each certification scenario and can be found in Table 19.2.

$$EPNdB_{total} = 10 \cdot \log_{10}\left(\sum_{i=1}^{n} 10^{\frac{EPNdB_i}{10}}\right) \tag{19.3}$$

Airframe noise

The airframe noise is caused by the aerodynamic interaction of the atmosphere and the exterior of the aircraft. A first-order estimation method is established by NASA [72]. It uses the following relationship derived from airframe noise measurements:

$$SPL_{\text{clean}} = 10 \cdot \log_{10}(V^5) + 10 \cdot \log_{10}(W) - 74.0 \tag{19.4}$$

Where SPL_{clean} is the sound pressure level in dB for a clean aircraft configuration, normalized to an altitude of 152 meters from the aircraft. V is the aircraft velocity and W is the weight of the aircraft, both considered

at the noise certification point. The following steps are taken to obtain the noise level in EPNdB for the three certification points:

1. Equation 19.3 is considered at maximum takeoff weight for all certification points, and V is taken as 97.2 m/s due to limitations of Equation 19.3 [72];
2. Two correction factors are added to Equation 19.3 to account for the deployment of the flaps and landing gear, wich are $C_{\text{f}} = 7$ and $C_{\text{lg}} = 5$ respectively [72];
3. The sound pressure level in dB is adjusted to the distance to the certification points and converted to A-weighted sound pressure level in dBA using the method proposed in [70];
4. The A-weighted sound pressure level is converted to Effective Perceived Noise Pressure Level (EPNdB) by adding 13 as proposed in [73].

This results in the noise levels in EPNdB for the three certification points which can be found in Table 19.2.

Total noise and requirement compliance

The total noise is computed with Equation 19.3 using the EPNdB values caused by the airframe and propeller for each certification scenario. The resulting total noise is presented in Table 19.2 and compared to the noise certification limits. Since there is a large margin to the limit cases, it can be concluded that the aircraft meets the requirements in this first-order approximation.

Table 19.2: Noise breakdown, total and limit overview for the certification points

Certification point	Propeller Noise (EPNdB)	Airframe Noise (EPNdB)	Total Noise (EPNdB)	Noise limit (EPNdB)
Lateral	88.5	68.9	**88.5**	**94**
Flyover	85.3	64.2	**85.3**	**89**
Approach	85.9	82.6	**87.6**	**98**

In conclusion, SRP-22 complies with the noise requirements stated by ICAO and is also listed in RA-TOP-SUS-2.1, RA-TOP-SUS-2.2, and RA-TOP-SUS-2.3.

20 Operations and Logistics

In order for hydrogen-powered aircraft to take flight, a supported hydrogen infrastructure needs to be developed. This chapter describes the most important aspects of such infrastructure from production to ground operations at the airport. In addition, flight operations and logistics are outlined.

20.1. Hydrogen infrastructure

Production

Currently, one of the biggest challenges towards the use of hydrogen in aviation is the limited sustainable production capacity of hydrogen. Nowadays the majority of the hydrogen is produced by steam methane reforming (SMR), which uses natural gas as a raw material and creates CO2 as a byproduct. This CO2 could be captured and stored for a zero-emission production process of so called 'Blue hydrogen'. Numerous other production methods exist, often referred to with their color code as can be seen in Figure 20.1[1].

	Terminology	Technology	Feedstock/ Electricity source	GHG footprint*
PRODUCTION VIA ELECTRICITY	Green Hydrogen	Electrolysis	Wind | Solar | Hydro Geothermal | Tidal	Minimal
	Purple/Pink Hydrogen		Nuclear	
	Yellow Hydrogen		Mixed-origin grid energy	Medium
PRODUCTION VIA FOSSIL FUELS	Blue Hydrogen	Natural gas reforming + CCUS Gasification + CCUS	Natural gas | coal	Low
	Turquoise Hydrogen	Pyrolysis	Natural gas	Solid carbon (by-product)
	Grey Hydrogen	Natural gas reforming		Medium
	Brown Hydrogen	Gasification	Brown coal (lignite)	High
	Black Hydrogen		Black coal	

*GHG footprint given as a general guide but it is accepted that each category can be higher in some cases.

Figure 20.1: Hydrogen Production Methods with Color Codes

While a hydrogen powered aircraft may have zero in-flight emissions, it is important that the hydrogen is also produced without emissions to minimize the total climate impact of the aircraft. Therefore countries should strive for production of hydrogen with renewable or nuclear energy.

Since hydrogen is one of the few candidates for storage of renewable energy in the future, the transition to a hydrogen infrastructure should be seen in a larger national and supranational context. Many industries together will create a large demand for a sustainable energy source in the future, potentially pushed by governmental organizations to meet climate goals or reduce dependency on fossil fuels. Therefore blue hydrogen, albeit CO2 neutral, is not suitable for long term usage because of its dependency on natural gas.

With this perspective in mind, hydrogen production plants should be located near nuclear or renewable energy plants such as large wind parks or solar farms, depending on the nature of the region. Also, the hydrogen production plant should be near the relevant industries such as airports and industrial production plants to minimize the transport of hydrogen.

Transport

In the early stages of a hydrogen infrastructure, it would be ideal to minimize the adaption of airports to accommodate hydrogen aircraft. Hydrogen will need to be liquefied to increase its volumetric energy density,

before it can be used in aircraft. This could be done at the hydrogen production site, and then be transferred to the airport with insulated cryogenic tanker trucks, which is a proven and used means of transport[2]. Another option would be to transport hydrogen via a dedicated pipeline infrastructure. Since the hydrogen is gaseous in these pipelines, it would need to be liquefied at or close to the airport. Such hydrogen pipelines already exist to a limited extent in Europe and the United States[3] and there are concrete plans for the development of an extensive hydrogen pipeline infrastructure throughout Europe in the upcoming two decades which can be seen in Figure 20.2 [16].

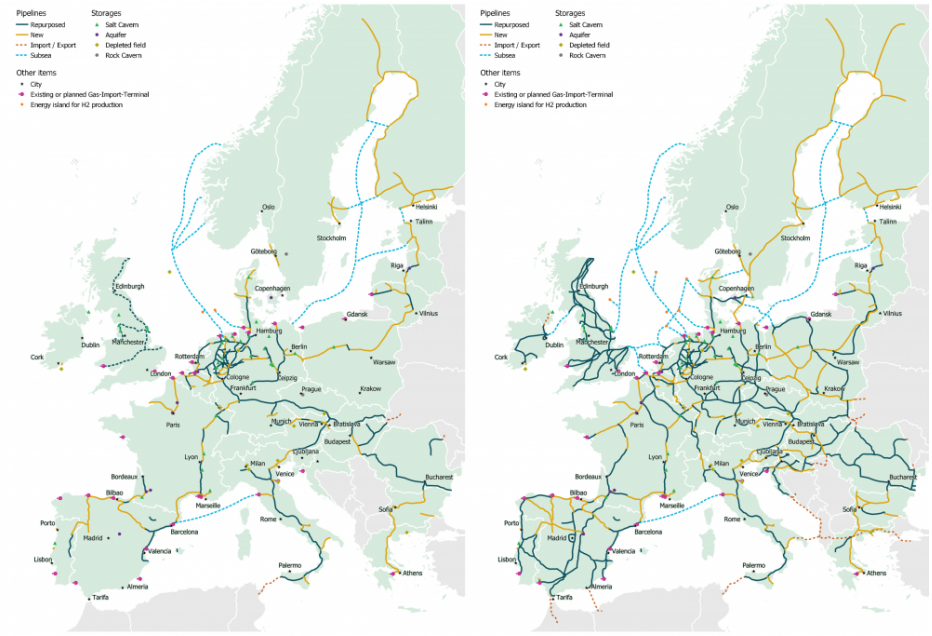

Figure 20.2: European Hydrogen Pipeline Network Plan for 2030 (left) and 2040 (right)

Storage

Storage of liquid hydrogen can be achieved in multiple ways, with the two main techniques being cooling to cryogenic temperature or pressurizing the storage tank to 700 bar. Both techniques are proven technology and are currently mostly used in the high-tech and space industry [4]. The port of Kobe in Japan currently operates a liquid hydrogen terminal with a tank capacity of 2,250 m^3 [5], which would be enough to completely tank the SRP-22 around 200 times.

20.2. Ground operations

The general ground operations of the regional aircraft are shown in 20.3. The majority of this process is identical for traditional kerosene powered aircraft, except for liquid hydrogen refueling. This process is explained in 20.2.

Refueling and turnaround time

The method of liquid hydrogen tanking depends on the available airport hydrogen infrastructure. The option that requires the least adaption to the airport is to use insulated tank trucks to maintain the liquid state of the hydrogen. Airbus is currently developing a liquid hydrogen refuelling station at Toulouse Airport, expected to be operational in 2025 [6].

Knowing the Liquid Hydrogen density of 71 kg/m^3, assuming a flow velocity of 2.5 m/s [12]. Two hose diameters were taken into account one of the inner diameter of 50 mm and another of 100 mm [7]. The smaller hose implies a fuelling time of 32 minutes, while the latter results in a much shorter fueling time of 8 minutes, meaning with both hose sizes **RA-SYS-OPM-4** is complied for.

The SRP-22 the aircraft is equipped with a lightweight extendable staircase to allow for fast passenger turnaround, avoid mobile stairway airport fees and increase independence in remote airports which might

not have suitable mobile stairways for SRP-22. The stairway is made of Aluminium alloy 2024-T3 to allow for lightweight design. The weight of the internal staircase is estimated to be around 150 kg based on the CAD model shown in Figure 20.4, around 1% of the operational empty mass. Due to this relatively low fraction and for sake of simplicity, it is not taken into account in the weight estimation, stability and control analysis and sizing of the aircraft in this design stage.

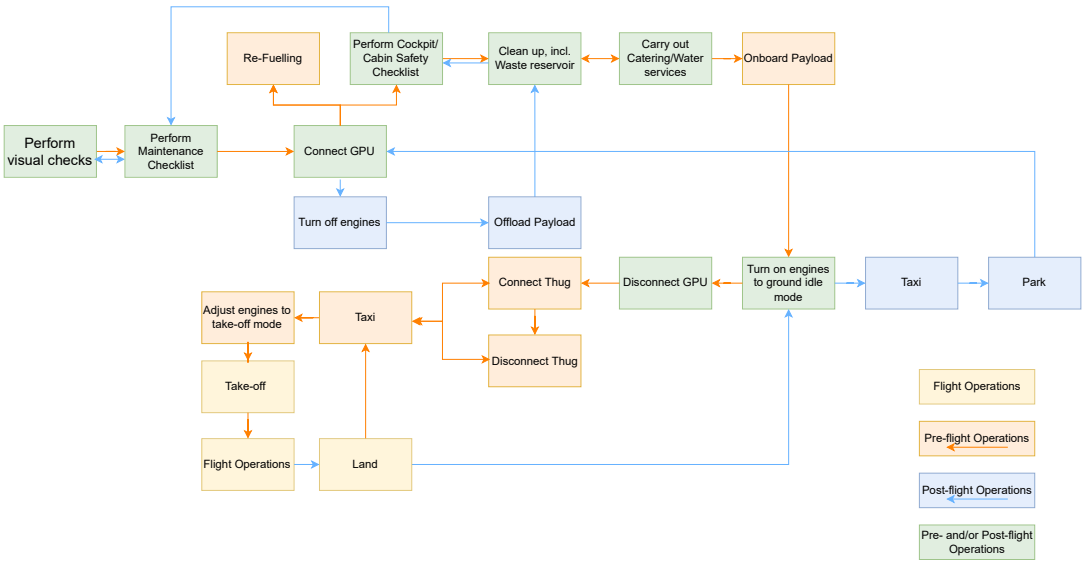

Figure 20.3: Ground Operations Flow Diagram

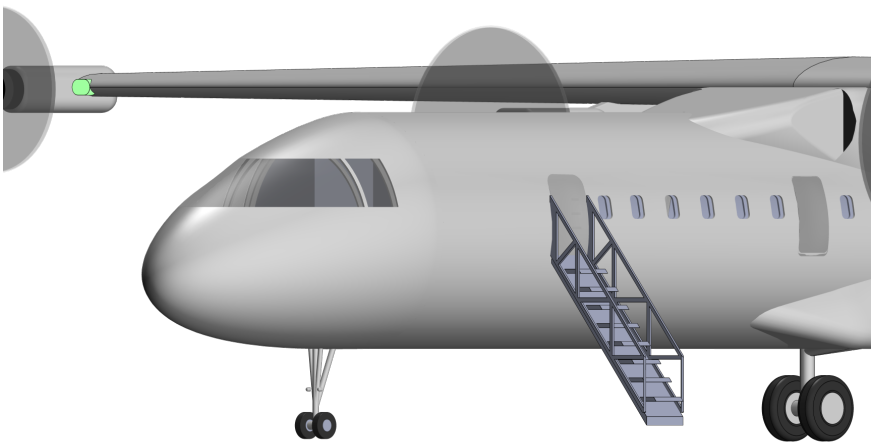

Figure 20.4: Internal extendable stairs of SRP-22 in deployed configuration

20.3. Flight Operations & Logistics

The typical mission profile of the regional aircraft is shown in Figure 20.5. The figure follows a typical mission profile, as any other aircraft with kerosene fuel would. Note that a diversion is taken into account as this is also present when calculating the weight estimations of the aircraft. Furthermore, the aircraft is equipped with a VHF communication system, which enables communication between the aircraft and the ground system or with other aircraft. This is crucial when it comes to safety, a prime example is when loitering is necessary and is communicated from the ground stations to the aircraft in flight, meaning **RA-SYS-OPM-2** is complied with.

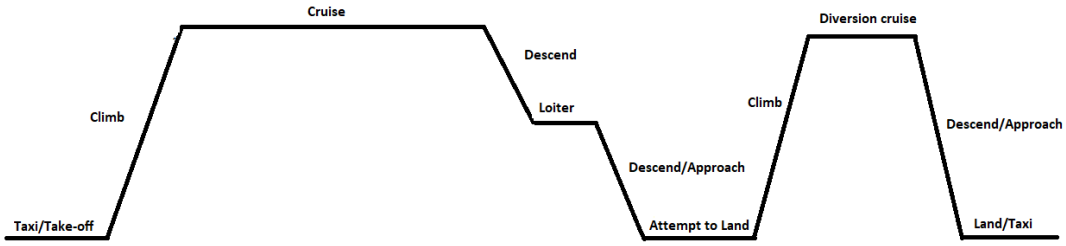

Figure 20.5: Mission Profile

The mission profile follows the following sequence:

1. **Taxi/take off**: The aircraft is taxied from the gate to the runway. Prior to takeoff, the lift devices are deployed. During takeoff, the aircraft is accelerated to takeoff speed. After taking off the aircraft starts to climb by accelerating to the target cruise altitude and velocity. The landing gear is retracted, the lift devices are adjusted to the climbing setting, and the climb angle is reached.
2. **Cruise**: Since the weight of the aircraft will decrease due to fuel consumption, the aircraft needs to maintain its cruise altitude and speed by adjusting the control surfaces.
3. **Descent/loitering**: Once the aircraft is approaching its destination, it can start descending, sometimes followed by loitering if the aircraft is not cleared to land by air traffic control. Once the aircraft is cleared to land, the aircraft proceeds to finalize the descent.
4. **Approach/Landing**: The high lift devices need to be adjusted to the approach setting. Furthermore, the landing gear is deployed and the aircraft is decelerated to approach speed. The last set is landing, in which the aircraft touches down on the runway. The aircraft is decelerated and the high lift devices are retracted, to taxi to the designated position at the airport and shut down the engines.
5. **Diversion**: In emergency cases, the aircraft needs to divert and climb to a diversion cruise altitude. The diversion can be to a different airport, a different runway, or the same runway under a different time slot. For these emergency and unusual situations, reserves of fuel need to be accounted for. After the diversion cruise, the aircraft is cleared for descent, during which the high lift devices are deployed to descent settings, and a descent angle needs to be reached.

[1]URL https://globalenergyinfrastructure.com/articles/2021/03-march/hydrogen-data-telling-a-story/ [cited 11 Jan. 2023]
[2]URL https://www.energy.gov/eere/fuelcells/liquid-hydrogen-delivery [cited 11 Jan. 2023]
[3]URL https://www.energy.gov/eere/fuelcells/hydrogen-pipelines [cited 11 Jan. 2023]
[4]URL https://energies.airliquide.com/resources-planet-hydrogen/how-hydrogen-stored [cited 12 Jan. 2023]
[5]URL https://energies.airliquide.com/resources-planet-hydrogen/how-hydrogen-stored [cited 12 Jan. 2023]
[6]URL https://www.airbus.com/en/newsroom/press-releases/2022-11-airbus-and-arianegroup-to-pioneer-liquid-hydrogen-technology [cited 12 Jan. 2023]
[7]URL https://hoseconfigurator.elaflex.de/GELBRING/VHD-C/Product3.html [cited 23 Jan. 2023]

21 RAMS Characteristics

The reliability, availability, maintainability, and safety characteristics of the aircraft are elements used to evaluate the operational performance of the SRP-22. For conventional subsystems, the RAMS characteristics are compared with reference aircraft [30]. For novel subsystems, an independent analysis is performed.

21.1. Reliability

Reliability inquires on how probable a system failure is, over the entire lifetime of the aircraft.

Fuel cell

Fuel cells have been applied to aeronautical sciences since the late 1980s [1]. Technology has developed exponentially since that date, and as recently as January 2023, the first fuel cell semi-commercial flight has taken place [2]. Nevertheless, a significant leap forward must take place before fuel cell flights become a regular occurrence. The current fuel cell chosen (Horizon VLS-III) is still in the certification phase, and has not yet been tested for such large-scale applications. This means that there exists a real possibility of fuel cell failure, which decreases the reliability of the aircraft.

Hydrogen tank insulation

The liquid hydrogen tank must store the propellant at a grand temperature of 20°K. However, the novel conservation technologies and materials are still in the experimental phase and have never flown on aircraft before [3]. As such, the reliability of the system is still to be determined, and a failure possibility must be accounted for.

Electric motor

Of the two electric motors chosen for the design, one of the motors is custom-made to fit the needs of the aircraft. While the H3X HPDM-250 has been previously tested, the custom motor has not commenced development, and as such the reliability of the system still needs experimental verification to ensure its reliability is adequate. Furthermore, the unconventional positioning of the wingtip-mounted propellers is a design choice that divides many engineers on whether it is an effective means of drag reduction or not.

Conventional subsystems

The conventional subsystems of the aircraft (controls, undercarriage, wing, empennage, landing gear) are similar to those currently implemented in similar transport aircraft. To quantify the reliability of these subsystems, the reliability of existing aircraft is documented. Not accounting for propulsion system / powertrain failures, the ATR 72-600, DHC-8 Q400, and CRJ 200 have dispatch reliability of 99.7% [4], 99.5% [5], and 99% [6], respectively.

21.2. Availability

The availability researches the operational availability of the aircraft during its entire lifespan. It attempts to quantify for how long every system can be in use.

Ground operations

Between flight routes, aircraft experience a turnaround, which comprises the time an aircraft is grounded for pre-flight checks, refueling, and passenger/luggage embarking/disembarking [7]. Refueling estimations take a maximum estimated time of 32 minutes, but can significantly decrease based on the tubing diameter used. Refueling must be performed however with no passengers within the cabin to limit the casualties in case of unexpected disaster. The low passenger capacity and easy access to luggage compartments are

beneficial to the turnaround time, since passenger offloading/onboarding can be performed in as little as 10 minutes each. As such, an approximate turnaround time can range anywhere between 28 minutes to 55 minutes, based on the airport's refueling capabilities and crew engagement.

Furthermore, the aircraft is designed to fly multiple trips on a single tank of hydrogen, should the destination not have a developed hydrogen infrastructure. With this in mind, the aircraft turnaround time can take as little as 20 minutes, with pre-flight inspections performed simultaneously while offloading.

Auxiliary power unit

While the aircraft does not have a dedicated APU, its motors act as ground power systems when the propeller brake is activated. Therefore, no huffer cart or similar alternative is required. With the fuel cell's cold start temperature, electrical systems can be powered within a matter of seconds. However, this system should run for a certain short period of time before the fuel cell reaches optimal operating temperature - crucial for take-off power.

Maintenance time

Maintenance is explored in more detailed within the following section. While it is hard to estimate the exactitude of time needed for maintenance, it is expected that overhaul ground times take longer than conventional aircraft, due to tedious process of examining the tank's feasibility. A-checks and B-checks, however, may take less time than conventional aircraft due to the design simplicity of the motor [74].

21.3. Maintainability

Maintainability characteristics focus on how effectively the aircraft can be maintained - with parts repaired and replaced - throughout the entirety of its lifetime. The greatest maintenance threats lie between the fuel cell system, and the integral tank.

Fuel cell system

The fuel cell system is a combination of the air intake supply and the electricity generation within the fuel cell. The system works harmoniously in a carefully regulated process to provide a source of electricity through a chemical reaction. As such, maintenance is an essential part in ensuring that the system works in optimal condition.

The fuel cell environment is very specific, requiring adjusted levels of oxygen, hydrogen, temperature, and hydration for the reaction to occur. If any of these is unbalanced, the result will be a sub-optimal production of power. First of all, intakes must be inspected regularly to ensure there are is no clogging or debris build-up that may restrict the airflow. Furthermore, the carbon, dust, and HEPA filters must also be inspected and replaced regularly to not contaminate the fuel cell and cabin environments. In the contrary, further maintenance will be required to repair any damaged internal parts, leading to extended grounded time and additional inquired costs.

The fuel lines require extended inspection to ensure there are no hydrogen leakages into the cabin environment, which risk providing a source of ignition and loss of propellant. Additionally, the fuel cell itself must be inspected to ensure that the membranes do not dry out and that temperature remains within the operational limits. To do this, the fuel cell can be accessed through a hatch in the cabin (as it lies in front of the aft pressure bulkhead), where stacks can be slid out for maintenance or replacement. Since the system is made up of ten separate stacks, it is advised that stacks are simply removed and interchanged periodically to avoid extended grounded time and a bulk inspection of ten stacks.

Hydrogen tank

Due to the tank operating outside pressurized conditions, the tank will go through pressure changes ranging from 1.2 bar at refueling to 0.3 bar in cruise. As such, these extreme cycles can have an effect the tank's structural integrity. Furthermore, the cryogenic environment of the tank can cause embrittlement of the tank walls. The tank is also integrated into the aircraft, meaning that replacement of the tank can lead to serious grounding time.

The tank can be accessed through hatches on the outside of the fuselage, through which periodic inspection is expected. If the tank is deemed unfeasible for flight, the aircraft must be grounded to further assess the options of replacing the tank structure.

Conventional subsystems

Conventional subsystems may continue to be inspected and maintained in the same manner that current airlines perform, through the following inspections [74]:

1. Pre-flight checks (visual inspection): Obvious mechanical problems that imminently threaten the scheduled route.
2. A-checks (every 150 flight hours): Inspection of interior and exterior, fluid servicing, visual inspection of power lines.
3. B-checks (every 750 flight hours): Preventive maintenance of aircraft lubrication, examination of airframe.
4. C-checks (every 3000 flight hours): Detailed inspection of airframe, propellers, and accessories. Flight control recalibration.
5. D-checks (every 20000 flight hours): Aircraft overhaul to return it to its original condition. Cabin interior is dismantled and structural checks performed.

21.4. Safety

Safety is a fundamental pillar of aircraft operations. Due to general public's reserved views on aviation, the commercial aircraft market must comply with stricter safety standards than other industries. To review the biggest safety risks of the system, please refer back to Section 22.1, risks R-TANK-02, R-TANK-03, R-FC-01, R-FC-03, R-UND-01, and R-CAB-01.

[1]URL https://www.fzt.haw-hamburg.de/pers/Scholz/dglr/hh/text_2020_11_19_HydrogenAircraft.pdf [last accessed 29-01-2023]

[2]URL https://www.prnewswire.com/news-releases/zeroavia-makes-aviation-history-flying-worlds-largest-aircraft-powered-with-a-hydrogen-electric-engine-301726022.html [last accessed 30-01-2023]

[3]URL https://newatlas.com/aircraft/hypoint-gtl-lightweight-liquid-hydrogen-tank/ [last accessed 30-01-2023]

[4]URL https://www.atr-aircraft.com/presspost/first-atr-72-600-high-capacity-delivered-to-cebu-pacific [last accessed 06-12-2022]

[5]URL https://www.aerocontact.com/en/virtual-aviation-exhibition/product/573-bombardier-q400 [last accessed 06-12-2022]

[6]URL https://https://en.wikipedia.org/wiki/Bombardier_CRJ100/200#cite_note-Flight20June2017-12 [last accessed 06-12-2022]

[7]URL https://www.faa.gov/air_traffic/publications/atpubs/aim_html/chap5_section_1.html [last accessed 31-01-2023]

22
Risks

For a more detailed in-depth look at how the risks are formulated, refer back to the baseline report [30]. This design project entails a significant number of risks that must be identified to ensure that the project life runs efficiently with minimal setbacks. The risk register for the technical and operational risks is presented below and divided into multiple sections for easier comprehension: The main technical risks are identified alongside their cause, event, and effect. A risk assessment is then performed, which assigns each risk a numerical rating of importance through its likelihood of occurrence and impact rating, as shown in. Lastly, a mitigation strategy is defined for each risk, along with a responsible team member, and the risk assessment is reevaluated to give each risk a residual likelihood and impact rating *after* the mitigation strategy has been put in place.

22.1. Risk Identification

Since risk analysis is a continuous process - new risks may be discovered until the design project is complete. The initial project organizational risks may be consulted in the project plan and baseline report [75, 30]. The initial technical design risks are presented in the midterm report [76].

An abbreviated risk register is presented in Table 22.3 at the end of this section. These are the ten risks that prove to be most fatal to the safe use, operation, and development of the project.

22.2. Risk Assessment

To evaluate the likelihood of a risk occurring, a method called the *Probability of Occurrence* (PoO) is used [77]. This method assigns a weight, from one to five, to each risk based on the likelihood of its occurrence. To evaluate the impact of a risk, a weight method is used to assign a numerical value to the impact of every risk. This method, appropriately named *Severity of Consequences* (SoC), transforms the abstract concept of impact into a quantifiable value[1].

The risk rating is the final numerical value assigned to each risk. This is the value that rates and positions the risks. With this number, the team is able to identify the risks that require more elaborate mitigation methods, and the risks that are the most prevalent. To evaluate the risk rating, the likelihood and and impact are multiplied, to give a value between 1 and 25: The higher the risk rating, the more severe the risk is to the project. Once these values have been assigned, each individual risk can now be plotted on a risk map, as seen in Figure 22.1.

Table 22.1: Technical risk rating

ID	Likelihood (1-5)	Impact (1-5)	Rating (1-25)
R-TANK-01	3	3	9
R-TANK-02	2	4	8
R-TANK-03	3	5	15
R-OPER-01	4	3	12
R-FC-01	2	4	8
R-FC-02	2	3	6
R-FC-03	3	3	9
R-MOT-01	2	4	8
R-UND-01	1	5	5
R-CAB-01	1	5	5

22.3. Risk Mitigation

Once the initial risks have been quantified, it is crucial to determine a mitigation strategy for the relevant risks. As seen in Figure 22.1, the most crucial risks are the ones that lie in the red region. The objective is to reduce their risk rating so that they lie mostly within the green region. Nevertheless, a mitigation strategy must be put in place for every risk, no matter how small the risk may be. This is because, as previously stated, risk rates evolve throughout the project: what may seem like a small risk now might eventually grow to become a critical one.

The risk mitigation strategies are classed into one of four main methods:

- **TREAT:** A system is put in place to reduce the risk rate before the risk occurs.
- **TRANSFER:** The risk is passed on to a third party, who then bears the risk and decides on how to mitigate it.
- **TERMINATE:** The risk is deemed fatal to the project, and a system is put in place beforehand to minimize the risk rate to the absolute minimum possible.
- **TOLERATE:** The risk is a positive risk, or nothing can be done by the team or third parties to minimize the risk. As such, the risk must be accepted and expected.

Following this, all risks are assigned mitigation strategies, as seen in Table 22.2, and the likelihood, impact, and rate of the residual risks are formulated. Additionally, a team member is assigned to bear the responsibility of each risk. Lastly, the residual risks are mapped on a new risk map. This allows to see which risks are the most critical after the mitigation and contingency strategies are put in place. These can be observed on Figure 22.2.

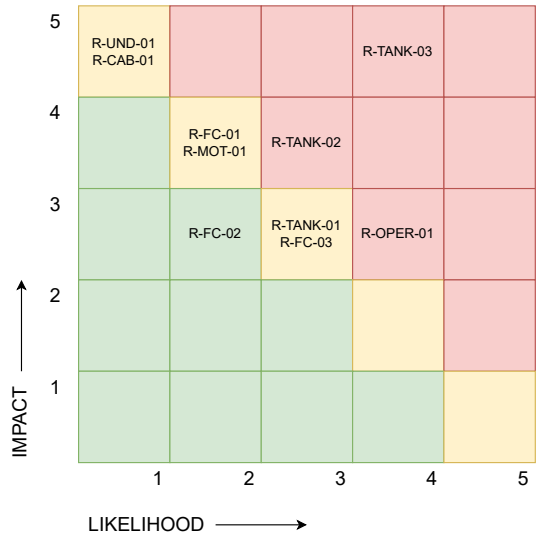

Figure 22.1: Risk Map for Unmitigated Fatal Design Risks

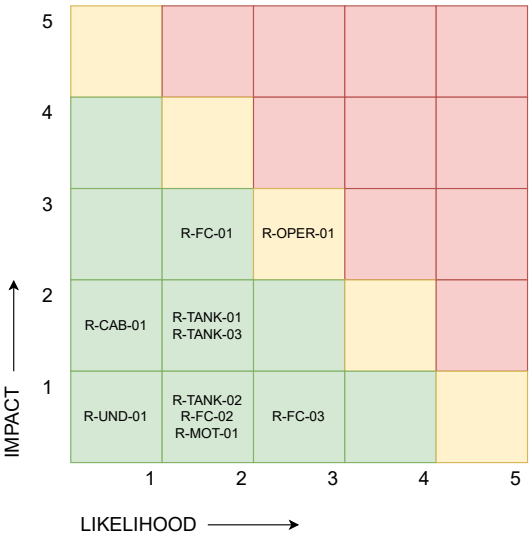

Figure 22.2: Risk Map for Mitigated Residual Technical Design Risks

Table 22.2: Technical Risks Mitigation Strategies

ID	Planned Response	Res. Likelihood	Res. Impact	Res. Rate	Responsible
R-TANK-01	TREAT: Discuss the feasibility of introducing either a BOG compressor [78] or an IRAS cooler design [79] to actively control the temperature of the tank	2	2	4	Manufacturing manager / Structural engineer
R-TANK-02	TREAT: Replace conventional TPRV with a TPRV that has active open-close mechanism, in order to regulate accurately the amount of hydrogen vented instead of full dumping	2	1	2	Manufacturing manager / Propulsion engineer
R-TANK-03	TREAT: Discuss the feasibility of introducing an IRAS cooler design [79] to actively control the temperature of the tank	2	2	4	Manufacturing manager / Structural engineer
R-OPER-01	TREAT: Establish rapport with airports to come within feasible timeline of operative LH2 infrastructure. If timeline exceeds service date, establish contacts between LH2 storage plants and airports to temporarily provide regular delivery of LH2 to airport during necessary time	3	2	6	Operations manager
R-FC-01	TREAT: Integrate hydrogen-in-air sensor to assess concentration of hydrogen in air to determine leak. If determined, (partially) turn off fuel cell while hydrogen concentration drops	2	3	6	Flight performance engineer
R-FC-02	TREAT: Integrate heat exchangers to passively transfer the heat generated by the fuel cell to other systems which require heat. Reroute the water vapor biproduct back into the fuel cell membrane and intake air fans to regulate operating environment humidity	2	1	2	Propulsion engineer
R-FC-03	TREAT: Reroute part of the current generated by the fuel cell to a supercapacitor, capable of delivering power to temporarily replace fuel cell output during emergency operation	3	1	3	Propulsion engineer
R-MOT-01	TREAT: Size motors so that minimum mission can be completed with either of the engines inoperative (under one-engine inoperative condition). Have crossover electricity lines so that electricity input to inoperative engine can be rerouted to alternative engines for extended flight time	2	1	2	Propulsion engineer
R-UND-01	MITIGATE: Design undercarriage so that a gravity-assisted deployment may be executed, and undercarriage extended and locked in place	1	1	1	Structural engineer
R-CAB-01	TREAT: Size air inlets to provide greater mass flow than the minimum pressurization required. Provide oxygen backup system onboard for a limited oxygen supply while descending to a breathable altitude	1	2	2	Propulsion engineer / Flight-performance engineer

Table 22.3: Fatal risk identification

ID	Name	Cause	Event	Effect
R-TANK-01	Control of the boil-off rate	Boil-off rate cannot be regulated	Too much / too little boil-off is available for GH2 propulsion	Propulsion systems does not generate required thrust
R-TANK-02	Control of TPRV venting	TPRV can only be activated, but not deactivated	Excessive pressure in tank activates the TPRV venting mechanism	All H2 is drawn from the tank, leaving aircraft with no propellant for remainder of flight
R-TANK-03	Regulation of tank temperature	Tank temperature cannot be sustained at cryogenic needs	Excessive boil-off occurs	Premature consumption of all fuel, risk of explosion, or activation of TPRV
R-OPER-01	Underdeveloped airport LH2 infrastructure	Regional airports do not have appropriate logistics to accommodate storing of LH2 onsite	Airports do not have LH2 available	LH2 aircraft cannot be refueled pre/post flight at airports
R-FC-01	Fuel cell leakage	Leakage in the tubing that relays tank with fuel cell	Loss of hydrogen	Risk of explosion and loss of thrust
R-FC-02	Regulation of fuel cell environment	Changes in temperature and humidity within fuel cell casing	Fuel cell does not operate in optimal conditions	Decrease of power
R-FC-03	Fuel cell failure	Fuel cell malfunction	Fuel cell stops operations	Partial loss of power available and electrical system
R-MOT-01	Motor failure	Technical or disruption failure of electric motor	Motor becomes unavailable for thrust	Less total thrust available and a new moment is introduced
R-UND-01	Undercarriage deployment	Mechanical disruption of deployment system	Landing gear is not deployed	Belly landing and potential hull loss
R-CAB-01	Cabin depressurization	Inlets cannot sustain required air intake	Pressure level inside cabin cannot be maintained	Passenger discomfort and potential loss of consciousness

[1] URL `https://institute.acs.org/lab-safety/hazard-assessment/fundamentals/risk-assessment.html` [last accessed 26-01-2023]

23 Project Development

This chapter is aimed at providing an overview of the required design phases and certification process. A future development flow diagram together with a project Gantt chart, provide an overview of the required steps until entry into service in 2035.

23.1. Design Phase Timeline

After the initial phase of the design process, also called the conceptual design phase, a number of additional development phases will take place. A general timeline shows these phases in Figure 23.1.

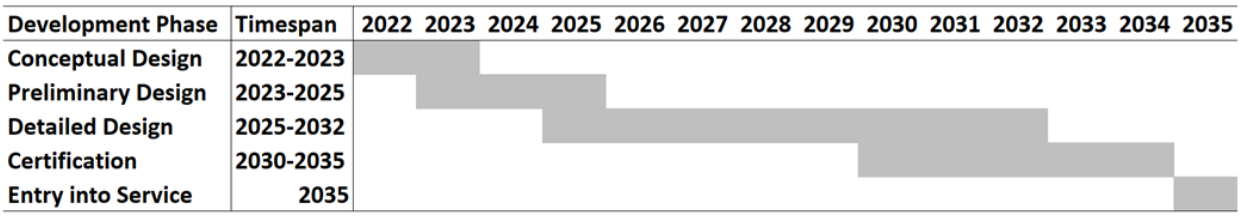

Figure 23.1: Entry into Service Timeline for the SRP-22

During the DSE, the conceptual design process is performed. However, this phase is not finished by the time of DSE completion and therefore continues for the first few months of 2023. The next phase is the preliminary design, which commonly takes about two years [20]. Next, the detailed design is performed. As this is extremely complicated, it is the most time consuming phase. Throughout the aviation industry the required time for this phase varies a lot. The detailed design usually starts near the end of the preliminary design phase and continues during the certification process, as things shall need to be altered as a result of flight tests etc. Therefore the detailed design phase runs from 2025 all the way to 2032. The certification for an entirely new aircraft takes between five to nine years[1]. As the proposed aircraft is relatively small compared to some wide body aircraft which are also certified within this timeframe, a certification time of five years is considered for the SRP-22.

Conceptual Design

The conceptual design process is aimed at discovering all options available to design the product requested by the costumer/stakeholder. These options are compared and initial configurations are created, which are mainly based on statistics, reference aircraft and assumptions. Once these concepts have been presented to the costumer together with an initial requirement check, one design will be chosen and the development will move on the the next phase.

Preliminary Design

During the preliminary design phase engineers will focus on aerodynamics, flight mechanics, structural analysis and stability together with initial wind tunnel tests[2]. Detailed calculations will be performed, showing an initial proof of concept which is used at the final evaluation of the design phase so the go/no-go decision can be made. Furthermore, a detailed cost analysis is performed to ensure the aircraft is able to comply with the user requirements for the desired unit price.

Detailed Design

The final design phase is aimed at outlining every detail of the aircraft as much as possible. The detailed design phase mainly focuses on the structural implementation of all subsystems, thus determining ribs, spars and rivet locations. In addition to the aircraft design itself, a flight simulator must be developed and

the manufacturing process set up. This process is extremely important to be able to efficiently produce the aircraft once fully developed. For the manufacturing unique machines and tools must be made. During the detailed design process the first tests are also performed, preparing for the certification process. These test will result in many alterations to the design, causing this to be a very lengthy design phase.

Certification

During the detailed design phase the certification process of the aircraft will also be initiated. To be able to perform the civil transport flights for which the SRP-22 is designed, the aircraft must comply with authority regulations. Many counties have their own regulations, but the FAA and EASA are considered to be the leading authorities. They have an extensive regulation manual with which all aircraft of similar type must comply with.

To be able to perform all the test required to certify the aircraft, usually multiple prototypes are build. This is generally an expensive approach, but reduces development time. These prototypes will be put through a rigorous and extensive test flight program, testing the aircraft in the most extreme conditions it should ever encounter. This could contain high loading through manoeuvres and maximum take-off weight tests, but also for circumstances such as a bird strike or engine failure[3]. Once the aircraft is certified pilots will also be able to obtain a type rating for the aircraft and it will be able to enter service.

23.2. Future Development Flow Diagram

To provide a general overview of the mentioned design phases and certification, a future development flow diagram is provided in Figure 23.2. Each block shows a task and in which estimated time frame it should be performed, such that the entry into service date of 2035 can be met.

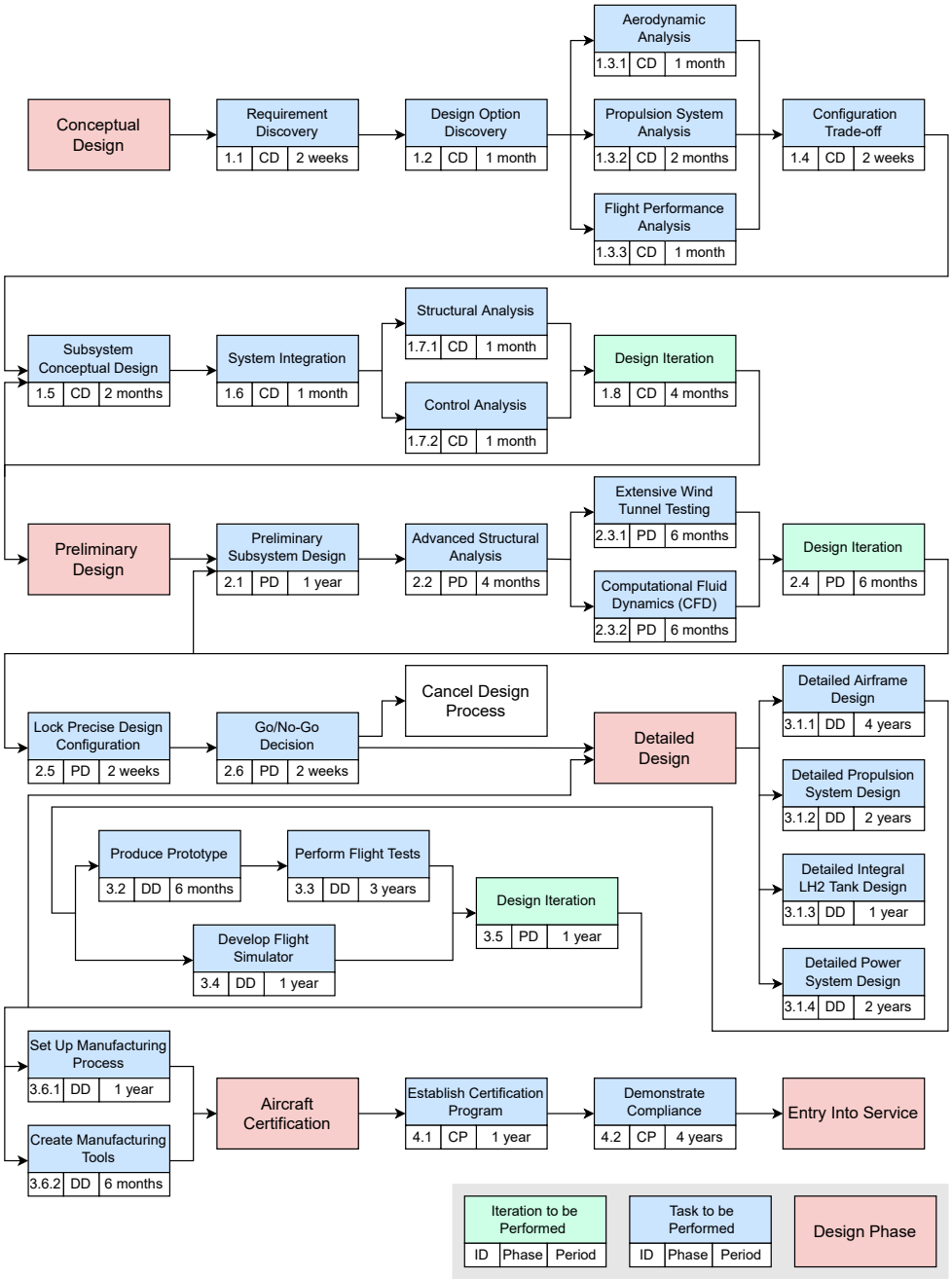

Figure 23.2: Future Development Flow Diagram

23.3. Future Project Gantt Chart

In Figure 23.3 and Figure 23.4 the project Gantt chart up to the entry into service date of 2035 is shown. This gives an overview of the timeline and the tasks that must be performed till SRP-22 aircraft service. To comply with **RA-TOP-TIM1** requirement, further studies throughout the design process will be evaluated.

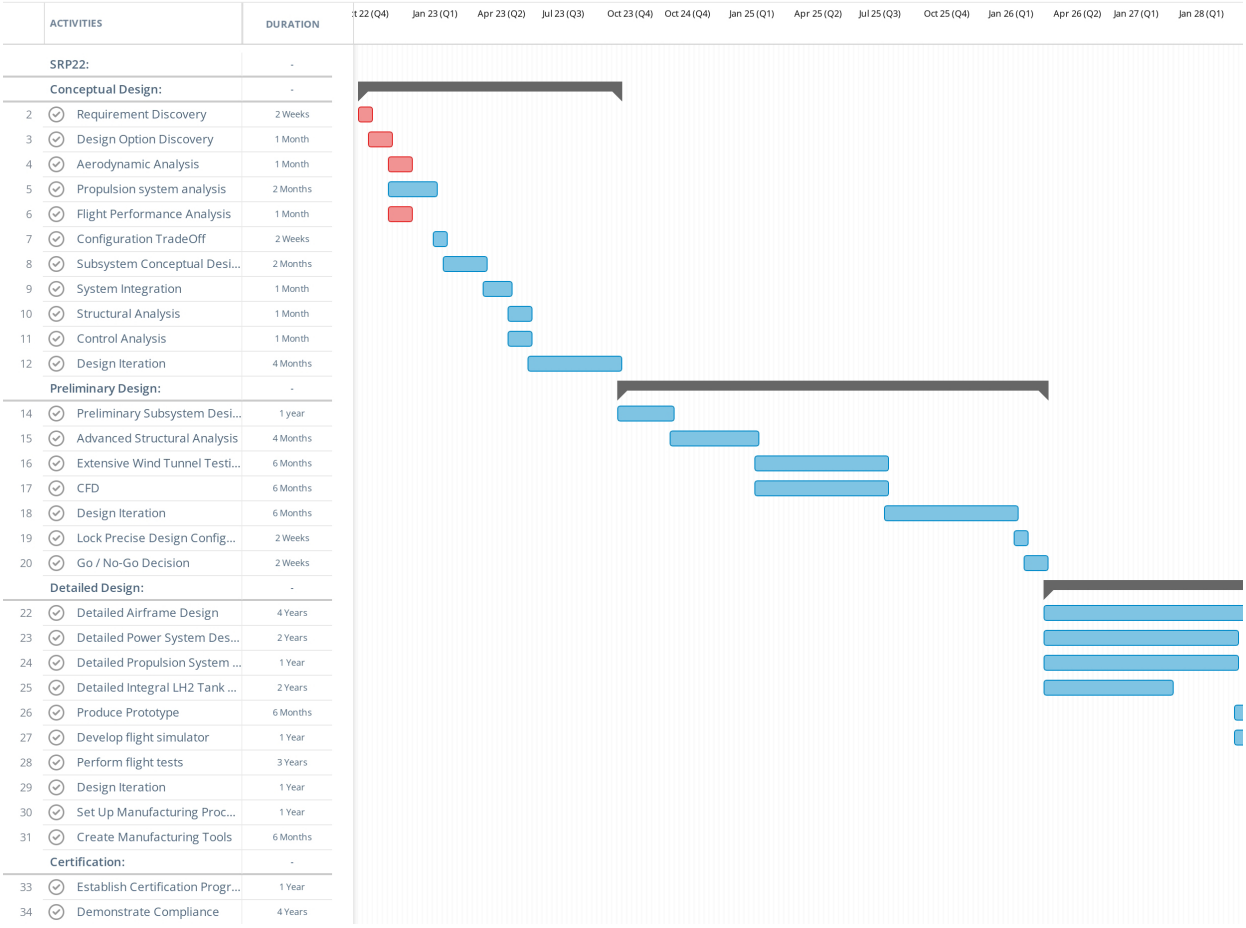

Figure 23.3: Future Project Gantt Chart [1]

Figure 23.4: Future Project Gantt Chart [2]

[1]URL `https://www.faa.gov/aircraft/air_cert/airworthiness_certification` [cited 22 Dec. 2022]
[2]URL `https://www.engineeringclicks.com/aircraft-design-process/` [cited 22 Dec. 2022]
[3]URL `https://www.easa.europa.eu/en/domains/aircraft-products/aircraft-certification` [cited 22 Dec. 2022]

24
Verification and Validation

During the course of the conceptual design of the SRP-22, it is important to check that the procedure is correct and as expected. This is especially important for the integration between the different component subsystems and/or systems. Unit tests (UT) are performed on small pieces of code that can be separated from the entire script. This helps to find potential errors in the code early in the design process and make the necessary improvements. System tests (ST) are performed on larger pieces of code in order to test the interactions between the code and check that the whole system behaves as expected.

The validation of the aircraft is aimed at showcasing the similarities in real-life tests and numerical solutions for the proposed aircraft design. Normally, the design would be validated during the test phase of the aircraft. However, since this is currently not feasible, the subsystems of the proposed design were validated by comparing the numerical solutions to other similar existing aircraft or literature.

24.1. Verification

Model Verification

The verification tests are implemented to confirm that the used methods produce the right output. The Unit tests and System tests have been performed on all codes. A summary of the unit tests performed on the codes is presented in Table 24.1. Units are the smallest parts of code that can be separated from the entire script.

Table 24.1: List of the unit and system tests performed on the Class I and Class II weight estimation.

Test ID	Test Description	Status
UT-WE-01	Check that units are consistent	PASSED
UT-WE-02	Check that formulas are correct	PASSED
UT-WE-03	Check that units are converging between the codes	PASSED
UT-WE-04	Check the unit calculations manually	PASSED
ST-WE-01	Check system convergence between the codes	PASSED

The first two tests are walk-through type tests. The units and methods used in the code have earlier been presented in the relevant sections. The relevant codes have been checked for convergence relative to each other, with the values related to the requirements. This step is called the system test. At last, a manual verification calculation is performed, by comparing the results of manual calculations of the units to the code results. By performing these calculations by hand as a sanity check, the code is ultimately verified. An example of performing the calculations by hand for the Class I resulted in an error of approximately 0.1% and the Class II by 0.0%. Therefore the code is considered correct. For all parts containing code or methods from literature, this verification process is applied such that the outcome can be considered correct.

Design Verification

To verify the design output and check the requirement compliance, different types of tests can be performed. Each requirement is able to be verified by using one or a combination of the following four verification methods.

- **Analysis**
  Using numerical simulations and code to analyse if the design is able to meet the requirement.
- **Inspection**
  A visual inspection and measurement of dimensions to verify requirement compliance.

- **Test**
  Using special equipment and simulation techniques, such as a wing whiffle tree, system tests can be performed and requirements verified.
- **Demonstration**
  Performing tests to check the functional operation of the system, without any special equipment or simulation techniques.

Table 24.2: Design Verification using Analysis, Inspection, Test and Demonstration

Analysis	Inspection	Test	Demonstration
RA-TOP-PER-2	RA-TOP-PER-1	RA-TOP-PER-3.1	RA-TOP-SRE-1
RA-TOP-PER-3.1	RA-TOP-SRE-1	RA-TOP-PER-3.2	RA-TOP-SRE-2
RA-TOP-PER-3.2	RA-SYS-SRE-1	RA-TOP-PER-5.1	RA-TOP-SRE-3
RA-TOP-PER-4.1	RA-SYS-SRE-2.1	RA-TOP-PER-5.2	RA-SYS-SRE-3
RA-TOP-PER-4.2	RA-SYS-SRE-2.2	RA-TOP-SRE-1	RA-SYS-SRE-4
RA-TOP-PER-5.1	RA-SYS-SRE-6	RA-SYS-SRE-4	RA-TOP-SUS-2
RA-TOP-PER-5.2	RA-TOP-DIM-1	RA-SYS-MSC-1.1	RA-SYS-OPM-4
RA-SYS-SRE-5	RA-TOP-DIM-2	RA-SYS-MSC-1.2	
RA-TOP-SUS-1	RA-SYS-DIM-1	RA-SYS-MSC-1.3	
RA-TOP-COS-1	RA-SYS-DIM-2	RA-SYS-MSC-2	
RA-TOP-COS-2	RA-TOP-CRE-1.1	RA-SYS-MSC-3	
RA-TOP-TIM-1	RA-TOP-CRE-1.2	RA-SYS-MSC-4	
RA-SYS-UCG-1	RA-TOP-PAS-1	RA-SYS-MSC-6	
RA-SYS-UCG-2	RA-SYS-OPM-1	RA-SYS-MSC-7	
RA-SYS-UCG-3		RA-SYS-MSC-8	
RA-SYS-MSC-1.1		RA-SYS-MSC-9	
RA-SYS-MSC-1.2		RA-SYS-MSC-10	
RA-SYS-MSC-2		RA-SYS-MSC-11	
RA-SYS-MSC-3		RA-SYS-MSC-12	
RA-SYS-MSC-4		RA-SYS-MSC-13	
RA-SYS-MSC-5		RA-SYS-MSC-14	
RA-SYS-MSC-6		RA-SYS-MSC-15	
RA-SYS-MSC-7		RA-SYS-OPM-1	
RA-SYS-MSC-8		RA-SYS-OPM-2	
RA-SYS-MSC-9		RA-SYS-OPM-3	
RA-SYS-MSC-10			
RA-SYS-MSC-11			
RA-SYS-MSC-12			
RA-SYS-MSC-13			
RA-SYS-MSC-14			
RA-SYS-MSC-15			

During the conceptual design phase, only the Analysis and Inspection verification can take place. Test and Demonstration will take place during later phases such as certification. To comply with the requirements that can only be confirmed using these methods, a simplified analysis is applied for the conceptual design.

24.2. Validation

Weight Estimation

The design point chosen for the SRP-22 is compared to the design points of several reference aircraft as can be seen in Figure 7.1. From the figure it is evident the design points lay around the same region, while as explained in Section 7.1 the power of the SRP-22 is relatively lower, whereas its surface area is bigger. The actual design points are shown in Table 24.3.

The validation for the Class I and Class II was performed by comparing the outputs of the design to the DASH 8-Q300 and ATR 42-600. This is done for the OEM and MTOM in Table 24.4. These weight estimations are within an allowable range when accounting for the increased weight of the alternative propulsion system requiring fuel cells and a hydrogen storage tank. The new propulsion system increases the OEM by about 2300 kg, but can be reduced by 1100 kg due to the elimination of turboprop engines. This results in an increase of 1200 kg for the OEM, relatively close to the expected increase of 1000 kg when comparing values in Table 24.4.

Table 24.3: Wing Loading Design Points

Aircraft	W/P	W/S
SRP-22	0.077	3270
ATR 42-600	0.057	3350
ATR 72-600	0.069	3665
DASH 8-Q300	0.051	3400

Table 24.4: OEM and MTOM Comparison

Aircraft	MTOM	OEM
SRP-22	18,650	12,770
ATR 42-600	18,600	11,700
DASH 8-Q300	19,505	11,791

Aircraft Sizing

For the validation of the design of the SRP-22, it has been geometrically compared to the ATR 42-600 and DASH 8-Q300. The values are presented in Table 24.5. The difference in fuselage diameter comes from the fact that the SRP-22 does not have a flatter belly fuselage whereas the ATR 42-600 and Dash 8-Q300 do. When comparing the aspect ratios, **the respective aspect ratios are 12, 11.1 and 13.3** from top to bottom as seen in Table 24.5.

Table 24.5: Sizing Comparison Between SRP-22 and Reference Aircraft

Aircraft	n_{pax}	Fus. Length [m]	Fus. Diameter [m]	Wing Span [m]	Wing Surface [m^2]
SRP-22	48	23.9	3.0	26.8	59.9
ATR 42-600	50	22.7	2.7	24.6	54.5
DASH 8-300	56	25.7	2.7	27.4	56.2

Structures

Validating the airframe (fuselage, empennage, and undercarriage) is very difficult as it is ultimately designed during the detailed design phase. Using a visual comparison between an ATR 42-600 and SRP-22 similarities in the spacing of frames and stringers can be seen, but no more can be validated. For the validation of the wing structure can also be done by comparing the design wing weight to those of estimation methods. This is done in Table 24.6

Table 24.6: Wing Mass Estimation

	SRP-22	Raymer	Torenbeek
Wing Mass [kg]	2188	1667	2218

These results show a relatively wide range of estimations. From the Baseline Report, a weight fraction of the MTOM was calculated to be 10.5% [30]. This would estimate a wing weight of 1960 kg. The lower estimate by Raymer can be clarified by the low MTOM of the SRP-22, as the prediction mainly depends on that mass [19]. Moreover, these wings have bending relief due to heavy turboprops and fuel stored in the wings. The Torenbeek method normally takes the MZFW, such that this bending relief is not taken into account [20]. As the wings of the SRP-22 will be empty, this method was used with the MTOM as an input

rather than the MZFW. Therefore, this estimation is a bit high but relatively more comparable. The overall wing structural design is difficult to validate with reference aircraft wings. However, the wing mass provides a general approximation that provides partial validation.

For the Hydrogen storage tank there is very little data with which it can be compared as its implementation into aviation is currently being researched. The structural connection of the hydrogen tank using carbon rods is comparable to that used in rockets, but would need additional research to be validated. The structural tank weight and thus gravimetric index ($\frac{m_{\text{tank}}}{m_{\text{fuel}}}$) can be compared.

Table 24.7: Gravimetric Index Comparison

	SRP-22	**HyPoint GTL** [1]	**McKinsey** [2]
G.I. Tank	0.64	0.45	
G.I Entire System			1.4

This validation remains a bit indecisive as such few reference tanks are actually produced. The tank G.I. is estimated to be higher than of the HyPoint/GTL tank, mainly due to the SRP-22 tank being load bearing. Moreover, in a recent press conference Airbus announced an expected gravimetric index of 1.8 for the entire storage system. For the calculations for the SRP-22 a gravimetric index of 1.4 was assumed. Therefore, the current assumption is considered to be acceptable as values vary significantly among sources and a relatively conservative G.I. is assumed.

Aerodynamics

The aerodynamic characteristics are more difficult to validate, as little data is available on reference aircraft. Therefor the types of airfoils where compared and the lift coefficient during cruise. From the comparison in Table 24.8, it is clear that the type of airfoil is somewhat different. This can be clarified by the different cruise speed and flight level the different aircraft are designed to fly at.

Table 24.8: Aerodynamic Comparison

	SRP-22 NACA 63(4)421	**ATR 42 NACA 43018**
t/c	0.21	0.145
$C_{l_{\text{max}}}$	1.4	1.68
$(C_l/C_d)_{\text{max}}$	120	105.2
$C_{L_{\text{cr}}}$	0.63	0.49

Stability and Control

The stability and control derivatives of reference aircraft are not easily obtainable, as they mostly follow from flight data. However, the output of the tail sizing can be compared. In Table 24.9, the values of the tail sizing are shown alongside the tail sizes of the ATR 42-600. The ratio of the horizontal area relative to the wing surface area is interesting as the SRP-22 has a relatively aft c.g. because of the hydrogen storage in the tail cone. However, as is evident from Table 24.3, the W/S ratio of the SRP-22 is higher than for the ATR 42-600 and hence the wing surface area was expected to be higher. Still, the relative difference in the horizontal tail area to the wing area is bigger, which is unexpected.

Table 24.9: Tail Sizing [80]

Aircraft	**Av**	**Ah**	$\lambda_{\mathbf{v}}$	$\lambda_{\mathbf{h}}$	$\Lambda_{\mathbf{v_{LE}}}$ [°]	$S_{\text{h}}/S_{\text{w}}$
SRP-22	1.3	4.0	0.5	0.78	26	0.17
ATR 42-600	1.6	4.1	0.61	0.60	32	0.21

Aircraft Performance

Aircraft performance can mainly be validated by the usage of flight data. As it is not possible to acquire real flight data and reference flight data is hard to come by, this is something that would need to be done at a

later design stage. However, it is possible to compare some of the flight performance parameters, such as cruise altitude and cruise velocity. The certified velocities for the DASH 8-Q300 are provided by EASA [81]. Other values are taken from the Midterm Report [76]. The overview is given in Table 24.10. The range of the SRP-22 is slightly higher, whereas the velocity is lower.

Table 24.10: Aircraft Performance Parameters

Aircraft	Cruise Speed [KTAS]	Cruise Altitude [FL]	Range with max PAX [nmi]
SRP-22	275	280	1000
ATR 42-600	300	250	716
Dash 8-Q300	287	250	924

Sustainability

The calculated noise levels are compared to reference aircraft. These aircraft are turboprops, hence the similarity lies in the mass and presence of a propeller, but these are airbreathing engines rather than electric motors. The data from the ATR 42-500 and DASH 8-315 are taken as these have the same mass and engine as the ATR 42-600 and DASH 8-Q300 respectively and had very detailed data available [82] [83]. As can be seen in Table 24.11, the noise levels of the SRP-22 are mostly close to the ATR 42. Furthermore, the noise levels are the highest in the approach category for all, while flyover results in the lowest noise level.

Table 24.11: Noise Levels

Aircraft	MTOM [kg]	Lateral [EPNL]	Flyover [EPNL]	Approach [EPNL]
SRP-22	18,650	82.1	77.7	89.0
ATR 42-500	18,600	80.9	77.8	94.2
DASH 8-315	19,505	86.9	80.0	94.9

[1]URL `https://newatlas.com/aircraft/hypoint-gtl-lightweight-liquid-hydrogen-tank/` [cited 13 Jan. 2023]

[2]URL `https://hydrogencouncil.com/wp-content/uploads/2020/01/Path-to-Hydrogen-Competitiveness_Full-Study-1.pdf` [cited 25 Jan. 2023]

25
Future Recommendations

This report was constructed as part of the requirements for a Bachelor's course and within a limited time frame, with certain aspects of the content remaining outside of the scope of work and knowledge required. As such, certain findings should be investigated further to assess their accuracy and developments. The most important recommendations are presented below.

Investigations Into Boil-Off Control
Using boil-off is a great improvement in fuel efficiency and cost. Current research into the technology involves using a cryogenic pump to extract the liquid hydrogen from the tank and eventually heating to a gas. The boil-off is then considered as losses, becoming a source of consumed yet unused fuel. The SRP-22 uses a pump to extract the boil-off and feed it directly to the fuel cell, with no latent energy expenditure. However, this system implies that the power available is directly related to the quantity of boil-off available: Having too little boil-off means that there is not enough power available, and having too much boil-off means that the pressure build up in the tank can cause tank rupture. The boil-off must also be controlled based on the power required for each phase of flight.

Rudimentary techniques exist to control the boil-off, through the use of glass rods to regulate the heat inside the tank. However, more investigation into this is required to find an effective way of timely regulating the heat flow.

Investigations Into Cryogenic Tank Storage
There is exists a vast array of theoretical research into the cryogenic storage of propellant on aircraft. However, of the limited aircraft that have flown on hydrogen, all of them have been on compressed gaseous hydrogen. As such, experimental data on the feasibility of cryogenic storage is limited, and needs greater investigation.

Additionally, the tank onboard the SRP-22 has no active cooling mechanisms: It relies purely on insulation conditions to maintain the temperature. As previously mentioned in Chapter 21, the material technologies used are still very premature, and the results portrayed theoretically may be discrepant from experimental data. The assumptions made for the tank's gravimetric index also proved to be reliant on data that is disputed by fellows in industry: While some research estimates indexes between 0.4 to 0.6, other research is much more conservative with values ranging up to 1.8. To get a clearer idea of what to use, further research is required in this aspect.

CFD and Wind Tunnel Testing of Inlets
Boundary layer aerodynamics is a complex area of physics that largely remains outside the scope of this report. Analytical equations were used to determine an average flow velocity inside the boundary layer, but this approach remains simplistic and may differ from computational fluid dynamics models, or wind tunnel testing.

Since the entire inlet design is characterized by the average flow velocity inside the boundary layer, the inlet geometry should be numerically and experimentally tested to ensure that the analytical findings of this report match. For this, further investigation is recommended.

CFD and Wind Tunnel Testing of Wingtip Propellers
The design choice of including wingtip-mounted propellers is one that divides many engineers on whether it is an effective means of drag reduction or not. While certain research suggests that it is beneficial, other research also points out downsides such faster wingtip stall. As such, these characteristics should be computationally tested on the aircraft before further implementation is progressed.

Future Investigation Into Water Vapor Emissions
The SRP-22 prouds itself in not emitting any NOx or carbon emissions during operation. However a biproduct of the fuel cell is the generation of water vapor. While some of this vapor is reinjected into the aircraft for air and membrane hydration, a large majority of the vapor produced must be expelled back into the air. Water vapor itself can be considered a greenhouse gas due to its short yet potent warming effect. As such, to limit these emissions, a mechanism is proposed to freeze the outgoing vapor into water pellets which fall back down to the ground, in the same style as light hail. It is recommended to investigate this alternative further to obliterate the potential argument of SRP-22 greenhouse emissions through water.

Improved Cost Estimations
The unpredictability of financial markets makes preliminary cost estimations vary drastically from conservative to optimistic outcomes. These unpredictabilities are greatly affected by the past, current, and future states of the world, as observed in the 21st century through the World Trade Center attacks of 2001, the 2007 economic recession, the Novel Coronavirus crisis of 2020, and the ongoing war in Ukraine. Fuel and hydrogen costs vary drastically within time periods, and predictions may be inaccurate. Considering there are still 13 years before the aircraft is expected to enter service, improving technologies for hydrogen acquisition, developments in manufacturing of fuel cells and cryogenic tanks, and diversification of operations, means that the preliminary estimates presented in this report have a margin of error. As such, it is recommended that as the entry-into-service date nears the present, a revision of these cost estimations is assessed.

Vertical Tail and Rudder Design Improvements
In Figure 15.4 it assumed that in an engine inoperative case the sideslip angle is 0 degrees. This assumption could be slightly unrealistic and thus in order to make a more precise calculation of the the vertical tailplane dimensions a sideslip angle of 5° could be used. This means that an additional force on the vertical tailplane should be considered when taking moments around the center of gravity, and as such the vertical tailplane dimensions would vary. Thus the total vertical tailplane force could be defined as

$$Y = \frac{1}{2} \cdot \rho \cdot V^2 \cdot S \cdot (C_{Y_\beta} \cdot \beta + C_{Y_{\delta_r}} \cdot \delta_r) \tag{25.1}$$

Additionally, the rudder is sized for one of its most critical conditions, an engine failure. However, it could also be sized for a crosswind landing, in which tail and rudder have to work oppositely. Following the method presented in [60] the ratio of chord lengths between the vertical tail and the rudder may be obtained. Then, the rudder span, tip chord, root chord and other geometric aspects are derived with the use of simple Aspect Ratio, and Area equations.

26 Conclusion

The objective of this project was to present the steps that have been taken in the conceptual design of a regional passenger aircraft with at least a 20% reduction of block fuel per seat over 500 nmi compared to market competitors, entering service by 2035. In order to do so, a trade-off was performed from which it was clear that the aircraft would be powered by a fuel cell running on hydrogen, while this hydrogen is stored in its liquid state, located in the tail cone of the aircraft. With this basis in mind, the further aircraft architecture was created. The resultant was four abreast seating, with a T-tail and high wing configuration. Furthermore, the wing contains four electric motors, all powering their own propeller.

The aircraft has been designed for minimum power required instead of minimum surface area, in order to size down on the power train. The hydrogen has to be stored cryogenically in order to be kept in its liquid form. This is done by the use of a carbon-fiber-reinforced polymer tank which is integrated into the fuselage such that it is load-bearing. An insulation layer of 20 cm is added to ensure the boil-off rate is kept sufficiently low. This boil-off rate however will be increased while in flight, to control the gaseous hydrogen rate entering the fuel cell. The performed design results in some general characteristics (Table 26.1) and general performance parameters (Table 26.2).

Table 26.1: SRP-22 General Characteristics

Number of Crew	3	[-]
PAX	48	[-]
Design Payload	5225	[kg]
Length	23.9	[m]
Wingspan	26.8	[m]
Wing Area	59.9	[m^2]
Airfoil	NACA 63(4)421	[-]
OEM	12,770	[kg]
MTOM	18,650	[kg]
Max Fuel Mass	683	[kg]
No. Propellers	4	[-]
Fuel cell Type	PEM	[-]
Fuel	LH2	[-]

Table 26.2: SRP-22 General Performance

Cruise Speed	275	[kts]
Cruise Altitude	FL280	[-]
Stall Speed, clean config.	118	[kts]
Design Range	1020	[nmi]
Ferry Range	2440	[nmi]
Takeoff Field Length	1160	[m]
Landing Field Length	1125	[m]
Horizontal Climb Distance	74.5	[nmi]

Revisiting the design objective, the reduction in block fuel per seat over a 500 nmi mission was found to be equal to 81.7% when comparing fuel mass and 48.7% when comparing energy consumption to the ATR 42-600. Furthermore, it has been shown that the current design indeed is able to enter service by 2035, with the novel technologies included.

Furthermore, there was a need to minimize the environmental impact of regional passenger aircraft while providing market-competitive performance, price, and operational costs. The environmental impact was minimized by usage of a fuel cell running on liquid hydrogen, which lead to an average temperature response 83 times smaller than that of the ATR 42-600 by 2065. Furthermore, the design range of the aircraft exceeds that of the main competitors, while its price and operational costs are comparable.

In general, it can be concluded that the SRP-22 is capable of performing its assigned tasks. After the next phases will be performed, the SRP-22 will be ready to depart on its journey towards clean skies.

References

[1] EASA. *Easy Access Rules for Large Aeroplanes (CS-25)*. Amendment 27. EASA. Aug. 2022.

[2] ICAO. *Operation of Aircraft*. Annex 6, Part I. ICAO.

[3] ICAO. *Environmental Protection*. Eighth Edition. ICAO. July 2017.

[4] R. Vos. *Introduction to Airplane Design*. (unpublished). Lawrence, KS. (USA): DARcorporation, 2023.

[5] Y. Brouwer. "Constrained Aerodynamic Optimization of the Flying V Nose Cone and Center-Body Fairing". MA thesis. Delft University of Technology, Apr. 2022.

[6] W. Bhatti. *Fuel Cells - Roadmap Report*. Tech. rep. Aerospace Technlogy Institute -FlyZero, 2022.

[7] M. Mitici, M. Pereira, and F. Oliviero. "Electric flight scheduling with battery-charging and battery-swapping opportunities". In: *EURO Journal on Transportation and Logistics* 11 (2022). DOI: 10.1016/j.ejtl.2022.100074.

[8] Schlömer S. et al. *Annex III: Technology-specific cost and performance parameters. In: Climate Change 2014: Mitigation of Climate Change. Contribution of Working Group III to the Fifth Assessment Report of the Intergovernmental Panel on Climate Change*. Cambridge, United Kingdom and New York, NY, USA: Cambridge University Press, 2014.

[9] J. Mukhopadhaya and D. Rutherford. *Performance Analysis of Evolutionary Hydrogen-Powered Aircraft*. Tech. rep. International Council of Clean Transportation, 2022.

[10] M. Studic. *Study into the impact of the global economic crisis on airframe utilisation*. Tech. rep. European Organisation for the Safety of Air Navigation (EUROCONTROL), Central Office for Delay Analysis (CODA), Jan. 2011.

[11] T. Cooper et al. *Global Fleet & MRO Market Forecast Summary*. Website. Subsidiary of Marsh McLennan Companies. Dec. 2017.

[12] L. Powis J. Cole W. McClintock. *MARKET FORECASTS & STRATEGY*. Tech. rep. Aerospace Technology Institute, 2022.

[13] A. Von Schoenberg. *Large Turboprop Report*. Tech. rep. Truenoord, 2020.

[14] A. Von Schoenberg. "Market review: turboprops punch above their weight". In: *Air finance Annual* (2021/2022).

[15] Avions de transport régional. *Turboprop market forecast 2022-2041*. Tech. rep. Avions de transport régional, 2022.

[16] Rik van Rossum et al. *A EUROPEAN HYDROGEN INFRASTRUCTURE VISION COVERING 28 COUNTRIES*. Tech. rep. European Hydrogen Backbone, 2022.

[17] FAA. *Economic Values for Evaluation of FAA Investment and Regulatory Decisions*. 2021 Update, Section 5. FAA. 2022.

[18] FAA. *Economic Values for Evaluation of FAA Investment and Regulatory Decisions*. 2021 Update, Section 4. FAA. 2022.

[19] D. Raymer. *Aircraft Design: A Conceptual Approach*. 6th ed. ISBN: 978-1-62410-490-9. American Institute of Aeronautics and Astronautics, Sept. 2018.

[20] E. Torenbeek. *Synthesis of Subsonic Airplane Design*. First ed. ISBN: 978-94-009-9582-6. Delft University Press, 1976.

[21] F. Babir. "Vehicles with Hydrogen-Air Fuel Cells". In: *Energy Carriers and Conversion Systems* 2 (2002). Copyright held by Encyclopedia of Life Support Systems. UNESCO/EOLSS Publishers Co., pp. 4245–4270.

[22] D. F. Finger, C. Braun, and C. Bil. “An Initial Sizing Methodology for Hybrid-Electric Light Aircraft”. In: *2018 Aviation Technology, Integration, and Operations Conference*. American Institute of Aeronautics and Astronautics. June 2018. DOI: 10.2514/6.2018-4229.

[23] R. Vos. *The Design of the Fuselage*. Aerospace Design and Systems Engineering Elements I, Delft University of Technology. Unpublished. Mar. 2020.

[24] D. Scholz. *Innovative Aircraft Design – Options for a New Medium Range Aircraft*. Hamburg Aerospace Lecture Series (DGLR, RAeS, VDI, HAW Hamburg), Hamburg (Germany). Zenodo. Hamburg University of Applied Sciences. 2015. DOI: 10.5281/zenodo.22468.

[25] J. Roskam. *Airplane Design Part I: Preliminary Sizing of Airplanes*. Published by DARCorporation. ISBN: 188488542X. June 1989.

[26] R. Vos, J.A. Melkert, and B.T.C. Zandbergen. *Wing and Propulsion system design and layout*. Aerospace Design and Systems Engineering Elements I, Delft University of Technology. Unpublished. Feb. 2020.

[27] T. Sinnige et al. “Wingtip-Mounted Propellers: Aerodynamic Analysis of Interaction Effects and Comparison with Conventional Layout”. In: *Journal of Aircraft* 56.1 (Jan. 2019). DOI: 10.2514/1.C034978.

[28] R. Vos and J.A. Melkert. *Wing Positioning, Landing Gear and Empennage Design*. Aerospace Design and Systems Engineering Elements I, Delft University of Technology. Unpublished. Mar. 2019.

[29] A. K. Kundu. *Aircraft Design*. Affiliated with Queen’s University. Cambridge University Press, June 2012. DOI: 10.1017/CBO9780511844652.

[30] DSE Group 1. *Baseline Report - Regional Passenger Transport*. Version 1. Unpublished. Faculty of Aerospace Engineering, TU Delft. Nov. 2022.

[31] V. N. Divakaran, G. V. V. Ravikumar, and S. R. Patnala. *Aircraft Landing Gear Design & Development*. 2018.

[32] J. Roskam. *Part IV: Layout Design of Landing Gear and Systems*. 8th ed. Design Analysis and Research Corporation (DARcorporation), 2022. Chap. 2.6. Brakes and Braking Capabilities, pp. 57–61. ISBN: 978-1-884885-53-2.

[33] A. E. Von Doenhoff and I. Abbott. *Theory of Wing Sections*. ISBN 978-0486605869. New York (U.S.A.): Dover Publications, 1949.

[34] F. Olivero. *Aircraft aerodynamic analysis: Mobile surfaces of the wing*. Aerospace Design and Systems Engineering Elements II, Delft University of Technology. Unpublished. Oct. 2019.

[35] F. Olivero. *Aircraft aerodynamic analysis: Lift and Drag*. Aerospace Design and Systems Engineering Elements II, Delft University of Technology. Unpublished. Oct. 2020.

[36] J. Roskam. *Machines, Mechanism and Robotics*. Lawrence: Springer, 2019.

[37] Micheal C.Y. Niu. *Airframe stress analysis and sizing*. second. Hong Kong Conmilit Press LTD, 1999.

[38] M. Ardema et al. “Fuselage and Wing Weight of Transport Aircraft”. In: *Journal of Aerospace* 105 (Jan. 1996), pp. 1536–1552.

[39] I. Sen. *Aircraft Fuselage Design Study*. Tech. rep. Aerospace Engineering at Delft University of Technology, Dec. 2010.

[40] F. Al-Mahmoud. *Nanotechnology in Eco-efficient Construction (Second Edition)*. Chapter Comprehensive Composite Materials II. Woodhead Publishing, 2019.

[41] G. Onorato. *Fuel Tank Integration for Hydrogen Airliners*. Tech. rep. Delft University of Technology, 2021.

[42] C. Winnefeld et al. *Modelling and Designing Cryogenic Hydrogen Tanks for Future Aircraft Applications*. Tech. rep. TU Braunschweig and Leibniz Universität Hannover, 2018.

[43] A. Gomez and H. Smith. *Aerospace Science and Technology Journal*. Liquid hydrogen fuel tanks for commercial aviation: Structural sizing and stress analysis. Elsevier, 2019.

[44] R. C. Hibbeler. *Mechanics of Materials*. 10th ed. Pearson, Jan. 2017.

[45] D. Silberhorn et al. *ASSESSMENT OF HYDROGEN FUEL TANK INTEGRATION AT AIRCRAFT LEVEL*. Tech. rep. German Aerospace Center (DLR) Institute of System Architectures in Aeronautics, 2019.

[46] H. Guoa et al. *Joining of carbon fiber and aluminum using ultrasonic additive manufacturing (UAM)*. Tech. rep. 2019.

[47] L. Kameni et al. “Feasibility Analysis of a New Thermal Insulation Concept of Cryogenic Fuel Tanks for Hydrogen Fuel Cell Powered Commercial Aircraft”. In: *International Journal of Hydrogen Energy* 47 (Aug. 2022). Affiliated with Technische Universität Braunschweig, pp. 31395–31408. DOI: 10.1016/j.ijhydene.2022.07.069.

[48] G. Onorato, P. Proesmans, and M. F. M Hoogreef. “Assessment of Hydrogen Transport Aircraft - Effects of Fuel Tank Integration”. In: *CEAS Aeronautical Journal* 13 (2022). Affiliated with the department of Flight Performance and Propulsion, Delft University of Technology, pp. 813–845. DOI: 10.1007/s13272-022-00601-6.

[49] Australian Civil Aviation Safety Authority. *Aircraft Electrical Load Analysis and Power Source Capacity*. Title 14. Advisory Circular AC 21-38 v2.1. ACASA. Dec. 2022.

[50] M. Biddanda et al. “Collins Aerospace Galley Thermal Power Optimization”. In: *Collins Aerospace* 56.1 (Dec. 2020). Designed by members of the College of Engineering, University of Michigan.

[51] M. Winter and R. J. Brodd. “Batteries, Fuel Cells, and Supercapacitors”. In: *Chemical Reviews* 104.10 (Sept. 2004). Published by the American Chemical Society, pp. 4245–4270. DOI: doi.org/10.1021/cr020730k.

[52] S. Um, C. Y. Wang, and K. S. Chen. “Computational Fluid Dynamics Modeling of Proton Exchange Membrane Fuel Cells”. In: *Journal of The Electrochemical Society* 147.12 (Aug. 2000), p. 4488.

[53] A. Salama. “Velocity Profile Representation for Fully Developed Turbulent Flows in Pipes: A Modified Power Law”. In: *Fluids* 6.10 (Oct. 2021). Article belongs to the Special Issue Turbulent Flow, p. 369. DOI: 10.3390/fluids6100369.

[54] H. D. Yao et al. “Blade-Tip Vortex Noise Mitigation Traded-Off against Aerodynamic Design for Propellers of Future Electric Aircraft”. In: *Journal of Aerospace* 9.12 (Dec. 2022). Article belongs to the Special Issue Aeroacoustics and Noise Mitigation. DOI: 10.3390/aerospace9120825.

[55] F. Woodruff. *Propeller Brake for a Turbo-Prop Engine*. United States Patent 4376614, Mar. 1983.

[56] Souad Kadi. *Aircraft Life Support Systems Part 2: Water and Waste System*. 2020. (Visited on 01/17/2023).

[57] J. Sinke. *Production of Aerospace Systems Reader*. Feb. 2022.

[58] R. Kumar, V.S. Chauhan, and H. Pathak M. Talha. *Part I: Airplane Flight Dynamics and Automatic Flight Controls*. Design Analysis and Research Corporation (DARcorporation), 1995.

[59] J.A. Mulder et al. *Flight Dynamics Lecture Notes*. AE3212-I Aerospace Flight Dynamics & Simulation including Flight Test, Delft University of Technology. Unpublished. 2013.

[60] Mohammad H Sadraey. *Aircraft Design A Systems Engineering Approach*. (unpublished). The Atrium, Southern Gate, Chichester, West Sussex, PO19 8SQ, United Kingdom: WILEY, 2013.

[61] G.J.J. Ruijgrok. *Elements of Airplane Performance*. Stevinweg 1: Delft University Press, 1990.

[62] Paul Jackson. *Jane’s All the World’s Aircraft: 2000-2001*. first. Jane ’s Information Group, July 2000.

[63] J. Roskam. *Part VIII: Airplane Cost Estimation: Design Development Manufacturing and Operating*. 8th ed. Design Analysis and Research Corporation (DARcorporation), 2018. ISBN: 978-1-885885-52-5.

[64] W. Bhatti et al. *Fuel Cells - Roadmap Report*. Tech. rep. Affiliated with the Department for Business, Energy and Industrial Strategy (UK). Aerospace Technology Institute, Mar. 2022.

[65] P. Proesmans and R. Vos. “Airplane Design Optimization for Minimal Global Warming Impact”. In: *AIAA Scitech 2021 Forum* (2021).

[66] E. Dallara. “Aircraft design for reduced climate impact”. PhD thesis. Stanford University, Feb. 2011.

[67] Leifsson and Leifur. “Multidisciplinary Design Optimization of low-noise transport aircraft [electronic resource] /”. In: (Jan. 2006).

[68] Carlo E.D. Riboldi et al. “Predicting the effect of electric and hybrid-electric aviation on acoustic pollution”. In: *Noise Mapping* 7.1 (2020), pp. 35–56. DOI: doi:10.1515/noise-2020-0004.

[69] N. Dickson. “ICAO Noise Standards”. In: *ICAO Symposium on Aviation and Climate Change “Destination Green”*. 2013.

[70] Snorri Gudmundsson. “Chapter 15 - Thrust Modeling for Propellers”. In: *General Aviation Aircraft Design (Second Edition)*. Ed. by Snorri Gudmundsson. Second Edition. Butterworth-Heinemann, 2022, pp. 597–656. ISBN: 978-0-12-818465-3. DOI: https://doi.org/10.1016/B978-0-12-818465-3.00015-X. URL: https://www.sciencedirect.com/science/article/pii/B978012818465300015X.

[71] Bronz M., Moschetta J., and Hattenberger G. “Multi-Point Optimisation of a Propulsion Set as Applied to a Multi-Tasking MAV”. In: (July 2012).

[72] Paul L. Lasagna et al. *Landing Approach Airframe Noise Measurements and Analysis*. Tech. rep. NASA, 1980.

[73] Robert Horonjeff et al. *Planning & Design of airports*. 5th ed. New York, NY, USA: McGraw-Hill, 2010.

[74] B.S.M Augustine et al. “Evaluation of Aircraft Maintainability and Aircraft Maintenance”. In: *International Conference and Exhibition on Emerging Challenges in Design and Manufacturing Technologies* 1 (Nov. 2007).

[75] DSE Group 1. *Project Plan - Regional Passenger Transport*. Version 1. Unpublished. Faculty of Aerospace Engineering, TU Delft. Nov. 2022.

[76] DSE Group 1. *Midterm Report - Regional Passenger Transport*. Version 1. Unpublished. Faculty of Aerospace Engineering, TU Delft. Dec. 2022.

[77] E. K. A. Gill. *Risk Management & Concurrent Engineering*. Version 0.7. Extract from AE3211-I Systems Engineering Methods. Faculty of Aerospace Engineering, TU Delft. Feb. 2022.

[78] M. Kalikatzarakis et al. “Model Based Analysis of the Boil-off Gas Management and Control for LNG Fuelled Vessels”. In: *Energy* 251 (2022). Affiliated to the Department of Maritime and Transport Technology, Delft University of Technology. DOI: 10.1016/j.energy.2022.123872.

[79] A. M. Swanger et al. “Integrated Refrigeration and Storage for Advanced Liquid Hydrogen Operations”. In: *Cryocoolers* 19 (June 2016). Published by International Cryocooler Conference, Inc., Boulder, CO (USA).

[80] N.J. van Wonderen. “Analysis of propeller slipstream effects on the directional stability using a potential flow model”. MA thesis. TU Delft, Jan. 2017.

[81] *TYPE-CERTIFICATE DATA SHEET FOR DHC-8*. Issue 15. EASA. Sept. 2021.

[82] *TYPE-CERTIFICATE DATA SHEET FOR NOISE for ATR 42 / ATR 72*. Issue 16. EASA. 1, Allée Pierre Nadot, Dec. 2022, p. 18.

[83] *TYPE-CERTIFICATE DATA SHEET FOR NOISE for De Havilland DHC-8*. Issue 8. EASA. Toronto, Ontario, Mar. 2022, p. 36.

A
Technical Drawing

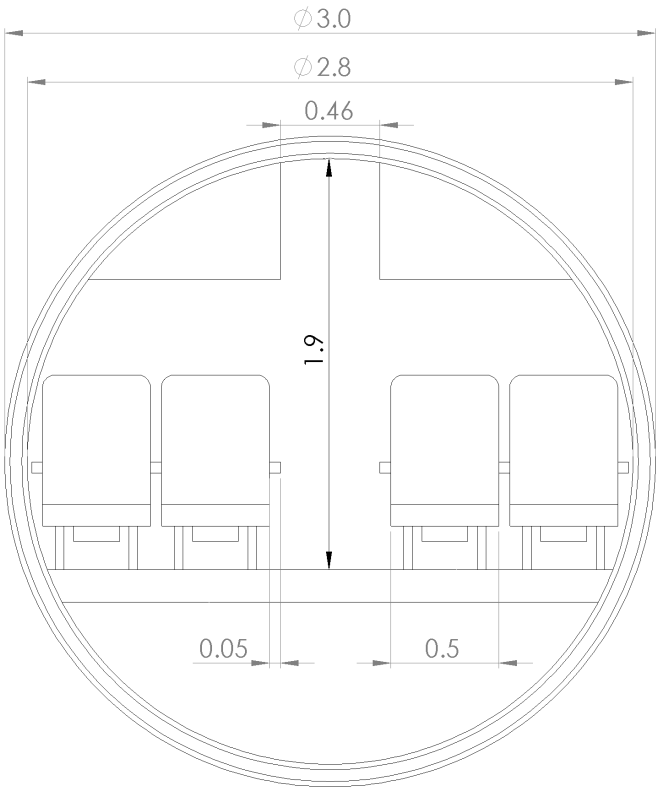

Figure A.1: Cabin cross section of SRP-22

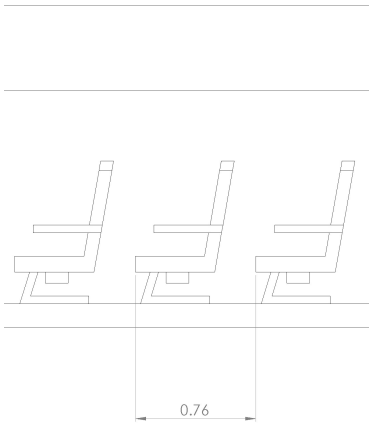

Figure A.2: Seat Pitch

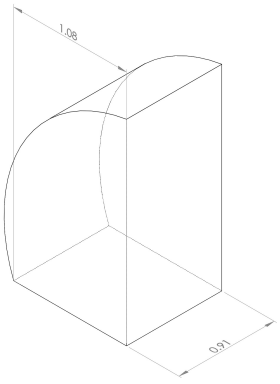

Figure A.3: Dimensions of lavatory and galley units in the SRP-22

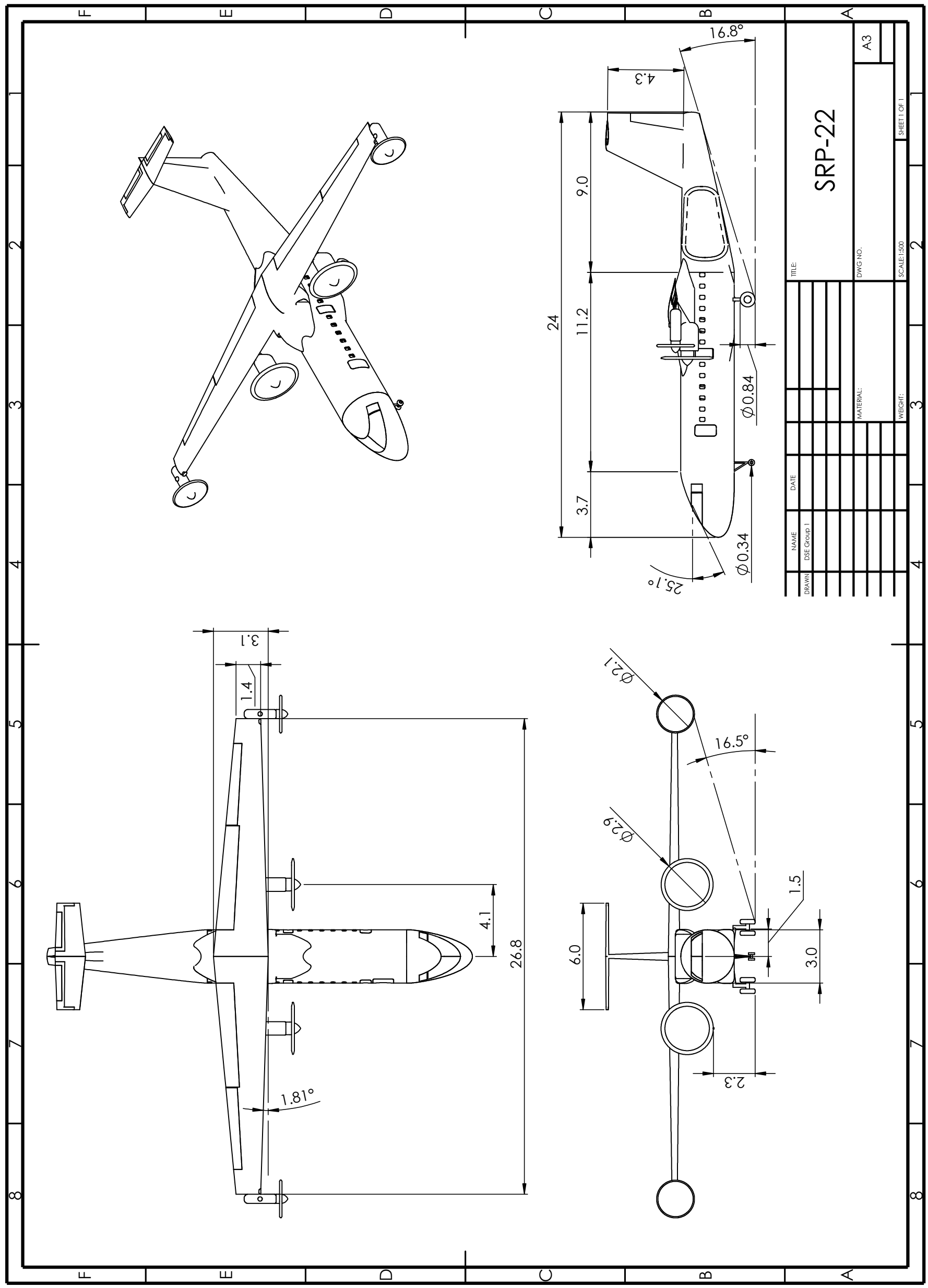

Figure A.4: Four view drawing of SRP-22